Modelling, Detection and Mitigation of Impulsive Noise and Narrowband Interference for Indoor Broadband Power Line Communication

Thesis submitted in accordance with the requirements of
the University of Liverpool for the degree of Doctor in Philosophy
by
Jun Yin

October 2016

Declaration

The work in this thesis is based on research carried out at the University of Liverpool. No part of this thesis has been submitted elsewhere for any other degree or qualification and it is all my own work unless referenced to the contrary in the text.

Abstract

Broadband power line communication (PLC) is a promising technology for the convergence of Internet, data and video for indoor networking. Impulsive noise (IN) and narrowband interference (NBI) are crucial affecting factors of the PLC system performance and cause harmful pollution to the PLC spectrum. In this thesis, a thorough study of IN and NBI is presented ranging from measurement, modelling, detection and mitigation techniques, and performance analysis.

In the first contribution, the modelling of aperiodic IN for PLC is investigated. To the best of our knowledge, this is the first work to model the correlation between consecutive impulses for PLC, using a hybrid model which includes the weighted contributions of deterministic and random patterns of individual impulses in a burst. The occurrence dependence between bursts and between impulses in a burst is described by a two-level Markov Chain (MC) based model. An intensive performance analysis of the proposed models is provided. The effectiveness of the models is verified by measured results.

In the second contribution, the modelling of radio NBI for PLC is investigated. A novel three-dimensional (3D) MC based statistical model is developed, to model the occurrence of NBI which is associated with the behaviours of certain radio users. An intensive performance analysis on the impact of the NBI on PLC is provided. The effectiveness of the proposed model is verified by measured results. The 3D MC model can be used for optimising cognitive PLC networks.

In the third contribution, detection and mitigation of aperiodic IN over uncoded orthogonal frequency division multiplexing (OFDM) PLC systems is inves-

tigated. A null subcarriers assisted IN mitigation scheme is proposed, to mitigate IN in the scenarios of NBI absence and NBI presence, respectively. The IN vector is first reconstructed at the receiver, and then cancelled out from the received signal. Theoretical analysis shows that the proposed scheme outperforms the existing blanking method. Also, the implementation of pre-joint NBI/IN mitigation with the aid of null subcarriers in the proposed scheme can combat intensive NBI, and achieve a near-optimal bit error rate (BER) performance with no iteration. The effectiveness of the proposed mitigation scheme is verified by simulation results.

In the fourth contribution, NBI detection over PLC systems is investigated. A novel higher-order statistics (HOS) based NBI detection scheme is proposed for cognitive PLC systems. In particular, the presence of IN is addressed for NBI detection, which was not considered in the previous work. An intensive performance analysis is provided, including the NBI detection probability and system capacity. The proposed NBI detection scheme outperforms the existing detection schemes and also leads to an enhanced system capacity over the existing schemes.

As a conclusion, the proposed work in this thesis is applicable to the PLC systems under the disturbance of IN and NBI, and enables optimisation of system performance. In the future work, a single-carrier frequency-domain equalisation (SC-FDE) PLC system will be investigated in order to reduce the high peak-to-average power ratio (PAPR) of signals in OFDM PLC systems. Also, different PLC channel attenuation models will be considered.

Acknowledgement

First of all, my gratitude goes to my supervisors Dr. Xu Zhu and Prof. Yi Huang for their valuable support, patient guidance and constant encouragement over the past years.

I would like to thank the University of Liverpool for providing me a studentship which makes this research possible.

I would also like to thank my colleagues who have offered kindly suggestions and encouragement during my study.

Finally, my gratitude is dedicated to my parents for their greatest support and deepest love all the time.

Contents

List of Figures

List of Tables

Abbreviations

3D	Three-Dimensional
AWGN	Additive White Gaussian Noise
BER	Bit Error Rate
BG	Bernoulli-Gaussian
BPSK	Binary Phase Shift Keying
CCDF	Complementary Cumulative Distribution Function
CDF	Cumulative Distribution Function
DFT	Discrete Fourier Transform
DSO	Digital Storage Oscilloscope
DUT	Device Under Test
FD	Frequency-Domain
FDM	Frequency Division Multiplexing
FEQ	Frequency-Domain Equalizer
FFT	Fast Fourier Transform
FSK	Frequency Shift Keying
HF	High Frequency
HOS	Higher-Order Statistics

HPAV	HomePlug AV
HV	High-Voltage
i.i.d.	independent and identically distributed
IFFT	Inverse Fast Fourier Transform
IN	Impulsive Noise
LISN	Line Impedance Stabilisation Network
LV	Low-Voltage
MC	Markov Chain
MIMO	Multiple-Input and Multiple-Output
MV	Medium-Voltage
NBI	Narrowband Interference
NTU	Network Termination Unit
OFDM	Orthogonal Frequency-Division Multiplexing
OPERA	Open PLC European Research Alliance
PAPR	Peak-to-Average Power Ratio
PDF	Probability Density Function
PLC	Power Line Communication
PSD	Power Spectral Density
PSK	Phase-Shift Keying
ROC	Receiver Operating Characteristic
SC-FDE	Single-Carrier Frequency-Domain Equalisation
SLC	Square-Law Combining

SLS	Square-Law Selection
SNR	Signal-to-Noise Ratio
SOS	Second-Order Statistics
SPP	Steady-Plane Probability
SSP	Steady-State Probability
TD	Time-Domain
WSS	Wide-Sense Stationary
ZF	Zero-Forcing

Chapter 1

Introduction

1.1 Background

Power line communication (PLC), which enables transmission of data over existing power cables, is a cost-effective and energy-efficient solution for the integration with growing ecosystem of indoor networking [8], smart grid [9] and other applications [10]. PLC for in-vehicle communication networks can also be found in the literature [9, 11].

The deployment of outdoor PLC [12] has been discouraged in most countries due to strong competition of cable services. Great attention has been drawn from utility companies to utilise low-voltage distribution lines as a last-mile technology [13] for indoor PLC applications, such as laptop and entertainment services in small offices and homes. Generally, the applications of PLC fall into three categories in terms of the operational bandwidth: ultra narrowband (0.3-3 KHz), narrowband (3-500 KHz) and broadband (1.8-250 MHz) [14]. The regulations prohibit PLC transmission between 500 KHz and 1.8 MHz to avoid interference with AM radio applications [1]. Automatic meter reading and two-way automatic communications are the applications for ultra narrowband PLC, which provides about 100 bps data rate. Narrowband PLC provides a few kbps for single-carrier and up to 500 kbps for multi-carrier. PRIME and G3-PLC are two commercial initiatives, and ITU-T G.hnem (G.9955/G.9956) and IEEE 1901.2 are the stan-

dards for narrowband PLC. Broadband PLC can achieve a data rate of several hundred Mbps for home area networks. The well-known PLC standards include IEEE 1901 [15], ITU-T G.hn (G.9960/G.9961) [16] and HomePlug AV/AV2 [17].

Future home networks are expected to support more high speed applications such as high-definition video, interactive gaming and broadband networking, driving the need for higher throughput. Broadband PLC is of interest [2], especially for indoor networks, in order to meet the demand for high throughput of Giga bits per second.

Some crucial issues of cable losses, multipath channel and added electromagnetic disturbance degrade the performance of indoor broadband PLC. Impulsive noise (IN) and narrowband interference (NBI) are the two main sources of high power electromagnetic disturbance causing harmful pollution to the PLC spectrum [2], which should be dealt with properly. In the HomePlug AV (HPAV) standard [17], the frequency band of 1.8 MHz-30 MHz is utilised. In [7], the frequency was extended to up to 100 MHz and the characterisation of PLC multipath channels was investigated. A dedicated system is required to deal with the PLC electromagnetic characteristics in the frequency range of 1.8 MHz-100 MHz.

1.2 Research Contributions

For the reason mentioned in Section 1.1, in the thesis, a thorough study of IN and NBI for indoor broadband PLC in the frequency band of 1.8 MHz-100 MHz is considered.

This PhD research was aimed to:

- Characterise the IN caused by various electric appliances, and the occurrence of NBI from potential radio users for broadband indoor PLC networking, through measurement-based approaches. Propose novel models for the time characteristics of the IN and NBI in PLC systems, respectively.

- Study novel and effective transmission techniques of detection and mitigation methods by considering the impact of both IN and NBI, in order to enhance the PLC system performance.

The research conducted during the PhD study has produced the following main contributions:

- Aperiodic IN for PLC is investigated using both measurement and modelling approaches. To the best of our knowledge, this is the first work to model the correlation between consecutive impulses for PLC, using a hybrid model which includes the weighted contributions of deterministic and random patterns of individual impulses in a burst, where the existing works mainly focus on independent and identically distributed (i.i.d.) samples. The occurrence dependence between bursts and between impulses in a burst is described by a two-level Markov chain (MC) based model. An intensive performance analysis of the proposed models is provided. The effectiveness of the models is verified by measured results.

- Radio NBI for PLC is investigated using both measurement and modelling approaches. A novel three-dimensional (3D) MC based statistical model is developed, to model the occurrence of NBI which is associated with the traffic of certain radio users. An intensive performance analysis on the impact of the NBI on PLC is provided. The effectiveness of the proposed model is verified by measured results. The 3D MC model can be used for optimising future cognitive PLC networks, through simulation-based approaches.

- IN mitigation over uncoded orthogonal frequency division multiplexing (OFDM) PLC systems is investigated considering the impact of NBI. A null subcarriers assisted IN mitigation scheme is proposed, to mitigate IN in the

scenarios of NBI absence and NBI presence, respectively. The IN vector is reconstructed at the proposed receiver first, and then cancelled out from the received signal. Capability of detecting nonzero entries in the IN vector for the proposed scheme is evaluated by means of receiver operating characteristic (ROC) comparing to that for the conventional blanking scheme reported in literature. According to the performance analysis, the proposed scheme outperforms the blanking method. Also, the implement of pre-joint NBI/IN mitigation with the aid of null subcarriers in the proposed scheme can combat the impact of intensive NBI, and achieve a near-optimal bit error rate (BER) performance with no iterations. The effectiveness of the proposed mitigation scheme is validated by simulation results, which is applicable to the PLC systems under the disturbance of joint IN and NBI.

- NBI detection over PLC systems is addressed considering potential power line IN source, which was not considered in the previous work. A novel higher-order statistics (HOS) assisted NBI detection scheme is proposed. Detection capability of the proposed scheme is evaluated by means of ROC comparing to those conventional methods reported in literature. An intensive performance analysis is provided, including the NBI detection probability and system capacity. The proposed NBI detection scheme outperforms the existing detection schemes and also leads to an enhanced system capacity over the existing schemes, which can be applied for optimising future cognitive PLC networks.

1.3 Thesis Organisation

The rest of this thesis is organised as follows. An overview of PLC channels and transmission techniques are given in Chapter 2. Chapter 3 presents a novel statistical modelling of IN. A 3D MC model for NBI is proposed in Chapter 4. Null

subcarriers aided IN mitigation scheme at PLC receivers is proposed in Chapter 5, considering the NBI environments. In Chapter 6, a higher-order statistics based NBI detection scheme for cognitive PLC is proposed, where detection in both scenarios of IN absence and IN presence is conducted, respectively. Conclusions and future work are provided in the final chapter.

1.4 Publications

- Jun Yin, Xu Zhu and Yi Huang, "Modeling of amplitude-correlated and occurrence-dependent impulsive noise for power line communication", *in Proc. IEEE International Conference on Communications (ICC)*, Jun. 2014, Sydney, Australia.
- Jun Yin, Xu Zhu and Yi Huang, "3D Markov chain based narrowband interference model for in-Home broadband power line communication", accepted by *IEEE Global Communications Conference (Globecom)*, Dec. 2016, Washington, DC, USA.
- Jun Yin, Xu Zhu and Yi Huang, "Higher-Order Statistics assisted Narrowband Interference Detection for Cognitive Power Line Communication", submitted to *IEEE International Conference on Communications (ICC)*.
- Jun Yin, Xu Zhu and Yi Huang, "Novel Statistical Modeling of Impulsive Noise and Narrowband Interference for in-Home Broadband Power Line Communication", submitted to *IEEE Transaction on Communications*.
- Jun Yin, Xu Zhu and Yi Huang, "Null Subcarriers assisted Impulsive Noise Mitigation for Indoor Broadband Power Line Communication", to be submitted *IEEE Transaction on Communications*.
- Jun Yin, Xu Zhu and Yi Huang, "Higher-Order Statistics assisted Narrowband Interference Detection for Cognitive Power Line Communication", to be submitted *IEEE Transaction on Communications*.

Chapter 2

Overview of Power Line Communications

In this chapter, the overall PLC infrastructure, channel characteristics and transmission techniques for indoor broadband PLC systems are reviewed. In Section 2.1, general structures for overall PLC architecture and a home area PLC networking are described. PLC specification by industry is also mentioned. Moreover, literature reviews on electromagnetic disturbance, channel attenuation and detection, mitigation techniques are presented in Section 2.2 and Section 2.3, respectively.

2.1 PLC Networking

2.1.1 Overall PLC Architecture

Normally, high-voltage (HV) transmission networks deliver power from power plants to the populated areas. Medium-voltage (MV) networks distribute power in a large scale while low-voltage (LV) networks distribute power to end-users. The structure of a typical broadband PLC network considering the overall communication architecture within the power grid is illustrated in Fig. 2.1. According to Fig. 2.1, the overall PLC network model contains the following parts:

- A service provider for Internet.

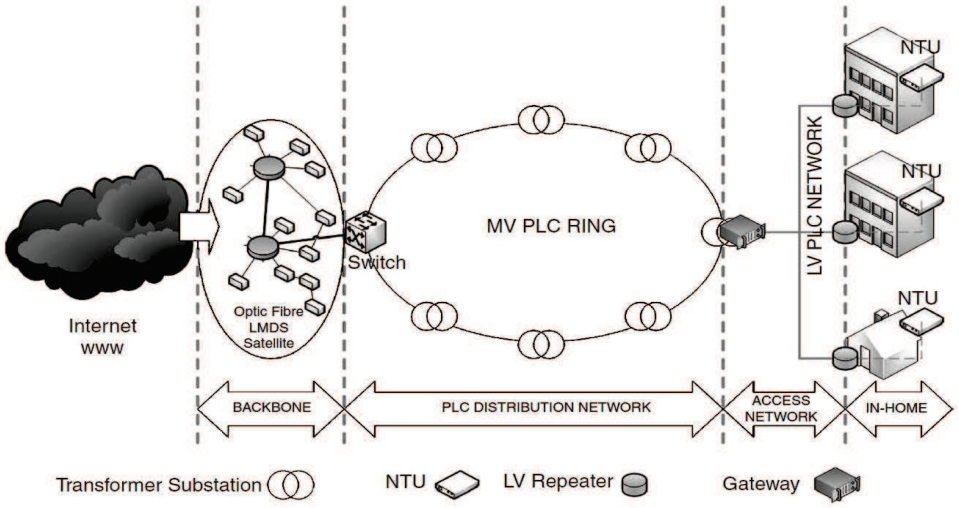

Figure 2.1: Overall PLC network structure [1].

- Backbone infrastructures for the communication between the MV PLC ring and the Internet service provider.
- A PLC distribution network, where all data from the MV PLC ring is concentrated at the MV to LV transformer substation.
- LV home area networks for the communication between the transformer substations and the customers.

The network termination unit (NTU) denotes the interface between the PLC networks and end-users. The repeaters are used to regenerate PLC signals in order to cover the whole networks for effective communications over a long distance. Among all the networking parts, the LV home area networking is of the interest as a last-mile to customers. In this thesis, the network for indoor broadband PLC is considered.

2.1.2 Indoor Broadband PLC Network Infrastructure

Due to the existing power line infrastructure, PLC makes it possible to deploy home area networks without new wiring facilities, yielding a cost-effective solution. Broadband PLC is of the interest [18, 2] for indoor networking [8] to enable

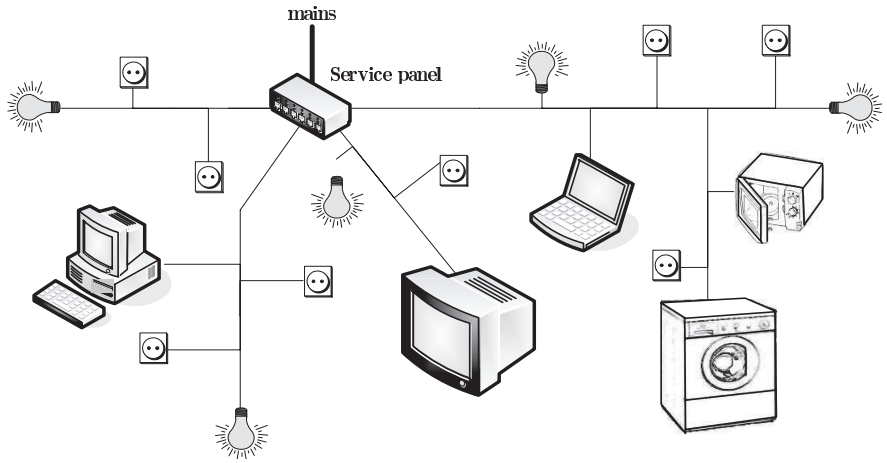

Figure 2.2: Block diagram of an indoor PLC network [1].

high data-rate applications, which provides an alternative to Ethernet and WiFi.

In Fig. 2.2, a typical layout of an indoor power grid is shown, which is connected to the outdoor LV network. Various electric appliances are connected to the network, such as computers, microwave oven, *etc.* Different types of disturbance inside the system can be generated due to the power distribution, running devices and connection/disconnection of appliances inside the grid, and also the external interference coupled into the network. The effect of multipath channel fading can be caused by the impedance mismatch between various loads and the power line.

2.1.3 Industry Specifications

The development in PLC technologies promotes a number of industry specifications for low data rate solutions or last-mile broadband Internet access of indoor networking. Practical PLC devices have been produced by a group of individual companies or alliance of companies, such as Lonworks, HomePlug, Open PLC European Research Alliance (OPERA) and Panasonic, *etc.* More details of the PLC industry companies can be found in [1].

The products from HomePlug Powerline Alliance [17], which is formed by a group of companies in April 2000 have already been widely accepted by mil-

lions of consumers. The HomePlug technology is driven by the demand of high-speed home networking. The first specification HomePlug 1.0 was designed with 14 Mbps physical rate using the frequency band of 4-28 MHz. Then, the HomePlug AV operating in 2-30 MHz was adopted in 2005 for the physical rate up to 200 Mbps. Moreover, HomePlug AV2 as the next generation enables a Gigabit-class physical rate using extra frequencies of 30-86 MHz and multiple-input and multiple-output (MIMO) technique. HomePlug AV2 meets the high throughput requirement for more indoor applications, such as whole home high-definition video/audio, interactive gaming and broadband Internet, *etc.*

2.2 Channel Characterisation

2.2.1 Noise

The noise environment for PLC is typically different from the noise in other communication systems and is one of the major challenges in the development of PLC systems. Generally, the existing power line noise characterisation [19, 20] from indoor PLC channels considers two main origins: noise incurred by the electric appliances connected to the power grid, and external noise coupled to the indoor networks by radiation or conduction. Detailed categorisation is given as

- Coloured background noise, is caused by overlaying of variety noise sources with low Power Spectral Density (PSD) in high frequency band (10-30 MHz), and relatively higher PSD in low frequencies (1-10 MHz) [21]. Due to a large number of low-frequency sources of noise, the PSD increases towards lower frequencies.

- Periodic IN asynchronous to the mains frequency with a repetition rate between 50 and 200 kHz.

- Periodic IN synchronous to the mains frequency with a repetition rate of 50 or 100 Hz (in Europe).

- Aperiodic IN caused by switching transients of electric appliances in the indoor PLC networks.

Unlike background noise, IN is distinctive in PLC system with extremely larger variance of noise amplitude. Periodic IN is induced by AC voltage change, which is cyclostationary with low repetition rates. However, aperiodic IN caused by any switching operations in PLC is randomly generated with probabilities. In the research area of PLC, IN has drawn many interests since its occurrence significantly increases the BER. A variety of models for simulating power line noise environments have been proposed. In the following, we introduce some well-known IN models for PLC channels, *i.e.*, the Middleton's class A model [22], the Bernoulli-Gaussian (BG) model [2] and the cyclostationary Gaussian model [23].

Middleton's Class A Model: The time-domain IN environment can be well reproduced through an infinite Gaussian mixture model, referred to as the Middleton's class A model, which has a probability density function (PDF) expressed as

$$p_\eta(\nu) = \sum_{k=0}^{\infty} \frac{e^{-A} A^k}{k!} \cdot \mathcal{N}(0, \sigma_k^2) \tag{2.1}$$

where $e^{-A}A^k/k!$ indicates the Poisson distributed probability for the kth IN term. Let $p_k = e^{-A}A^k/k!$, *i.e.*, $\sum_{k=0}^{\infty} p_k = 1$, where the first term ($k = 0$) is the probability for background noise only. $\mathcal{N}(0, \sigma_k^2)$ is the Gaussian PDF with zero mean and variance σ_k^2, which can be defined by

$$\mathcal{N}(x; 0, \sigma_k^2) = \frac{1}{\sigma_k \sqrt{2\pi}} \cdot e^{-\frac{x^2}{2\sigma_k^2}} \tag{2.2}$$

with

$$\sigma_k^2 = \left(1 + \frac{1}{\Gamma}\right) \left(\frac{(k/A) + \Gamma}{1 + \Gamma}\right) \sigma_{\mathrm{b}}^2 \tag{2.3}$$

where Γ is defined as the power ratio of background noise to impulsive noise, A represents the impulse index.

When the value of k is sufficiently large, the probability for the kth IN term becomes negligible. The first three terms in the Middleton's class A model are usually considered enough to approximate the model, which can be simplified as

$$p_\eta(\nu) \approx p_0 \cdot \mathcal{N}(0, \sigma_0^2) + p_1 \cdot \mathcal{N}(0, \sigma_1^2) + p_2 \cdot \mathcal{N}(0, \sigma_2^2) \tag{2.4}$$

Bernoulli-Gaussian Model: Referring to the Middleton's class A model, BG model is also based on the Gaussian mixture distribution but with only two terms. In order to simplify the IN modelling, only one IN term is considered in the BG model with the variance σ_{i}^2 while the other term is for the background noise only, expressed by

$$p_\eta(\nu) = (1-p) \cdot \mathcal{N}(0, \sigma_{\mathrm{b}}^2) + p \cdot \mathcal{N}(0, \sigma_{\mathrm{b}}^2 + \sigma_{\mathrm{i}}^2) \tag{2.5}$$

where p represents the probability of a Bernoulli random process, *i.e.*, the occurrence probability of IN. σ_{b}^2 and σ_{i}^2 are the variances for the background noise and IN, respectively.

Cyclostationary Gaussian Model: As categorised above, the IN can be periodically generated which is synchronous with the mains frequency. The periodic IN can be assumed as cyclostationary and modelled with zero mean and time-varying variance Gaussian process, yielding the amplitude PDF as

$$p_\eta(\nu(iT_s)) = \frac{1}{\sqrt{2\pi\sigma^2(iT_s)}} \cdot e^{-\frac{\nu^2(iT_s)}{2\sigma^2(iT_s)}} \tag{2.6}$$

where T_s is the sampling period, $\sigma^2(iT_s)$ is the instantaneous variance of the noise which is synchronous to the mains due to different phases of AC voltage, and expressed by

$$\sigma^2(t) = \sum_{l=0}^{L-1} A_l \left| sin\left(\frac{2\pi T}{T_0} + \theta_l\right)\right|^{n_l} \tag{2.7}$$

where T_0 is the duration of mains cycle, the parameters A_l, θ_l and n_l determine the noise characteristics. Due to the low rate of periodic IN, such noise is insignificant for broadband PLC transmission, while cannot be ignored for narrowband PLC systems.

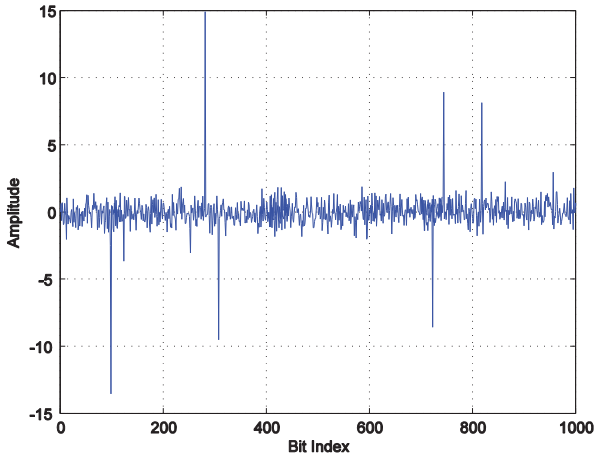

Figure 2.3: An example of IN environment reproduced by BG model [2].

In narrowband PLC, the coloured background noise and the low-frequency periodic IN is dominant [21, 24]. As learned previously, coloured background noise is caused by the superimposition of numerous noise sources. Such combination of multiple independent Rayleigh distributed sources is well modelled by the Nakagami-m PDF in [21]. A cyclostationary model in [23] is proposed for the periodic IN.

In broadband PLC, the dominant noise term is the aperiodic IN [25]. The background noise has low and constant PSD in high frequencies, which is often considered as additive white Gaussian noise (AWGN) [26, 27]. The periodic IN is cyclostationary with a low repetition rate comparable to that of the mains, and has relatively low amplitude [18], and hence is insignificant in broadband PLC. Aperiodic IN often occurs randomly in bursts with large amplitude variance and degrades the broadband PLC performance significantly [2, 25]. Due to the random behaviour, aperiodic IN is often reproduced statistically in a random model, such as the well-known BG model [28, 29], Middleton's Class A model [22] and MC model with memory in [25, 30]. Among them, BG model is most popular and widely applied [31, 32].

Fig. 2.3 shows an example noise environment for broadband PLC generated by the BG model [2], where noise is randomly generated by i.i.d. Gaussian samples.

Referring to (2.5), it is assumed $p = 0.01$ and $\sigma_{\mathrm{i}}^2 = 100\sigma_{\mathrm{b}}^2$. The horizontal axis denotes the time samples where the sparsity level of the IN entries are presented. The IN samples are uniformly distributed with a certain occurrence probability. In this thesis, modelling of the burst-type aperiodic IN is considered.

2.2.2 Interference

Power line noise has its power spread over the whole frequency spectrum, which shows wideband property, The disturbance type of interference can be easily detected in the power line spectrum, since it normally has much higher intensity of the PSD compared to that of the noise terms, referred to as NBI [18]. NBI can be classified according to different categories, *e.g.*, origins, shapes of PSD and statistical properties [18]. Considering the origins, NBI in PLC systems is mainly caused by two types of sources as

- Spurious disturbance inside the power grid caused by running electric devices. It is also called narrowband noise in [25, 33]. Narrow band noise between 3 and 148.5 kHz in Europe and below 450 kHz in Japan [23] is a reason to induce high level of noise power in low frequencies.

- Mostly sinusoidal signals, with modulated amplitudes caused by ingress of broadcast stations and amateur radio. This interference has PSD of a single narrowband term and a significant level above the background noise (even more than 30 dB). Normally below 2 MHz or above 20 MHz. NBI from commercial AM radio stations is an example of this category.

The power of the NBI caused by spurious disturbance is usually at a lower level than that from the external radio applications, and concentrates in the frequency band below 8 MHz. Therefore, in this thesis, we focus on characterising the NBI from various nearby radio applications.

For indoor broadband PLC, NBI from radio systems may become a salient issue that degrades the PLC system performance, since the unshielded power line can be a good antenna picking up the radios around [6]. Normally, there are various narrowband interferers inside the frequency range of 1.8 MHz-100 MHz, from broadcast radios, amateur radios, *etc.*, and the power level is generally time-varying in daytime [6, 25]. Accurate modelling of NBI supports comprehensive system performance analysis in order to achieve effective PLC transmission. Most of the existing NBI models are for wireless communication channels [34, 35], such as ad hoc networks. Currently, the analysis of the NBI for PLC is mainly through measurement-based approaches, and NBI needs to be modelled in a statistical manner. In this thesis, modelling of the radio NBI is considered.

2.2.3 Attenuation

The indoor power line channel attenuation due to multipath propagation and frequency dependent cable losses has crucial effects on PLC system performance. Some popular power line channel models have already been proposed and widely used, such as the bottom-up model [36] and the multipath model [37].

Due to the complexity of indoor PLC channel topology and the safety issues of power line related measurements within the high voltage environment, it is difficult to conduct research on developing a universally recognised channel model. According to the literature, two types of channel modelling approaches are considered, *i.e.*, the bottom-up approach [36, 8] and the top-down approach [30, 37]. The channel model used in this thesis is from a top-down based random channel generator.

2.2.3.1 Bottom-Up Channels

The bottom-up approach is normally to derive the channel attenuation mathematically using transmission line theory [3]. Perfect knowledge of the power network parameters is required, such as the topology, cables and loads. There-

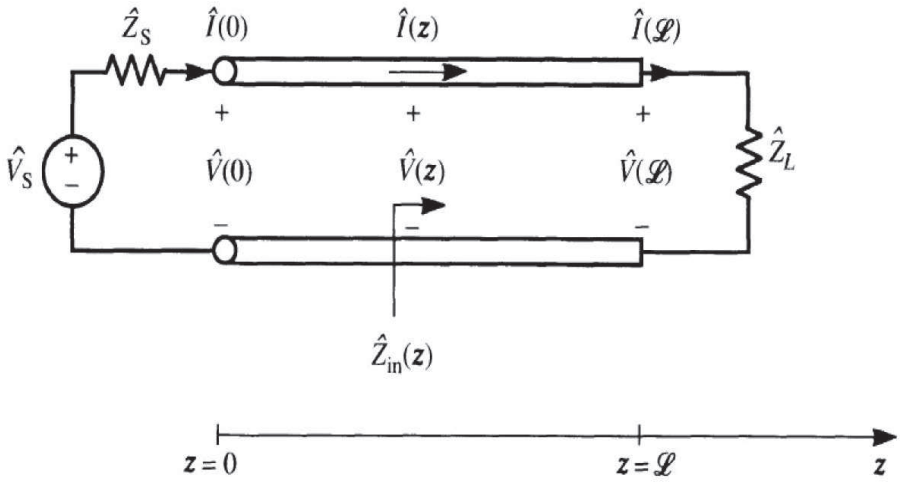

Figure 2.4: An example transmission line model [3].

fore, the bottom-up approach is closely related to physical power line networks. However, it is computational complex to collect all the network information.

An example transmission line model is shown in Fig. 2.4. The parameter $\mathcal{L}$ indicates the cable length with the characteristic impedance Z_{C}. The channel transfer function can be obtained by calculating the voltage ratio [36]. Considering the source voltage V_{S} with the impedance Z_{S}, the channel transfer function $H(f)$ can be calculated by the ratio $V(\mathcal{L})/V_{\mathrm{S}}$, yielding

$$H(f) = \frac{1+\Gamma_{\mathrm{L}}}{1-\Gamma_{\mathrm{L}}\Gamma_{\mathrm{S}}e^{-2\gamma\mathcal{L}}} \cdot \frac{Z_{\mathrm{C}}}{Z_{\mathrm{C}}+Z_{\mathrm{S}}} \cdot e^{-\gamma\mathcal{L}} \tag{2.8}$$

where Γ_{L} and Γ_{S} are the reflection coefficients for the load and the source, respectively. γ denotes the attenuation constant and $\mathcal{L}$ is the cable length.

Using the voltage ratio approach in [36], the channel transfer function of each segment can be derived as $H_n(f) = V_{n+1}(f)/V_n(f)$. Then, the overall channel transfer function is given by

$$H(f) = \prod_{n=1}^{N} H_n(f) \tag{2.9}$$

where the source impedance is assumed as zero, *i.e.*, $V_1(f) = V_{\mathrm{S}}(f)$.

2.2.3.2 Top-Down Channels

Unlike the bottom-up approach, the top-down approaches try to generate the channels statistically and then develop the channel models through data fitting. It is a low complexity method to model the channel but great effort is needed for the channel characterisation in order to get the statistical results.

The most popular top-down channel model can be found in [37], since it considers the joint effects of the multipath delay, the cable length and frequency dependent attenuation. The transfer function of the attenuation model can be specified as

$$H(f) = \sum_{i=1}^{N} g_i \cdot e^{-(a_0+a_1 f^k)d_i} \cdot e^{-j2\pi f \tau_i} \tag{2.10}$$

where N is the total number of paths. The first term g_i indicates the weighting factor for the ith path where $|g_i| \leq 1$. The attenuation term $e^{-(a_0+a_1 f^k)d_i}$ for the ith path shows that the cable loss increases with the distance d_i and frequency f. The parameters a_0, a_1 and k determine the dependency of attenuation on the distance and frequency. The third term $e^{-j2\pi f \tau_i}$ considers the multipath delay where the time delay τ_i is given by

$$\tau_i = \frac{d_i}{v_p} \tag{2.11}$$

which is determined by the path length d_i and the phase velocity v_p.

Using the top-down approach, the attenuation parameters can be estimated through measurements. The OPERA [30] defined 9 reference channels in respect to linking the distances. However, various parameters are not easy to determine for the model and the computational cost increases fast with the number of paths. It is more convenient to generate the reference channels in a statistical manner. Corresponding to the 9 reference channel, the nine-class channel model with 9 sets of parameters [7] presents its benefit of simple expression of the channel transfer functions, and is used in this thesis for indoor broadband PLC random channel generator.

Table 2.1: Capacities of the Nine-Class Model [7]

Class	Percentage of channels (%)	Capacity range (Gbps)	Average capacity (Gbps)
1	3.49	1 - 1.2	1.12
2	16.78	1.2 - 1.4	1.31
3	18.18	1.4 - 1.6	1.49
4	11.88	1.6 - 1.8	1.69
5	11.88	1.8 - 2	1.90
6	12.58	2 - 2.2	2.10
7	9.79	2.2 - 2.4	2.30
8	7.69	2.4 - 2.6	2.50
9	7.69	2.6 - 2.8	2.70

In [7], PLC channels are classified into 9 classes per ascending order of their capacities since it is not easy to calculate the distances between PLC transmitters and receivers. According to the Shannon's capacity under the same signal-to-noise power ratio, the capacity formula related to the channel response can be expressed as

$$C = \frac{\Delta f}{N} \cdot \sum_{i=1}^{N} \log_2 \left(1 + \frac{P_e |H(f_i)|^2}{P_b} \right) \tag{2.12}$$

where Δf is the bandwidth, P_e and P_b are the transmitted signal PSD and white noise PSD, respectively.

It can be seen in (2.12) that channel attenuation is a crucial factor to determine the channel capacity C. According to the Shannon's theorem, capacity states a maximum allowed data rate for error-free communication. Namely, in order to transmit the source data through the channel with no error, the data rate R should be limited by

$$R \leq \frac{\Delta f}{N} \cdot \sum_{i=1}^{N} \log_2 \left(1 + \frac{P_e |H(f_i)|^2}{P_b} \right) \tag{2.13}$$

otherwise, it will cause bit errors certainly.

The 9 classes were defined within the frequency band of 1 MHz-100 MHz, where the minimum capacity was around 1 Gbps and the maximum capacity was around 2.8 Gbps. Detail results of the nine-class channel were given in [7]

in reference to a number to indoor sites, while the classifications of the transfer functions are presented in Table 2.1.

2.3 Transmission Techniques

2.3.1 Modulation Schemes

Modulation is to translate a baseband signal to a waveform suitable for transmission over different channels. There are sever modulation schemes to be considered for PLC systems previously, such as single-carrier modulation, spread spectrum modulation and multi-carrier modulation [1, 38].

Recent research emphasises the transmission techniques and error control coding for the binary modulation schemes, such as binary phase shift keying (BPSK) and frequency shift keying (FSK). The single-carrier modulation leads the inter-symbol interference issue and is vulnerable to frequency selective fading channels. The spread spectrum modulation scheme is one of the candidates for broadband PLC, since it is robust against selective fading and NBI. However, the spread spectrum technique has a very low spectral efficiency and seems not feasible for future applications. The multi-carrier modulation schemes are expected for the future as exhibiting robustness against frequency selective fading and offering high spectral efficiency. OFDM is the most popular multi-carrier modulation technique and widely used in broadband PLC systems [21, 39].

2.3.2 OFDM Transmission

Power line channel is a very harsh media for transmissions which may suffer from frequency-selective fading due to signal reflections and impedance mismatching at transmission line discontinuities. The multi-carrier technique of OFDM is more robust compared to single-carrier modulation in frequency selective channels. The advantages of using OFDM can be listed in the following:

- The frequency selective fading channel can be divided into multiple narrow-

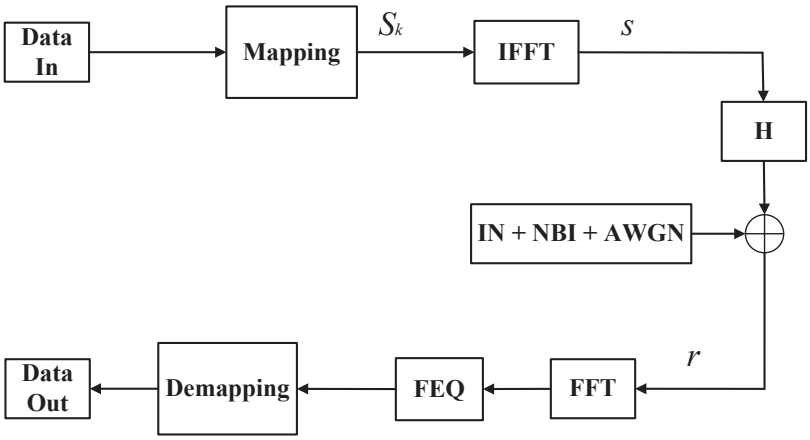

Figure 2.5: Block diagram of an OFDM based communication system for PLC under both IN and NBI (FEQ-frequency domain equalization).

band sub-channels where each sub-channel suffers from flat fading. Hence, BER performance in frequency selective fading channels is the same as that in flat fading channels.

- OFDM leads a higher spectrum efficiency than the conventional frequency division multiplexing (FDM), since it uses orthogonal subcarriers and all the subcarriers are overlapped with each other.

- Each subcarrier can be modulated and equalised independently, using conventional schemes for single-carrier systems.

OFDM is the most popular modulation technique and widely used in broadband PLC [21, 39] to achieve high-speed communications, which is also specified in current PLC standard [17]. The block diagram of a conventional baseband uncoded OFDM system for PLC transmission is presented in Fig. 2.5, where s is for the transmitted signal and r is the received signal.

To model the signal at a conventional OFDM transmitter for baseband communications [40, 31], the data symbol S_k is selected from binary mapping (*i.e.*, BPSK). Following OFDM modulation, the mth sample of transmitted signal can

be expressed by

$$s(m) = \frac{1}{\sqrt{N}} \sum_{k=0}^{N-1} S_k e^{j2\pi km/N} \tag{2.14}$$

where $m = 0, 1, ..., N-1$ and N is the number of subcarriers. The PLC signals then will be attenuated by channel effects and disturbed by additive noise and interference at receiver, where robust techniques like mitigation and detection are required.

The signal at the PLC receiver is a mixture of various noises. Let $r(m)$ denote the mth received signal sample, which can be expressed as

$$r(m) = \{h_{\mathrm{s}} * s\}(m) + n_{\mathrm{i}}(m) + v(m) + n_{\mathrm{b}}(m) \tag{2.15}$$

where $\{h_{\mathrm{s}} * s\}(m) = \sum_n h_{\mathrm{s}}(n)s(m-n)$ and h_{s} is the channel impulse response for PLC signal $s(m)$. A random PLC channel generator in [7] is applied as the channel model. The background noise $n_{\mathrm{b}}(m)$ is assumed to be AWGN with zero mean and variance σ_{b}^2. $n_{\mathrm{i}}(m)$ is the considered IN at PLC receiver, which has a zero mean and variance σ_{i}^2. It is assumed that the variance of the background noise is much lower than that of the IN, *i.e.*, $\sigma_{\mathrm{b}}^2 \ll \sigma_{\mathrm{i}}^2$. The NBI $v(m)$ is from radio applications and occurs with probabilities.

2.3.3 Noise Mitigation

IN has its power spread over all subcarriers in OFDM systems. Although Peak-to-average power ratio (PAPR) of IN is lowered after doing fast Fourier transform (FFT), it may still degrade the system performance significantly by damaging all subcarriers, which should be seriously treated to ensure high quality communications.

Nonlinear techniques are popular with existing IN mitigation schemes executed in OFDM systems, such as blanking [41], clipping/deep clipping [27] and weighted combinations of them [40, 42]. Some conventional nonlinear methods were studied in [40] and can be formulated as

Clipping:

$$\bar{r}(m) = \begin{cases} r(m), & |r(m)| \leq \lambda_1 \\ \lambda_1 e^{j\varphi}, & |r(m)| > \lambda_1 \end{cases} \tag{2.16}$$

Blanking:

$$\bar{r}(m) = \begin{cases} r(m), & |r(m)| \leq \lambda_2 \\ 0, & |r(m)| > \lambda_2 \end{cases} \tag{2.17}$$

Joint Clipping/Blanking:

$$\bar{r}(m) = \begin{cases} r(m), & |r(m)| \leq \lambda_1 \\ \lambda_1 e^{j\varphi}, & \lambda_1 < |r(m)| \leq \lambda_2 \\ 0, & |r(m)| > \lambda_2 \end{cases} \tag{2.18}$$

where $\varphi = \arg(r(m))$, λ_1 and λ_2 ($\lambda_1 < \lambda_2$) denote the thresholds for clipping and blanking respectively.

For the above nonlinear schemes, the detection performance on IN contaminated data subcarriers is disturbed by high PAPR OFDM signals. Higher values of threshold may miss detect some of the impulses, while lower threshold values may cause false alarms. Generally, the threshold chosen for blanking is larger than the threshold for clipping. Some sophisticated IN mitigation schemes were developed in [11, 26] with the aid of compressed sensing [43, 44] and sparse Bayesian learning [45]. Moreover, channel coding schemes were used in [46, 47] to correct the bit errors. In this thesis, the technique of IN mitigation is considered for indoor broadband PLC.

2.3.4 Cognitive Interference Detection

At PLC receivers, NBI caused by radio signals is another added disturbance as learned previously. Cognitive technique [48, 49] meets the need of flexible networking, which is defined in [50] as to sense the electromagnetic environment and then adjust the operating frequency bands dynamically, in order to mitigate interference and improve the throughput achievable. Some popular NBI detection methods are widely applied for cognitive radio [4, 51], such as matched filtering, amplitude detection and energy detection. Fig. 2.6 presents a comparison of the

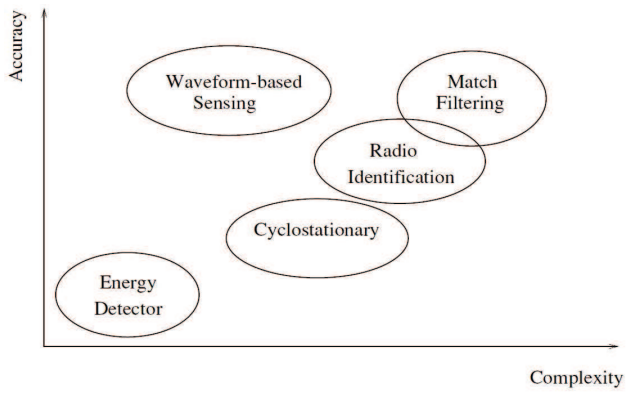

Figure 2.6: A comparison of main detection schemes in terms of the accuracy and complexity [4].

existing radio detection schemes. There is a trade-off between the performance and complexity while selecting a particular detection method. More details can be found in [4].

For indoor broadband networking, cognitive PLC is currently of the interest [52] to increase the transmission frequency bands by using the available radio frequencies. Test campaigns in PLC systems were performed within 1.8-30 MHz frequency band [17]. European project OMEGA [53] increases the bandwidth until 100 MHz for future PLC systems with the aim of achieving 1 Gbps data-rate. Cooperative scheme is widely used for NBI detection at PLC receivers from different sites, while in [54], short wave broadcast radio band (1.6-20 MHz) was investigated, and cognitive detection on the FM band (87.5-108 MHz) was considered in [6]. In this thesis, detection of the radio NBI for the application of cognitive PLC is considered.

Chapter 3

Modelling of Amplitude-Correlated and Occurrence-Dependent Impulsive Noise

High power electromagnetic disturbance of both IN and NBI are the two main sources causing harmful pollution to the PLC spectrum [2], which should be dealt with properly. This chapter focuses on investigating the burst-type IN. Accurate modelling of IN will support comprehensive system performance analysis in order to achieve effective PLC transmissions.

PLC IN can be classified as periodic and aperiodic [18]. Periodic IN, which is caused by power converters occurring in dimmers and the rectifiers using diodes, is either synchronous to the mains with a frequency of 50 or 100 Hz, or asynchronous with a frequency between 50 and 200 kHz. It is cyclostationary with a certain repetition period comparable to that of the mains, and has relatively low amplitude [18]. Aperiodic IN is mainly incurred by switching/plugging/unplugging transients of electric appliances such as heater, oven and incandescent lamp [18, 30]. It often occurs randomly in bursts and degrades the PLC performance significantly [2, 25]. Hence, we focus on aperiodic IN in this paper. The random Bernoulli-Gaussian (BG) model [28, 29] and Middleton's Class A model [22] are well-known for aperiodic IN modelling in PLC systems. However, it was assumed

in both models that the impulses are independent and identically distributed (i.i.d.), which is not practical. Markov chain (MC) is considered as an accurate tool to predict a random source [55]. In [25], an MC based model was proposed, which generates the impulses with occurrence probabilities dependent on the previous states. Aperiodic IN often occurs in a series of impulses, referred to as burst [25]. The occurrence of a burst is dependent on the previous states, which can be described by an MC based model [56]. In [30], a two-level hierarchical MC was applied to model the defence of bursts with each other and the dependence of the impulses. However, it was assumed in [30] that the impulses within a burst are uncorrelated, and the impulse variance is fixed, regardless of noise source. In practice, the impulses within a burst are not only dependent, but also correlated. Also, different noise sources could result in significantly different impulse variances. In [25], two measured impulse examples reveal the coloured power spectral density (PSD) and show different PSD levels above the background noise.

In this chapter, the measurement and modelling of correlated and occurrence-dependent aperiodic IN for indoor broadband PLC are conducted. Our work is different in the following aspects. First, to the best of our knowledge, this is the first work to investigate modelling of correlations between impulses within a noise burst for PLC. A hybrid model is proposed, where an adjustable weight coefficient is applied to trade-off the deterministic pattern and the random pattern of correlated impulses within a burst. The impact of different values of the weight coefficient is also investigated. The existing BG model [2] and any other Bernoulli process [57] can be regarded as a special case with weight coefficient set to zero. Second, an enhanced hierarchical two-level MC based model is proposed to describe the occurrence dependence of IN, where the first level chain models the occurrence of bursts, while the second level chain models the occurrence of impulses in a burst. Multiple impulse states, which represent IN induced by different sources, are introduced in the second level chain, unlike [30] where only

a single impulse state was assumed. The existing BG model [2] and any other Bernoulli process [57] can be regarded as a special case with assumed independent impulse samples. Third, we present an intensive performance analysis, including autocorrelation function and PSD of the IN, average duration and interval of IN, respectively, steady-state probabilities for the MC, and system capacity, using the parameters obtained from the measured results. Fourth, the IN at both source and receiver are investigated, while the existing noise characterisation is applied either at source [33] or at receiver [18], where the channel propagation effects on IN were not considered. The effectiveness of the proposed hybrid model and MC based models is verified by the measured results.

In Section 3.1, measurement setup and results of the burst IN for PLC are presented. A hybrid model to describe the correlation properties of IN, and a two-level MC based model for the occurrence dependence of IN are proposed in Section 3.2. A performance analysis is presented in Section 3.3. The summary is remarked in Section 3.4.

3.1 Measurement of Burst IN for Indoor PLC Systems

The block diagram of an indoor broadband PLC system disturbed by IN sources is depicted in Fig. 3.1, where $s(t)$ represents the transmit signal and $r(t)$ is the received signal. $n_{\mathrm{b}}(t)$ denotes the added background noise. We assume K aperiodic IN sources. At time t, $n_{\mathrm{s}k}(t)$ $(k = 1, \ldots, K)$ denotes the IN from the kth source ($n_{\mathrm{s}k}(t) = 0$ means no noise). Let $n_{\mathrm{i}}(t)$ denote the overall IN at the receiver as aperiodic IN, which can be treated as passing the noise from any potential switching/plug transients of the appliances in the system, through the corresponding channel. While h_{s} and $h_{\mathrm{n}k}$ are the channel impulse responses for PLC signal $s(t)$ and the IN at source $n_{\mathrm{s}k}(t)$, respectively.

In a discrete-time system, the signal at the PLC receiver is a mixture of various

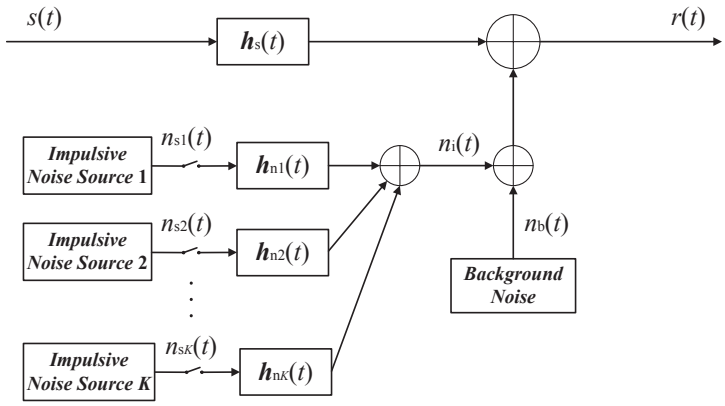

Figure 3.1: Block diagram of a PLC system disturbed by IN sources.

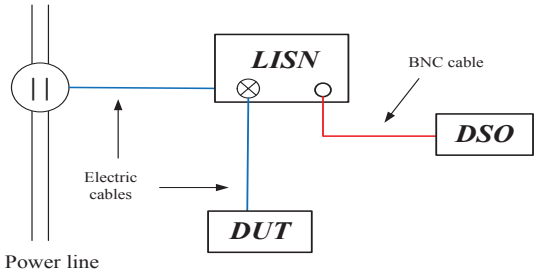

Figure 3.2: Measurement setup for PLC noise at source.

noises. Let $n(m)$ denote the mth sample of the added disturbance at receiver, expressed as

$$n(m) = n_{\mathrm{b}}(m) + n_{\mathrm{i}}(m) \tag{3.1}$$

where the background noise $n_{\mathrm{b}}(m)$ is assumed to be additive white Gaussian noise (AWGN) with zero mean and variance σ_{b}^2, and the output IN at PLC receiver $n_{\mathrm{i}}(m) = \sum_k \sum_q h_{\mathrm{n}k}(q) n_{sk}(m-q)$ $(k = 1, \ldots, K)$ is the discrete convolution between the IN at source and the corresponding channel impulse response, which has a zero mean and variance σ_{i}^2 . It is assumed that the variance of the background noise is much lower than that of the IN, *i.e.*, $\sigma_{\mathrm{b}}^2 \ll \sigma_{\mathrm{i}}^2$.

The measurements are divided into two aspects, the IN at source $n_{sk}(t)$ $(k = 1, \ldots, K)$, and the IN at the PLC channel output $n_{\mathrm{i}}(t)$, respectively.

3.1.1 IN at Source

It would be easier to characterise IN at source, since there are much less noise types at source than that at receiver [58, 59], and the noise at receiver is simply considered as the noise at source filtered by the channel.

The setup for measuring the noise at source for PLC is shown in Fig. 3.2. A digital storage oscilloscope (DSO) is used to record the transients of waveform generated by the device under test (DUT), and a line impedance stabilisation network (LISN) is applied to reject noise current from mains. The use of LISN protects the DSO input and also isolates the DUT, whose IN under measure.

The aperiodic IN measured often occurs in bursts. The impulses are associated with electric switch on/off events as well as plug in and unplug events of the DUTs within a laboratory of the University of Liverpool. Fig. 3.3 shows two examples of the measured impulsive noises from source, which are induced by hair dryer switch on and electric kettle unplug, respectively. The two presented examples represent a long burst duration case and a short burst duration case, respectively. They are considered to be representative as they show a clear difference in the statistical patterns. The statistics of IN can vary according to the in-device generators, appearing as short, medium and very long impulses. Other measured IN events like monitor plug-in and incandescent lamp unplug generate impulses in long and scattered form, while lamp switching on/off presents very short and weak impulses. The IN caused by microwave oven plug-in is characterised by several successive short bursts. Details of IN originating from more household electrical appliances can be found in [59].

The measurements for the example events are repeated for 100 times to ensure that sufficient samples are obtained for accurate analysis. A sampling rate of 100 Mega-samples per second is used. Hair dryer switch on event generates a longer burst, while electric kettle unplug event yields the higher noise power. The statistical results of the example noise durations, means and variances are

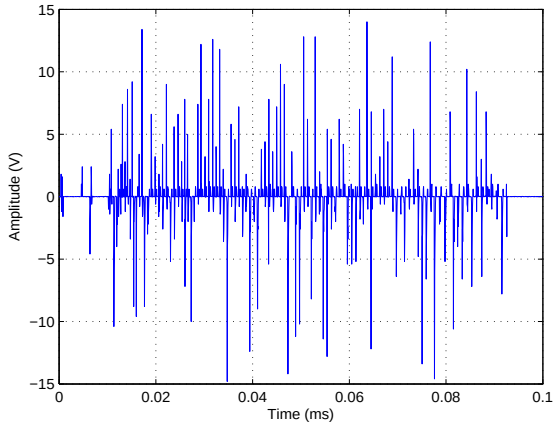

(a)

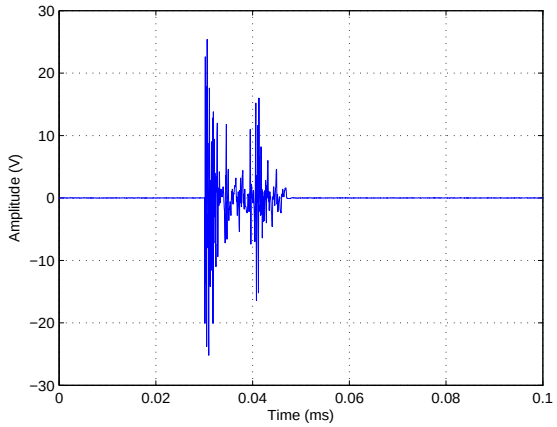

(b)

Figure 3.3: Measured IN at source caused by (a) hair dryer switch on; and (b) electric kettle unplug.

listed in Table 3.1. The variance is a measure of the average squared differences from the mean, *i.e.*, $\sigma_x^2 = \sum_i (x_i - \mu)^2$. The normalised variance indicates the noise power level, which is the variance of measured IN events normalised to the variance of background noise, *i.e.*, $\sigma_{\mathrm{i}}^2/\sigma_{\mathrm{b}}^2$. It can be seen that the higher power of kettle unplug noise refers to the bursts with shorter time durations at both source and receiver, *i.e.*, less than 20 μs, the means of all the measured noises are close to zero, which verify our assumption of zero-mean noise, and the variances of impulsive noises caused by different events vary significantly.

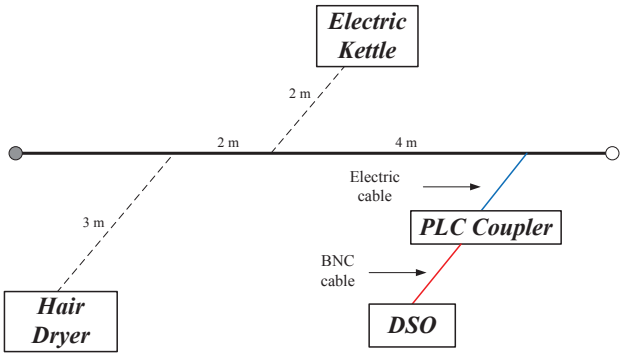

Figure 3.4: Measurement of example impulsive noises at a PLC channel output.

3.1.2 IN from Power Line Channel Output

The setup for measuring IN from a simple electric grid is given in Fig. 3.4, where the example devices of hair dryer and electric kettle are the potential appliances to the power line. The solid circle implies an energy delivery point. A PLC coupler is essential to provide a smooth interface for the devices to pick up signals from the power line. The inductive coupling unit is designed as a high pass filter that suppresses the 50 Hz mains voltage.

The measured impulsive noises caused by the hair dryer switch on and the electric kettle unplug respectively, are shown in Fig. 3.5, which can be treated

Table 3.1: Measured Characteristics of the Example Impulsive Noises

	Duration (μs)	Mean (mV)	Variance (V^2)	Normalised Variance
Background noise	–	0.89	2.79e−3	1
Impulses by hair dryer switch on (Fig. 3.3(a))	92.5	2.61	13.1	4695
Impulses by kettle unplug (Fig. 3.3(b))	16.7	−5.6	54.89	19674
Impulses by hair dryer switch on (Fig. 3.5(a))	91.3	9.4	5.8e−2	21
Impulses by kettle unplug (Fig. 3.5(b))	14.1	−7.9	0.9	323

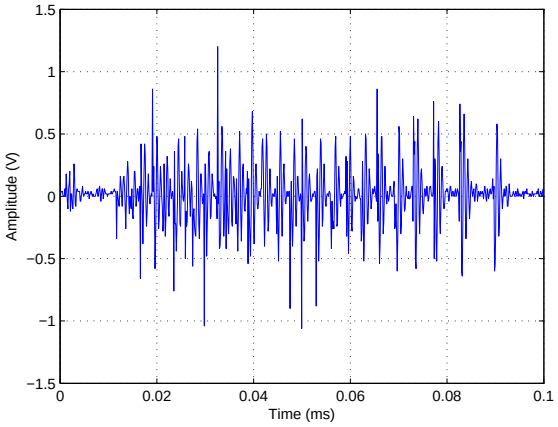

(a)

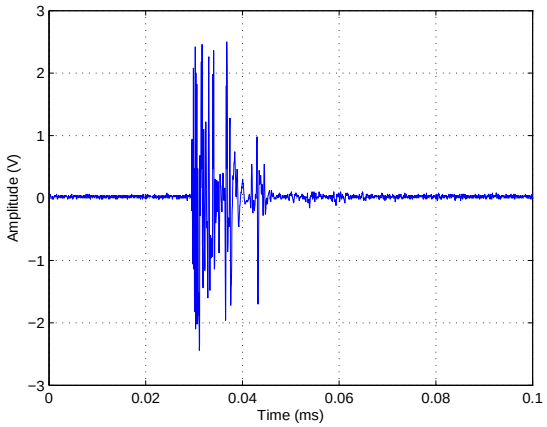

(b)

Figure 3.5: Measured IN at PLC channel output caused by (a) hair dryer switch on; and (b) electric kettle unplug.

as passing the corresponding IN in Fig. 3.3 through a certain channel block. As can be seen from the results in Fig. 3.5, although a large amplitude attenuation is caused due to channel propagation, the IN at the receiving end keeps a similar shape as measured at source. The parameters of the IN at PLC channel output is shown in Table 3.1, where channel propagation results in a reduction of the average noise magnitude by around 93% and 87% to the hair dryer switch on event and the electric kettle unplug event, respectively. For the frequency domain analysis, Fig. 3.6 shows the mean PSD of the two example impulsive noises. It can be seen the spectral power is concentrated towards lower frequencies which

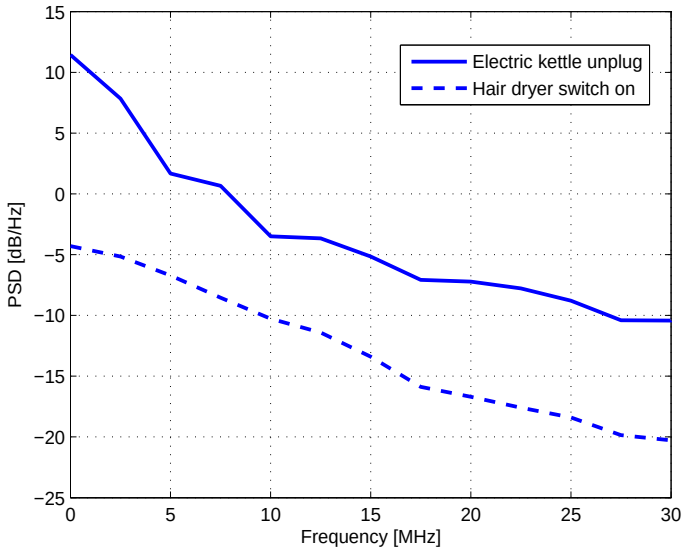

Figure 3.6: PSD of the impulsive noises from the power line (Fig. 3.5).

reveals coloured PSD, also shows different power levels for different IN events.

In practice, IN observed over a certain time period may be caused by multiple sources and therefore should be treated differently. This is discussed in detail in our noise models in Subsection 3.2.1 and Subsection 3.2.2.

3.2 Statistical Models for the Time Characteristics of IN

The measured results in previous section demonstrate the time behaviour of the noise bursts at source and channel output, respectively. Due to the randomness and time variation properties, modelling makes it straightforward to analyse the PLC IN environments statistically. In this section, two stochastic models are proposed for the IN in according to the measured results.

3.2.1 Hybrid Model for Correlated IN

The amplitude correlation between the impulses measured at the receiver is analysed in this subsection. Based on the measured results, the IN can be regarded as a wide-sense stationary (WSS) sequence. It is assumed that the current im-

pulse magnitude has correlation with its previous sample. Thus, we model the amplitude correlation in an autoregressive process. A hybrid model is proposed to formulate the correlated IN samples as

$$n_{\mathrm{i}}(m) = \frac{1}{\sqrt{1+w^2}}[w \cdot n_{\mathrm{i}}(m-1) + x(m)] \tag{3.2}$$

where $x(m)$ are the independent IN samples following the Gaussian distribution with zero-mean and variance σ_x^2, which is equivalent to the aforementioned BG model of IN in [2] and [28]; w ($w \geq 0$) is the weighting coefficient to determine the degree of correlation, and the larger the value of w, the higher the correlation between the current noise sample and its previous sample. Thus, in (3.2), a hybrid of the deterministic and random behaviours of the IN in a burst, are reflected by the first term and the second term, respectively. To keep the average total noise power constant, we apply a scaling factor $1/\sqrt{1+w^2}$ and also let $\sigma_{\mathrm{i}}^2 = \sigma_x^2$.

The autocorrelation function of $n_{\mathrm{i}}(m)$ can be expressed as $R(k) = E[n_{\mathrm{i}}(m+k) \cdot n_{\mathrm{i}}(m)]$. It can be further derived that

$$R(k) = \sigma_x^2 \cdot \left(\frac{w}{\sqrt{1+w^2}}\right)^{|k|} \tag{3.3}$$

where k is the discrete time separation between any two impulses. The complete derivation is given in Appendix A.

In the following, we analyse the impact of the value of coefficient w on the hybrid model for IN.

Scenario 1: If $w = 0$,

$$n_{\mathrm{i}}(m) = x(m) \tag{3.4}$$

and $R(k) = \sigma_x^2 \cdot \delta(k)$. In this case, the proposed model reduces to the BG model [2] and any other Bernoulli process [57], where the IN samples are uncorrelated.

Scenario 2: If $w = 1$, $n_{\mathrm{i}}(m)$ becomes

$$n_{\mathrm{i}}(m) = \left(\sqrt{2}/2\right) \cdot n_{\mathrm{i}}(m-1) + \left(\sqrt{2}/2\right) \cdot x(m) \tag{3.5}$$

which indicates that the current noise sample is determined by the deterministic behaviour (previous noise sample) and the random behaviour (uncorrelated noise sample) with equal weights. The corresponding autocorrelation function of $n_{\mathrm{i}}(m)$ becomes $R(k) = \sigma_x^2 \cdot \left(\sqrt{2}/2\right)^{|k|}$.

Scenario 3: If $w \gg 1$, $n_{\mathrm{i}}(m)$ can be approximated by

$$n_{\mathrm{i}}(m) \approx n_{\mathrm{i}}(m-1) + (1/w) \cdot x(m) \tag{3.6}$$

which implies that the current IN sample is dominated by its previous sample, as the second term in (3.6) is significantly suppressed by the large value of coefficient w. The autocorrelation function is nearly constant in time, *i.e.*, $R(k) \approx \sigma_x^2$, which shows a strong correlation between any two adjacent samples.

The effectiveness of the proposed hybrid model is shown by Fig. 3.7, comparing the autocorrelation function in (3.3) normalised to σ_x^2 with the normalised autocorrelation function of the impulsive noises showed in Fig. 3.5. A unit time separation is associated with a sampling interval of 0.01 μs. The value of w in the statistical model can be obtained through data fitting. The method of least squares is used to find the most fitted value provided from the model, which minimises the sum of squared difference between the observed curve and the fitted curve. Hence, by setting $w = 1.1$ (an example of Scenario 2), the hair dryer switch on event can be closely modelled. A larger value of $w = 2$ is applied to demonstrate higher correlation between the impulses caused by the kettle unplug event. The statistical results reflect that the hybrid model is more effective than the existing BG model [2] in autocorrelation analysis. It can be seen the hybrid model with a similar value of w can also be applied to the corresponding IN at source, implying that the channel has little impact on the autocorrelation of the IN when it passes through the channel.

The PSD of $n_{\mathrm{i}}(m)$ in (3.2) can be defined as the discrete-time Fourier transform of its autocorrelation function as $S(f) = \sum_k R(k) e^{-j2\pi kf/f_s}$, where the mag-

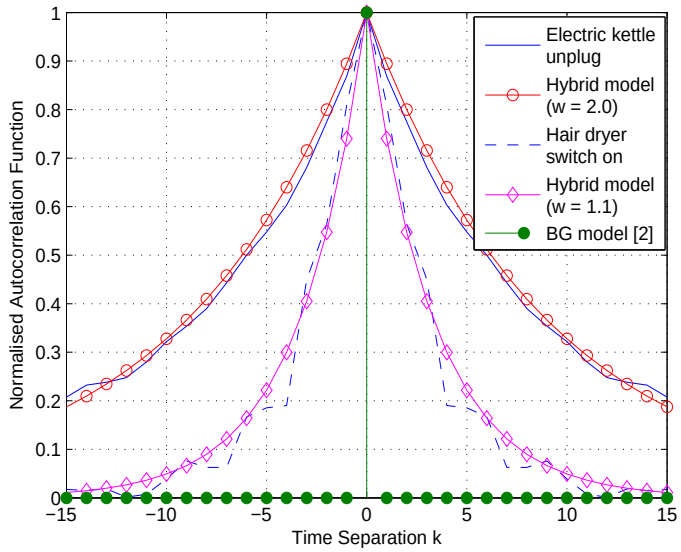

Figure 3.7: Comparison of the hybrid model with the impulsive noises from the power line (Fig. 3.5) in terms of normalised autocorrelation function.

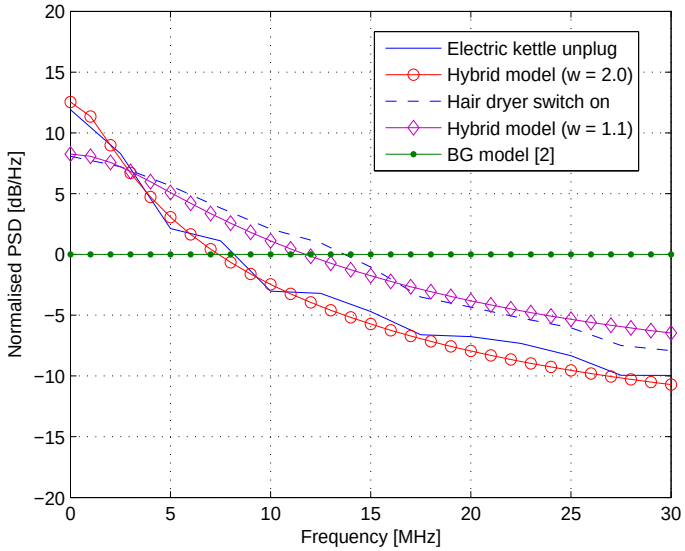

Figure 3.8: Comparison of the hybrid model with the impulsive noises from the power line (Fig. 3.5) in terms of normalised PSD.

nitude $|S(f)|$ of the PSD can be further derived in the linear form of

$$|S(f)| = \sigma_x^2 \cdot \frac{1}{1 - 2w\sqrt{1+w^2}\cos(2\pi f/f_s) + 2w^2} \tag{3.7}$$

where f_s is the sampling frequency. The complete derivation is given in Appendix B. In Fig. 3.8, the hybrid model is verified in frequency domain, by com-

paring the PSD function in (3.7) normalised to σ_x^2 with the measured results and the BG model [2]. It can be seen that the hybrid model, which demonstrates coloured PSD, is much closer to the measured results than the BG model which has white PSD.

3.2.2 Two-Level Markov Chain based Model for Occurrence-Dependent IN

After modelling the amplitude correlation between impulses in the hybrid model, we now propose a two-level hierarchical MC model to study the occurrence dependence of IN in PLC systems. This is an enhanced model over the model in [30] in that we consider multiple states in the second MC level.

It is assumed that impulses occur in bursts only, as the probability of the occurrence of single impulses is very low and the corresponding impulse power is usually low. Hence, the occurrence of a burst can be described by the first level MC, and the occurrence of individual impulses within a burst are characterised by the second level MC, as showed in Fig. 3.9. A burst is defined as a series of impulses, which has a minimum number (*e.g.*, three) of impulses and a maximum distance (*e.g.*, 4 ms) between two consecutive impulses [25]. In the first level MC, a relatively coarse time resolution is sufficient to model the bursts. For the second level MC, a finer time resolution is needed to model the impulse transitions within a burst.

In Fig. 3.9(a), 'I 0' represents the non-burst state where only consecutive background noise is present, and 'I 1' denotes the state that a burst occurs. The symbol $P_{I\ i,j}$ $(i = 0, 1; j = 0, 1)$ denotes the probability of transition from state 'I i' to state 'I j'. The first level transition probability matrix is given by

$$P_I^{(imp)} = \begin{bmatrix} P_{I\ 0,0} & P_{I\ 1,0} \\ P_{I\ 0,1} & P_{I\ 1,1} \end{bmatrix} \tag{3.8}$$

where $P_{I\ i,0} + P_{I\ i,1} = 1$ $(i = 0, 1)$.

When the first level state is 'I 0' (non-burst), the second level chain is not

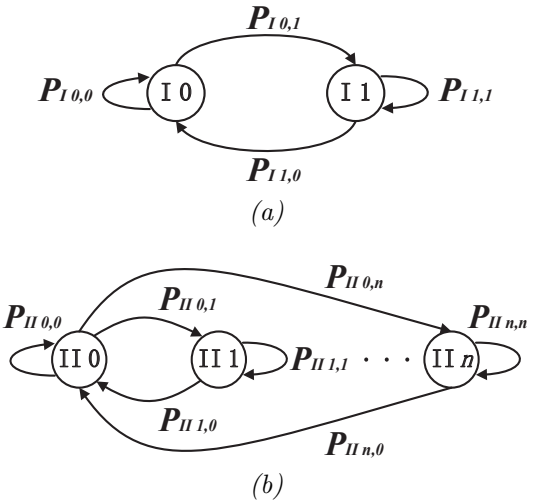

Figure 3.9: (a) First level Markov chain for modelling the occurrence of bursts ('I 0'—non-burst state; 'I 1'—burst state) (b) Second level Markov chain for modelling the occurrence of individual impulses in a burst ('II 0'—non-impulse state; 'II l'—impulse states with different impulse variances ($l = 1, \ldots, n$)).

needed. In the presence of a burst, *i.e.*, state 'I 1', the occurrence of impulses in a burst is depicted by Fig. 3.9(b), where 'II 0' denotes the non-impulse state (only background noise is present), and states 'II 1' to 'II n' represent occurrence of impulses of different variances. A selection of n typical variance values for impulses induced by different sources is used for different impulse states, *e.g.*, $\sigma_{\mathrm{i}}^2/\sigma_{\mathrm{b}}^2$ can be 10 dB for the state 'II 1' and raised to 20 dB for the state 'II 2'.

It is assumed that there is only one impulse state in a burst state, as the impulses in the same burst are likely to be induced by the same source. Hence, there are no transitions among impulse states 'II 1' to 'II n' in the second level model. When the lth ($l = 1, \ldots, n$) impulse state is in use, the symbol $P_{II\ i,j}$ ($i = 0, l; j = 0, l$) denotes the probability of transition from state 'II i' to state 'II j'. The corresponding transition matrix is given by

$$P_{II\ l}^{(imp)} = \begin{bmatrix} P_{II\ 0,0} & P_{II\ l,0} \\ P_{II\ 0,l} & P_{II\ l,l} \end{bmatrix} \tag{3.9}$$

where $P_{II\ i,0} + P_{II\ i,l} = 1$ ($i = 0, l$). In the scenario that $P_{I\ 0,i} = P_{I\ 1,i}$ ($i = 0, 1$) and $P_{II\ 0,i} = P_{II\ l,i}$ ($i = 0, l$), the proposed MC model is equivalent to the BG model [2] and any other Bernoulli process [57] where the occurrence of IN is

independent.

To validate the IN occurrence model in Fig. 3.9, the example IN generated by the MC based model at two different levels are shown in Fig. 3.10. To illustrate the IN clearly, the background noise is ignored in this case. It is assumed that two of the example bursts are induced by hair dryer switch on (denoted as state 'II 1'), and electric kettle unplug (denoted as state 'II 2'), respectively. In Fig. 3.10(a), the bursts are produced using $P_I^{(imp)} = \begin{bmatrix} 0.995 & 0.4 \\ 0.005 & 0.6 \end{bmatrix}$ as the first level transition probability matrix, and a relatively low sampling frequency of 100 kHz is employed. While Fig. 3.10(b) and Fig. 3.10(c) demonstrate the impulses caused by hair dryer switch on and kettle unplug events at the channel output, respectively, using the parameters in Table 3.1, and a sampling frequency of 100 MHz is applied. To evaluate the second level transition probabilities from Fig. 3.5, any sample that has the amplitude larger than the threshold $4\sigma_b$ is treated as an impulse sample, otherwise, a background noise sample is returned. Let '1' denote the impulse samples and '0' represent the non-impulse samples. The symbol $N_{i,j}$ $(i = 0, 1; j = 0, 1)$ denotes the number of sample combinations $[i, j]$ $(i = 0, 1; j = 0, 1)$. Hence, the value of transition probabilities $P_{II\ 0,1} = N_{0,1}/(N_{0,0} + N_{0,1})$ and $P_{II\ 1,1} = N_{1,1}/(N_{1,0} + N_{1,1})$. It can be calculated that the corresponding transition probability matrices for the second level MC are $P_{II\ 1}^{(imp)} = \begin{bmatrix} 0.7873 & 0.2663 \\ 0.2127 & 0.7337 \end{bmatrix}$ for hair dryer switch on event, and $P_{II\ 2}^{(imp)} = \begin{bmatrix} 0.9815 & 0.1205 \\ 0.0185 & 0.8795 \end{bmatrix}$ for kettle unplug event, respectively. Note that the impulses in a burst are not only occurrence-dependent, but also amplitude-correlated. Therefore, the hybrid model described in Subsection 3.2.1 is applied in the second level MC based model to produce the more realistic impulses in Fig. 3.10(b) (with weight coefficient $w = 1.1$) and Fig. 3.10(c) (with weight coefficient $w = 2$), respectively, which have consistent amplitude-correlation and occurrence-dependence as the measured impulses shown in Fig. 3.5. The proposed MC model is also applicable for the occurrence-dependent impulses at

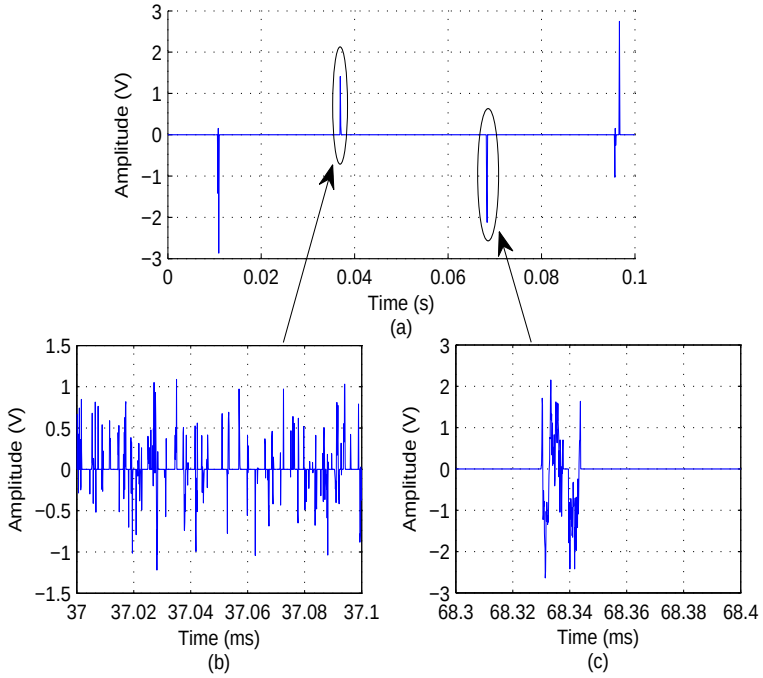

Figure 3.10: (a) Noise bursts produced by the first level MC based model at PLC receiving end; (b) Correlated and occurrence-dependent impulses by hair dryer switch on event in a burst produced by the hybrid model ($w = 1.1$) and the second level MC based model; (c) Correlated and occurrence-dependent impulses by electric kettle unplug event in a burst produced by the hybrid model ($w = 2$) and the second level MC based model.

source. The transition probabilities for the example impulses at source take similar values as that from receiver, implying that the channel has little impact on the transition probabilities.

In Fig. 3.11, the distribution of the random impulse amplitudes is presented by the means of complementary cumulative distribution function (CDF), which denotes the probability of impulse amplitude $|n_{\mathrm{i}}|$ exceeding a value x (abscissa), *i.e.*, $\Pr(|n_{\mathrm{i}}| > x)$. Compared to the measured results, the overall fitting of the two impulse events from modelling is fairly good.

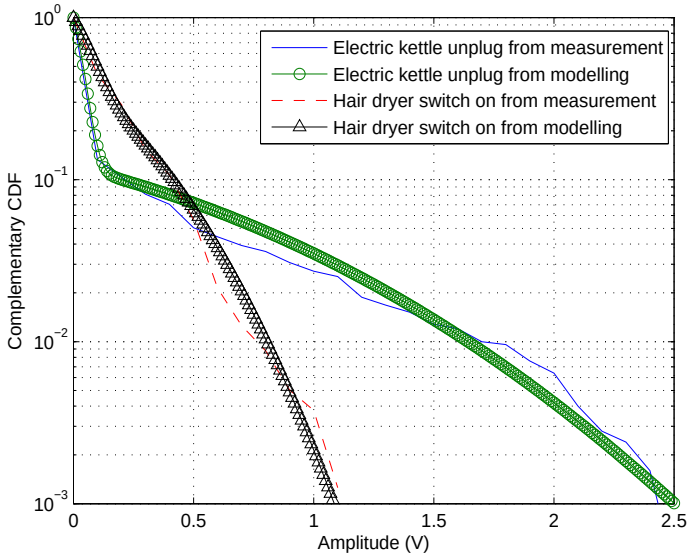

Figure 3.11: Statistics of the impulse amplitudes from measurement (Fig. 3.5) and modelling in terms of complementary CDF.

3.3 Channel Characteristics

In Section 3.2, we have presented the modelling of amplitude-correlated and occurrence-dependent IN using the tool of MC. In this section, we provide an intensive performance analysis of the MC models, including the average impulse duration and interval, steady-state probabilities of the MC, and maximum bandwidth efficiency achievable.

3.3.1 Transition Probability based Time Characteristics

3.3.1.1 Average Impulse Duration

Define $T_{S,II}^{(imp)}$ as the sampling interval for the second level in the two-level MC model. The average impulse duration is determined by both the probabilities of remaining in an impulsive state and the sampling interval $T_{S,II}^{(imp)}$. Define $P_{I1,IIl}$ $(l = 1, \ldots, n)$ as the probability of entering impulse state 'II l' in a burst state, which can be expressed as [60]

$$P_{I1,IIl} = e^{-A} \frac{A^{l-1}}{(l-1)!} \tag{3.10}$$

where $A = l\sigma_{\mathrm{b}}^2/\sigma_l^2$ is the impulse index or the disturbance ratio [25] with σ_l^2 denoting the variance of IN in state '$II\ l$'. The probability that the impulse state '$II\ l$' lasts for k samples in a burst can be expressed as

$$P_{width}(k) = P_{I1,IIl} \cdot P_{II\ l,l}^{k-1} \cdot (1 - P_{II\ l,l}) \tag{3.11}$$

The average impulse duration is given by $t_{width}^{(imp)} = T_{S,II}^{(imp)} \cdot \sum_{l=1}^{n} \sum_{k=1}^{\infty} k \cdot P_{width}(k)$. Using (3.10) and (3.11), it can be expressed as

$$t_{width}^{(imp)} = T_{S,II}^{(imp)} \cdot \sum_{l=1}^{n} \left[\frac{e^{-A} A^{l-1}}{(l-1)!} (1 - P_{II\ l,l}) \sum_{k=1}^{\infty} \left(k P_{II\ l,l}^{k-1} \right) \right] \tag{3.12}$$

3.3.1.2 Average Impulse Interval

It can be easily derived that the probability that interval between two consecutive impulses lasts for k samples in a burst, referred to as state '$II\ 0$', can be expressed as

$$P_{interval}(k) = P_{II\ 0,0}^{k-1} \cdot (1 - P_{II\ 0,0}) \tag{3.13}$$

The average impulse interval is given by $t_{interval}^{(imp)} = T_{S,II}^{(imp)} \cdot \sum_{k=1}^{\infty} k \cdot P_{interval}(k)$. Using (3.13), $t_{interval}^{(imp)}$ becomes

$$t_{interval}^{(imp)} = T_{S,II}^{(imp)} \cdot (1 - P_{II\ 0,0}) \sum_{k=1}^{\infty} k \cdot P_{II\ 0,0}^{k-1} \tag{3.14}$$

3.3.2 Steady-State Probabilities of the Two-Level Markov Chain

Normally, in a discrete-time MC model, the next state probabilities have dependence on the current state probabilities and are determined by the transition matrix as

$$\boldsymbol{\Pi}_{t+1} = \boldsymbol{P}\boldsymbol{\Pi}_t \tag{3.15}$$

where $\boldsymbol{P}$ is transition probability matrix, $\boldsymbol{\Pi}_t$ is a column vector whose elements represent the state probabilities at time t, and have a sum of 1. In the steady state, we have $\boldsymbol{\Pi}_{t+1} = \boldsymbol{\Pi}_t$.

In our two-level MC based model in Subsection 3.2.2, for the first level chain, we define $\pi_{I\ 1}$ as the steady-state probability (SSP) of incurring the burst state 'I 1', and $\pi_{I\ 0}$ as the SSP for the non-burst state 'I 0'. It is obvious that $\pi_{I\ 0} + \pi_{I\ 1} = 1$. We substitute $\boldsymbol{P} = P_I^{(imp)}$ into (3.15) and obtain

$$\begin{bmatrix} \pi_{I\ 0} \\ \pi_{I\ 1} \end{bmatrix} = \begin{bmatrix} P_{I\ 0,0} & P_{I\ 1,0} \\ P_{I\ 0,1} & P_{I\ 1,1} \end{bmatrix} \cdot \begin{bmatrix} \pi_{I\ 0} \\ \pi_{I\ 1} \end{bmatrix} \tag{3.16}$$

Solving (3.16) yields the values of π_{I0} and π_{I1} as

$$\begin{bmatrix} \pi_{I\ 0} \\ \pi_{I\ 1} \end{bmatrix} = \begin{bmatrix} P_{I\ 1,0} / \left(P_{I\ 0,1} + P_{I\ 1,0}\right) \\ P_{I\ 0,1} / \left(P_{I\ 0,1} + P_{I\ 1,0}\right) \end{bmatrix} \tag{3.17}$$

For the second level chain, define $\pi_{II\ l}$ as the SSP of remaining in the impulse state '$II\ l$', and $\pi_{II\ 0l}$ as the SSP for the associated non-impulse state. We have $\pi_{II\ 0l} + \pi_{II\ l} = 1$ $(l = 1, \ldots, n)$. It can be derived in a similar way as (3.17) that the steady-state probabilities for the second level Markov chain are given by

$$\begin{bmatrix} \pi_{II\ 0l} \\ \pi_{II\ l} \end{bmatrix} = \begin{bmatrix} P_{II\ l,0} / \left(P_{II\ 0,l} + P_{II\ l,0}\right) \\ P_{II\ 0,l} / \left(P_{II\ 0,l} + P_{II\ l,0}\right) \end{bmatrix} \tag{3.18}$$

The steady-state probabilities for the IN model in Fig. 3.9 are independent of the initial probabilities, and are important to evaluate the channel capacity.

3.3.3 Maximum Bandwidth Efficiency under IN

The terminology of maximum bandwidth efficiency is a measure of channel capacity over a given bandwidth in a specific communication system. The maximum bandwidth efficiency using the two-level MC model is expressed as

$$C = \sum\nolimits_{m=0}^{1} \pi_{I\ m} \cdot C_m^{(imp)} \tag{3.19}$$

where $C_0^{(imp)}$ and $C_1^{(imp)}$ denote the maximum bandwidth efficiencies achievable for the non-burst and burst states, respectively. We analyse the upper bound on channel capacity, where a full knowledge of the impulse state is assumed at the transmitter and receiver. Applying the Shannon's theorem [7], $C_m^{(imp)}$ can be expressed as

$$C_0^{(imp)} = \frac{1}{N} \sum_{i=1}^{N} \log_2 \left(1 + \frac{P_e |H(f_i)|^2}{P_b}\right) \tag{3.20}$$

and

$$C_1^{(imp)} = \sum_{l=1}^{n} \frac{e^{-A} A^{l-1}}{(l-1)!} \left[\frac{\pi_{II\ 0l}}{N} \sum_{i=1}^{N} \log_2 \left(1 + \frac{P_e |H(f_i)|^2}{P_b} \right) + \frac{\pi_{II\ l}}{N} \sum_{i=1}^{N} \log_2 \left(1 + \frac{P_e |H(f_i)|^2}{P_l^{(imp)}(f_i) + P_b} \right) \right] \tag{3.21}$$

where P_e denotes the transmitted PSD, and P_b is the background noise PSD, which is denoted by σ_{b}^2. N is the number of subcarriers, and $H(f)$ is the channel transfer function. $P_l^{(imp)}(f)$ denotes the PSD of IN in state '$II\ l$' ($l = 1, \ldots, n$), which is the discrete Fourier transform (DFT) of the corresponding autocorrelation function in (3.3).

If $n = 1$, *i.e.*, the MC model has a single impulse state in the second level chain, (3.19) reduces to

$$C \approx \frac{(1 - \pi_{I\ 1}\pi_{II\ 1})}{N} \cdot \sum_{i=1}^{N} \log_2 \left(1 + \frac{P_e |H(f_i)|^2}{P_b} \right) + \frac{\pi_{I\ 1}\pi_{II\ 1}}{N} \cdot \sum_{i=1}^{N} \log_2 \left(1 + \frac{P_e |H(f_i)|^2}{P_1^{(imp)}(f_i) + P_b} \right) \tag{3.22}$$

Let $H_j(f_i)$ denote the jth instantaneous channel frequency response on the ith subcarrier. Assuming low occurrence probability of IN bursts, *i.e.*, $\pi_{I\ 1}$ is close to 0, and $\pi_{I\ 0} = 1 - \pi_{I\ 1}$ is close to 1, the corresponding instantaneous maximum bandwidth efficiency in (3.19) is given by

$$C_j \approx \frac{\pi_{I\ 0}}{N} \sum_{i=1}^{N} \log_2 \left(1 + \frac{P_e |H_j(f_i)|^2}{P_b} \right) \tag{3.23}$$

Thus, the average maximum overall bandwidth efficiency under the burst IN can be simplified as

$$C = \lim_{M \to \infty} \frac{\pi_{I\ 0}}{NM} \sum_{j=1}^{M} \sum_{i=1}^{N} \log_2 \left(1 + \frac{P_e |H_j(f_i)|^2}{P_b} \right) \tag{3.24}$$

which implies that the system capacity is dominated by background noise and the channel attenuation.

In Fig. 3.12, the overall maximum bandwidth efficiencies under proposed IN models given by (3.24) is demonstrated, in comparison with the bandwidth efficiency for the case of AWGN background noise only, and the bandwidth efficiency

achieved by the BG model [2]. The horizontal axis denotes P_e/P_b, the signal-to-background-noise ratio, which varies from 0 dB to 20 dB. It is assumed that there are $n = 2$ IN sources, hair dryer switch on (state 'II 1') and electric kettle unplug (state 'II 2'). Using the measured impulses at the PLC receiving end, the noise variances are obtained from Table 3.1 as $\sigma_1^2 = 21\sigma_{\rm b}^2$ and $\sigma_2^2 = 323\sigma_{\rm b}^2$, respectively, and the transition probability matrices for the second level MC are $P_{II\ 1}^{(imp)} = \begin{bmatrix} 0.7873 & 0.2663 \\ 0.2127 & 0.7337 \end{bmatrix}$ and $P_{II\ 2}^{(imp)} = \begin{bmatrix} 0.9815 & 0.1205 \\ 0.0185 & 0.8795 \end{bmatrix}$, respectively (same as that used for Fig. 3.10(b) and Fig. 3.10(c)). The first level MC transition probability matrix is $P_I^{(imp)} = \begin{bmatrix} 0.995 & 0.4 \\ 0.005 & 0.6 \end{bmatrix}$ (same as that used for Fig. 3.10(a)). The number of subcarriers $N = 128$. To compare with the AWGN channel, a random PLC channel generator [7] is applied to obtain Fig. 3.12, for broadband PLC transmission. With the effect of channel propagation, the system performance is significantly degraded.

Fig. 3.12 shows that within AWGN channel, all cases achieve almost the same system capacity, implying that IN with low occurrence probability have little impact on system performance. In the AWGN channel, only noise effect is considered with no channel attenuation (the same applied for BG model in [2]). Meanwhile, the occurrence probability for the first level MC of the proposed model is assumed low enough (the same applied for BG model in [2]), *i.e.*, $\pi_{I\ 1}$ is close to zero. Hence, the maximum bandwidth efficiency in (3.21) is negligible and (3.19) can be reduced to (3.24), indicating that background noise is dominant for all cases. Considering the channel effect in the frequency range of 1.8 MHz-100 MHz, the maximum bandwidth efficiency is lowered by around 0.4 bps/Hz and 3 bps/Hz with class-9 and class-6 channels, respectively, verifying our analysis in (3.24) that the theoretical capacity is dominated by background noise and the channel attenuation.

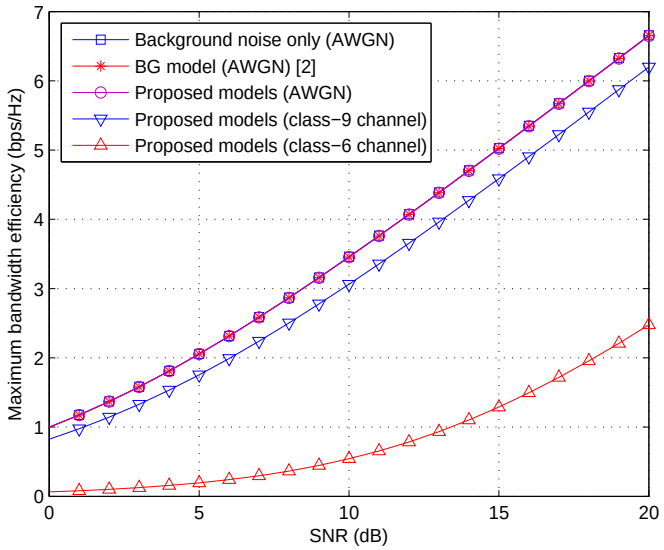

Figure 3.12: Analytical maximum bandwidth efficiency achievable under different channel models.

3.4 Summary

In this chapter, measured results have been presented to help investigate the nature of IN for indoor broadband PLC networks. A hybrid statistical model to describe the correlation of IN, and a two-level MC based model to describe the occurrence dependence of IN has been proposed, based on the measurement results. The models are generic and adaptive to different scenarios (the BG model [2] can be treated as a special case where impulses are independent). By simply adjusting the value of the weight coefficient in the hybrid model, the level of correlation between consecutive impulses can be changed. The example IN illustrates that MC is suitable to model the transitions among time states, where it is more realistic to consider multiple impulse states in the two-level MC. The proposed models are validated in reference to the measured results. The analytical throughput considering the impact of IN has been investigated.

Chapter 4

Three-Dimensional Markov Chain based Modelling of Narrowband Interference

Other than the IN modelled in Chapter 3, NBI from radio applications is also a major source of electromagnetic disturbance for broadband PLC, which should be dealt with properly. This chapter focuses on modelling the radio NBI. Accurate modelling of NBI supports comprehensive system performance analysis in order to achieve effective transmission. Currently, there still lack thorough modelling and performance analysis of the NBI for indoor broadband PLC.

NBI in PLC systems is mainly caused by two types of sources: spurious disturbance inside the power grid such as running electric devices [33] and radio applications such as broadcast radios and amateur radios [6]. The NBI caused by spurious disturbance is usually synchronous to the mains frequency with much lower power than that from the broadcast stations, and concentrates in the frequency band below 8 MHz. Therefore, in this chapter, we focus on characterising the NBI from various nearby radio applications. For indoor broadband PLC, NBI from radio systems may become a salient issue that degrades the PLC system performance, since the unshielded power line can be a good antenna picking up the radios around [6]. Normally, there are various narrowband interferers inside the frequency range of 1.8 MHz-100 MHz, from broadcast radios, amateur

radios, *etc.*, and the power level is generally time-varying in daytime [6, 25]. In [60], NBI was also called impulsive interference, and modelled by a Middleton's class A model, which shows a comparable behaviour as the IN modelling. Most of the existing NBI models are for wireless communication channels, such as [34, 35] for ad hoc networks, and the corresponding radio activities are modelled with random occurrence probabilities, such as Poisson point process in [35] and a simple Markov chain (MC) model in [61]. However, the existing models are assumed to be memoryless, and the produced NBI is not associated with particular radio bands. Currently, the analysis of the NBI for PLC is mainly through measurement-based approaches, and NBI needs to be modelled in a statistical manner.

In this chapter, the measurement and statistical modelling of the occurrence of NBI from nearby radio users for indoor broadband PLC are investigated. Our work is different in the following aspects. First, a novel three-dimensional (3D) MC model is proposed for the occurrence of narrowband radio interference, where the NBI inside the PLC frequency spectrum is reproduced in a series of time states, corresponding to the random activity of some certain radio bands. The occurrence dependence and multi-level power of the potential NBI according to the radio users traffic, are also reflected in our statistical model, which has not been fully considered for indoor broadband PLC channel. Second, we present an intensive performance analysis, including average interval of NBI, steady-state probabilities for the MC, and the system capacity under the joint impact of IN and NBI. Third, we observe the NBI in a broader spectrum of 1.8 MHz-100 MHz and investigate the time-varying behaviour in a given environment, while the existing NBI characterisation either from 80 MHz-100 MHz in [6] or up to 20 MHz in [54] can only view the NBI variation from different sites. Thus, with our work, it is possible to detect NBI in a single network for future cognitive PLC rather than detect NBI cooperatively from different networks. The effectiveness of the

proposed MC based model is verified by the measured results.

In Section 4.1, a system model is presented to describe the overall noise and interference scenarios for an indoor broadband PLC. In Section 4.2, measurement setup and results of NBI for PLC are presented. A 3D MC based model for the random activities of radio interference is proposed in Section 4.3. The system performance analysis is given in Section 4.4. The summary is remarked in Section 4.5.

4.1 System Model

The block diagram of an indoor broadband PLC system under the high power electromagnetic disturbance of both IN and NBI is depicted in Fig. 4.1, where $s(t)$ represents the transmit signal and $r(t)$ is the received signal. $n(t)$ denotes the combined noise and interference at the receiver, including the aperiodic IN $n_{\mathrm{i}}(t)$, the NBI $v(t)$ and the background noise $n_{\mathrm{b}}(t)$. We assume K aperiodic IN sources and L narrowband interferers. At time t, $n_{\mathrm{s}k}(t)$ $(k = 1, \ldots, K)$ denotes the IN from the kth source ($n_{\mathrm{s}k}(t) = 0$ means no noise). Let $n_{\mathrm{i}}(t)$ denote the overall IN at the receiver as aperiodic IN, which can be treated as passing the noise from any potential switching/plug transients of the appliances in the system, through the corresponding channel. While $v_l(t)$ $(l = 1, \ldots, L)$ denotes the lth narrowband interferer ($v_l(t) = 0$ means no interference). Let $v(t)$ denote the combined NBI at the PLC receiver, from various nearby radio applications.

In a discrete-time system, the signal at the PLC receiver is a mixture of various noises. Let $r(m)$ denote the mth received signal sample, expressed as:

$$r(m) = \{h_{\mathrm{s}} * s\}(m) + \sum\nolimits_k \{h_{\mathrm{n}k} * n_{\mathrm{s}k}\}(m) + \sum\nolimits_l v_l(m) + n_{\mathrm{b}}(m) \tag{4.1}$$

where $\{h_{\mathrm{s}} * s\}(m) = \sum_n h_{\mathrm{s}}(n)s(m-n)$ and $\{h_{\mathrm{n}k} * n_{\mathrm{s}k}\}(m) = \sum_n h_{\mathrm{n}k}(n)n_{\mathrm{s}k}(m-n)$ $(k = 1, \ldots, K)$, while h_{s} and $h_{\mathrm{n}k}$ are the channel impulse response for PLC signal $s(m)$ and the IN at source $n_{\mathrm{s}k}(m)$, respectively. $v_l(m)$ $(l = 1, \ldots, L)$ is the

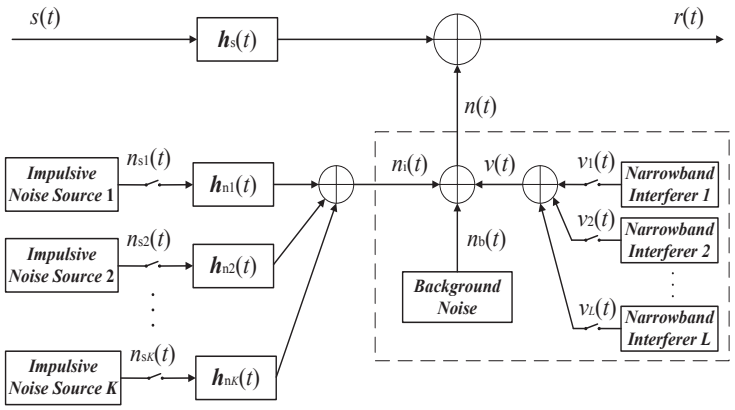

Figure 4.1: Block diagram of a PLC system.

NBI sample from the lth interferer added at PLC receiver, and the background noise $n_{\mathrm{b}}(m)$ is assumed to be AWGN with zero mean and variance σ_{b}^2 . Since both IN and NBI occur with probabilities, the general added disturbance $n(m)$ in impulsive noise plus interference scenario can be expressed as

$$n(m) = \alpha \cdot n_{\mathrm{i}}(m) + \beta \cdot v(m) + n_{\mathrm{b}}(m) \tag{4.2}$$

where $n_{\mathrm{i}}(m)$ is the output IN at PLC receiver, which has a zero mean and variance σ_{i}^2 . It is assumed that the variance of the background noise is much lower than that of the IN, *i.e.*, $\sigma_{\mathrm{b}}^2 \ll \sigma_{\mathrm{i}}^2$. In (4.2), α, $\beta \in \{0,\ 1\}$ are the parameters indicating the occurrence states (absent or present) of the IN and NBI respectively. $\Pr(\alpha = 1)$ denotes the IN occurrence probability, while $\Pr(\beta = 1)$ reflects the NBI occurrence probability.

The scenario of IN only ($\alpha = 1, \beta = 0$) is considered in Chapter 3, while Chapter 4 focuses on the electromagnetic disturbance of NBI only ($\alpha = 0, \beta = 1$). Joint impact of IN and NBI on system capacity is analysed in Subsection 4.4.3 of Chapter 4.

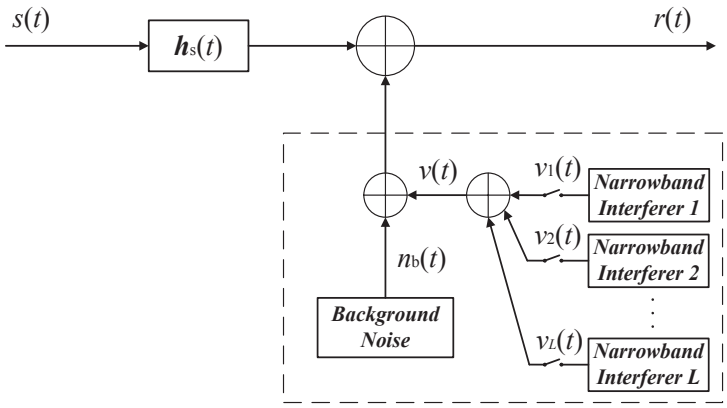

Figure 4.2: Block diagram of a PLC system disturbed by NBI only.

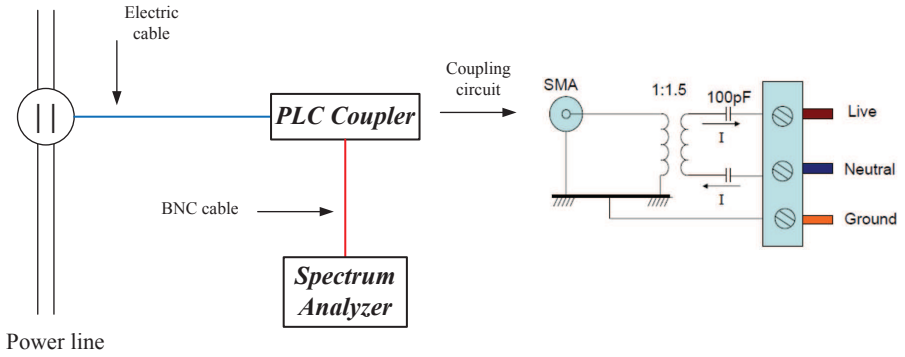

Figure 4.3: NBI measurement setup.

4.2 Measurement of NBI for Indoor Broadband PLC

The block diagram of an indoor broadband PLC system disturbed by narrowband interferers only is depicted in Fig. 4.2, *i.e.*, $\alpha = 0, \beta = 1$ in (4.2), which yields

$$n(m) = n_{\mathrm{b}}(m) + \sum\nolimits_{l} v_l(m) \tag{4.3}$$

Fig. 4.3 illustrates the setup of viewing NBI caused by the potential radio services inside the PLC spectrum, using a Rohde & Schwarz-FSP30 spectrum analyser. The measurement is made in different time during a day, in a certain indoor environment. The spectrum analyser mode is applied to record the NBI in the frequency range 1.8 MHz-100 MHz, with 10 KHz resolution bandwidth and 10 times averaging. The coupler provides an interface in order to protect the

spectrum analyser input. The inductive coupling circuit diagram is also shown in Fig. 4.3, where the mains voltage can be physically isolated from the spectrum analyser. Two 100 pF capacitors are used to block the DC. Besides, a transformer can isolate the mains voltage completely.

Fig. 4.4 shows two examples of NBI and background noise in frequency domain in the same lab at two different times during a day. It can be seen the NBI inside the spectrum has a randomness and time-varying behaviour. Normally, Above 80 MHz, a massive local and international broadcast radios can be received, while some radio users exist to communicate below 60 MHz, where the presence of NBI is more random and likely to be generated by amateur radios, mobile-radios, emergencies, astronomer-radios [62], *etc.*

To view the time variation of the particular NBI bands statistically, three function generators are applied transmitting certain radio signals using the amateur radio bands [5] around 14 MHz (band 1), 28 MHz (band 2) and 50 MHz (band 3). The three radio bands are selected referring to the UK radio band plans in [5], since they are primarily allocated for amateur services. The preferable modes to be used for the particular NBI bands can be any digital modulation

Table 4.1: Activities of Three Example Narrowband Interferences around 14 MHz (Band 1), 28 MHz (Band 2) and 50 MHz (Band 3) from the Measured Results

Spectrum sweeps (10 s interval)	Number of active NBI	Occurrent NBI band	Max. peak power (dBm)
1	2	Bands 1 & 2	-58.31
2	3	Bands 1, 2 & 3	-69.01
3	3	Bands 1, 2 & 3	-70.02
4	2	Bands 1 & 3	-61.47
5	2	Bands 1 & 3	-57.54
6	2	Bands 1 & 2	-71.54
7	1	Band 2	-59.80
8	0	None	-88.96
9	1	Band 3	-57.33
10	1	Band 3	-45.66
11	2	Bands 2 & 3	-60.73

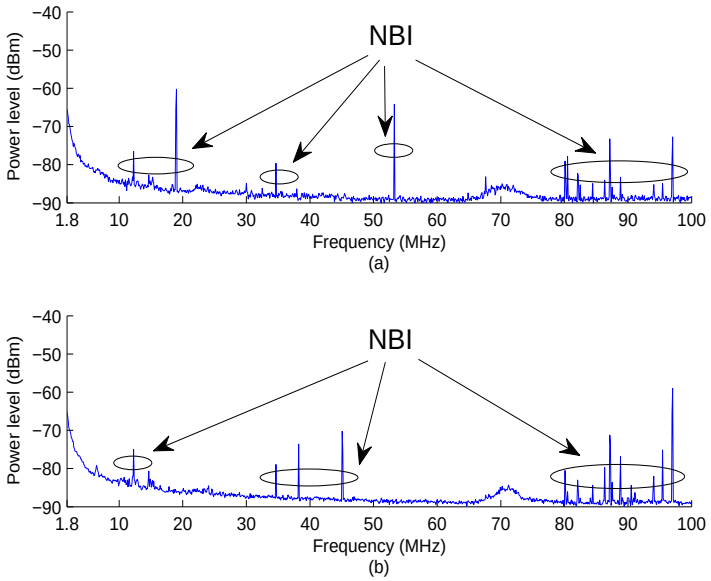

Figure 4.4: Measured NBI (amateur radios below 60 MHz [5]; broadcast radios above 80 MHz [6]) and background noise spectrum at two different times on the same site.

such as phase-shift keying (PSK), with the maximum bandwidth of 500 Hz. The status of noise spectrum is recorded in Table 4.1 for every 10 seconds. The eleven samples of the spectrum show a time-varying behaviour, according to the radio users activities.

It can be seen that the spectrum status varies with both the number and the frequencies of the active NBI, and that the highest peak NBI power is also different, which is associated with the number of radio users in the occupied bands. The random occurrence of the example NBI is further analysed in our statistical NBI model in Section 4.3.

4.3 3D Single-Level Markov Chain for the Occurrence of NBI

The measured results in previous section demonstrate the time behaviour of the presence of potential interferences inside the PLC transmission spectrum. Due to the randomness and time variation properties, modelling makes it straightforward

to analyse the PLC interference scenarios statistically. In this section, we propose a stochastic model for the PLC interference scenarios.

For the indoor broadband PLC, we put forward a novel structured 3D MC model for the occurrence of NBI inside the PLC spectrum. It is assumed there are some potential amateur radio users around transmitting and receiving signals in some particular radio bands within the PLC spectrum, which causes the occurrence-dependent NBI to PLC networks.

First, let the variables ϕ_1, ϕ_2 denote the number of radio bands in the PLC spectrum, and the number of potential radio users using the radio bands, respectively. To simplify the 3D Markov analysis, we assume that $\phi_1 = \phi_2 = \phi$. Then, let the random variable a be the number of active radio channels (NBI) at current state, let b represent the index of possible frequency locations of the presented NBI channels, let c denote the index of possible radio user distributions in the corresponding NBI channels, respectively.

In the proposed 3D MC model, the transition states are constructed by the random variables $\{a, b, c\}$. For the non-NBI state, in which all the ϕ radio channels are non-active (no NBI), the variable $a = b = c = 0$.

Once NBI occurs, $a = 1, 2, \ldots, \phi$. The variation of the value in the random variable a means a radio band is occupied or released. The total number of the possible locations of NBI is actually a calculation of the combinations $C(\phi, a)$, *i.e.*, the binomial coefficient C_ϕ^a. Thus, the random variable $b = 1, 2, \ldots, C(\phi, a)$. The value change in the variable b represents the occupation of a radio band is switched to another free radio band. To determine the value of c, it is assumed that each active radio band is occupied by at least one radio user. The number of the possible user distributions when j users appear on the a radio bands can be calculated by C_{j-1}^{a-1}, $j = a, a+1, \ldots, \phi$. It can be derived using the Pascal's triangle and the binomial identity $C_n^k + C_n^{k+1} = C_{n+1}^{k+1}$, that the total number of the possible user distributions is equal to the value of combinations $\sum_{j=a}^{\phi} C_{j-1}^{a-1}$,

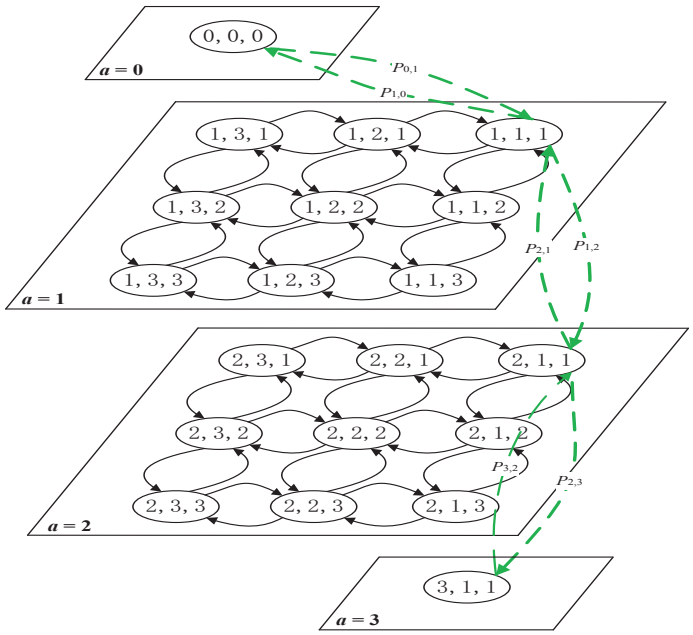

Figure 4.5: Structure of the 3D Markov chain for modelling the occurrence of potential ($\phi = 3$) NBI in a series of time.

i.e., $C(\phi, a)$. Thus, the random variable $c = 1, 2, \ldots, C(\phi, a)$. The variation of c reflects a radio user occupies, drops or switches in the presented a radio bands with the location index b.

Fig. 4.5 shows the corresponding NBI state transition diagram for $\phi = 3$. The total number of transition states is $\sum_{a=0}^{\phi}(C_{\phi}^{a})^2 = C_{2\phi}^{\phi} = C_6^3 = 20$. Its steady-state probabilities of the MC model need to be figured out to evaluate the PLC performance in the occurrence of NBI, which is analysed in the next section.

Refering to the transition probability matrix in the aforementioned two-level Markov chain, which denotes the transitions among the states, for the interference model in Fig. 4.5, we first define P_a as the probability of remaining in the same state in plane a, where $\{a_k, b_k, c_k\} = \{a_{k-1}, b_{k-1}, c_{k-1}\}$. It is clear that $P_0 = P_{\phi} = 1$. Then, the symbol $P_{i,j}$ is defined as the transition probability from plane '$a = i$' to plane '$a = j$', where $i, j = 0, 1, 2, 3$. The relationships are denoted by the dashed green arrows in Fig. 4.5, and the corresponding transition probability

matrix can be formulated as

$$P^{(int)} = \begin{bmatrix} P_{0,0} & P_{1,0} & 0 & 0 \\ P_{0,1} & P_{1,1} & P_{2,1} & 0 \\ 0 & P_{1,2} & P_{2,2} & P_{3,2} \\ 0 & 0 & P_{2,3} & P_{3,3} \end{bmatrix} \tag{4.4}$$

where the summation in each column equals one.

According to the model, if we assume no active radio band in the current state, the next state can either be no active radio band with the probability $P_{0,0}$ or one active radio band with the probability $P_{0,1}$. If there are three active radio bands in the current state, the next state can either be two active radio bands with the probability $P_{3,2}$ or three active radio bands with the probability $P_{3,3}$. Also, the proposed model can be adaptive to different NBI environments with a more general expression of the transition probability matrix as

$$\boldsymbol{P}^{(int)} = \begin{bmatrix} P_{0,0} & P_{1,0} & 0 & \cdots & 0 \\ P_{0,1} & P_{1,1} & \ddots & \ddots & \vdots \\ 0 & P_{1,2} & \ddots & P_{\phi-1,\phi-2} & 0 \\ \vdots & \ddots & \ddots & P_{\phi-1,\phi-1} & P_{\phi,\phi-1} \\ 0 & \cdots & 0 & P_{\phi-1,\phi} & P_{\phi,\phi} \end{bmatrix} \tag{4.5}$$

which has the element $P_{i,j}$ with $i, j = 0, 1, 2, \ldots, \phi$.

To validate the NBI occurrence model in Fig. 4.5, the example NBI generated by the proposed model of $\phi = 3$, is shown in Fig. 4.6. To clearly show the occurrence-dependence of NBI in the system, we only illustrate the NBI reproduced by the 3D MC model where the background noise is ignored in this case. It is assumed that the potential NBI inside the PLC spectrum is from three radio bands [5] around 14 MHz, 28 MHz and 50 MHz respectively. The ingress of the interference power in a particular radio band varies from the number of active radio users in that band, where more radio users cause higher NBI power at the particular band. Thus, three levels of NBI are roughly set as 20 dB, 30 dB and 40 dB above the noise floor at the corresponding radio bands with zero mean Gaussian amplitudes, respectively. The ingress of NBI power to the noise floor may be lower when the IN occurs, which results in a higher power line

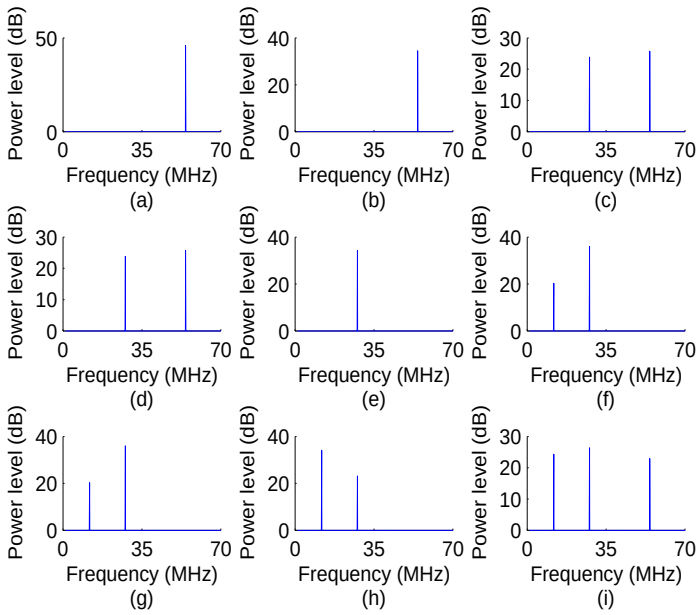

Figure 4.6: Occurrence-dependent NBI produced by the 3D MC based model and started with $a = 1$ at time sequence (10 s interval): (a) $t = 1$, (b) $t = 2$, (c) $t = 3$, (d) $t = 4$, (e) $t = 5$, (f) $t = 6$, (g) $t = 7$, (h) $t = 8$, (i) $t = 9$.

noise floor and may submerge the relatively weak radio signals. In Fig. 4.6, the potential occurrence of NBI is produced using the transition probability matrix $P^{(int)} = \begin{bmatrix} 0.7 & 0.1 & 0 & 0 \\ 0.3 & 0.8 & 0.1 & 0 \\ 0 & 0.1 & 0.8 & 0.3 \\ 0 & 0 & 0.1 & 0.7 \end{bmatrix}$, and $P_1 = 0.44, P_2 = 0.44$ for the probabilities of remaining in the same state in plane $a = 1$ and $a = 2$, respectively. The results are associated with a unit time separation of 10 s sampling interval, which is consistent as recorded in Table 4.1. It can be seen the time variation of NBI channel is generated randomly. The transition of the NBI occurrence from Fig. 4.6(b) to Fig. 4.6(c), implying that the value of variable a is changed from 1 to 2. Then, the value of a becomes 3 for Fig. 4.6(i). In the case of $a = 1$, let the indices of frequency location 1, 2 and 3 indicate the three radio bands 14 MHz, 28 MHz and 50 MHz, respectively. Then, the variable b is equal to the index value of 3 for Fig. 4.6(a) and Fig. 4.6(b), and becomes 2 for Fig. 4.6(e). Besides, the variation in c is equivalent to the change on power levels, *e.g.*, the values of a and

b are the same for Fig. 4.6(a) and Fig. 4.6(b), while the value of c is different. Moreover, the identical values of a, b and c during the transitions reflect a strong dependence of the NBI occurrence by remaining on the same plane, or even in the same state, such as Fig. 4.6(c) and Fig. 4.6(d); Fig. 4.6(f) and Fig. 4.6(g). It denotes that the occurrence of NBI in the broadband PLC system can be well modelled by the statistical 3D Markov chain based model.

4.4 Performance Analysis

In Section 4.3, the modelling of NBI using the 3D MC has been presented. In this section, we provide an intensive performance analysis of the MC based model, including the average NBI interval, steady-state probabilities of the MC, and maximum bandwidth efficiency achievable.

4.4.1 Transition Probability based Time Characteristics

4.4.1.1 Average NBI Interval

In the 3D MC model, NBI interval is associated with the transition probability that the non-NBI state $\{0, 0, 0\}$ lasts for k samples, referred to as $P_{0,0}$. Thus, the average NBI interval can be expressed as

$$t_{interval}^{(int)} = T_S^{(int)} \cdot (1 - P_{0,0}) \sum_{k=1}^{\infty} k \cdot P_{0,0}^{k-1} \tag{4.6}$$

where $T_S^{(int)}$ is the sampling time in the NBI model.

4.4.1.2 NBI Arrival Rate

If we know the value of the average NBI interval, the average NBI rate can also be determined, which is approximately the reciprocal value of the average duration of the non-NBI state. Since (4.6) can be simplified as $t_{interval}^{(int)} = T_S^{(int)}/(1 - P_{0,0})$, the NBI arrival rate is formulated as

$$n_{arrival}^{(int)} = \frac{1 - P_{0,0}}{T_S^{(int)}} \tag{4.7}$$

4.4.2 Steady-State Probabilities of the MC Model

In the proposed 3D MC model, the structure is constructed by the number of $(\phi + 1)$ planes. Each plane indicates the corresponding number of a active radio bands. To analyse the steady-state probability (SSP) of the discrete-time MC model, we first learn the transition probabilities among the planes, which have dependence with the previous state. To separate from SSP, let steady-plane probability (SPP) denote the steady state of the plane probabilities, which is the occurrence probability of the corresponding a active radio bands.

To obtain the SPP in Fig. 4.5, π_a is defined as the SPP for plane a, where $a = 0, 1, 2, 3$. It is obvious that $\pi_0 + \pi_1 + \pi_2 + \pi_3 = 1$. We substitute $\boldsymbol{P} = P^{(int)}$ and π_a into (3.15) and obtain

$$\begin{bmatrix} \pi_0 \\ \pi_1 \\ \pi_2 \\ \pi_3 \end{bmatrix} = \begin{bmatrix} P_{0,0} & P_{1,0} & 0 & 0 \\ P_{0,1} & P_{1,1} & P_{2,1} & 0 \\ 0 & P_{1,2} & P_{2,2} & P_{3,2} \\ 0 & 0 & P_{2,3} & P_{3,3} \end{bmatrix} \cdot \begin{bmatrix} \pi_0 \\ \pi_1 \\ \pi_2 \\ \pi_3 \end{bmatrix} \tag{4.8}$$

Solving (4.8) yields the values of SPP as

$$\begin{bmatrix} \pi_0 \\ \pi_1 \\ \pi_2 \\ \pi_3 \end{bmatrix} = \begin{bmatrix} q_0 / \sum_{m=0}^{3} q_m \\ q_1 / \sum_{m=0}^{3} q_m \\ q_2 / \sum_{m=0}^{3} q_m \\ q_3 / \sum_{m=0}^{3} q_m \end{bmatrix} \tag{4.9}$$

where

$$\begin{bmatrix} q_0 \\ q_1 \\ q_2 \\ q_3 \end{bmatrix} = \begin{bmatrix} P_{3,2}P_{2,1}P_{1,0} \\ P_{3,2}P_{2,1}P_{0,1} \\ P_{3,2}P_{1,2}P_{0,1} \\ P_{2,3}P_{1,2}P_{0,1} \end{bmatrix}.$$

In Fig. 4.5, there are 20 transition states in total constructed by the random variables $\{a, b, c\}$, where $\{0, 0, 0\}$ for the non-NBI state, and $a = 1, 2, \ldots, \phi$; $b, c = 1, 2, \ldots, C(\phi, a)$ when NBI arrives. To obtain the SSP, we define $\lambda_{a,b,c}$ as the SSP for the state $\{a, b, c\}$. Combine the normalised condition $\sum_{a=0}^{\phi} \sum_{b=1}^{C_\phi^a} \sum_{c=1}^{C_\phi^a} \lambda_{a,b,c} = 1$ and the values of SPP derived in (4.9), the values of SSP can be obtained as

$$\lambda_{a,b,c} = \begin{cases} \pi_a / \left(C_\phi^a \cdot C_\phi^a\right) & if (a_k \neq a_{k-1}) \, or \left(C_\phi^a = 1\right), \\ P_a \cdot \pi_a & if (a_k = a_{k-1}) \,\&\, (b_k = b_{k-1}) \,\&\, (c_k = c_{k-1}), \\ (1 - P_a) \cdot \pi_a / \left(C_\phi^a \cdot C_\phi^a - 1\right) & if \left(C_\phi^a \neq 1\right). \end{cases} \tag{4.10}$$

where $a = 0, 1, 2, \ldots, \phi$, and $b, c = 0, 1, 2, \ldots, C(\phi, a)$.

The steady probabilities for the NBI model in Fig. 4.5 are independent of the initial probabilities, and are important to evaluate the channel capacity.

4.4.3 Maximum Bandwidth Efficiency Achievable

4.4.3.1 Maximum Bandwidth Efficiency under NBI

The terminology of maximum bandwidth efficiency is a measure of channel capacity over a given bandwidth in a specific communication system. The maximum bandwidth efficiency using the 3D MC model is expressed as

$$C = \sum_{a=0}^{\phi} \pi_a \cdot C_a^{(int)} \tag{4.11}$$

where $C_a^{(int)}$ denotes the normalised channel capacity for plane a ($a = 0, 1, \ldots, \phi$). Applying the Shannon's theorem [7], for the non-NBI case ($a = 0$), $C_0^{(int)}$ can be simply expressed as

$$C_0^{(int)} = \frac{1}{N} \sum_{i=1}^{N} \log_2 \left(1 + \frac{P_e |H(f_i)|^2}{P_b} \right) \tag{4.12}$$

where P_e denotes the transmitted PSD, and P_b is the background noise PSD, which is denoted by σ_{b}^2. N is the number of subcarriers, and $H(f)$ is the channel transfer function. In the case of $\phi = 3$ as shown in Fig. 4.5, $C_a^{(int)}$, where $a = 1, 2, \ldots, \phi$ for the number of a active NBI bands can be expressed as

$$\begin{aligned} C_a^{(int)} \approx \frac{1}{N} \cdot \Bigg[& \sum_{i=1}^{N-a} \log_2 \left(1 + \frac{P_e |H(f_i)|^2}{P_b} \right) \\ & + \sum_{\theta=1}^{\phi-a+1} \Delta_\theta \log_2 \left(1 + \frac{P_e |\bar{H}(f)|^2}{P_\theta^{(int)} + P_b} \right) \Bigg] \end{aligned} \tag{4.13}$$

where Δ_θ is the coefficient calculated with the assumption of $\phi_1 = \phi_2 = \phi$ for the capacity on the subcarriers interfered by the active radio bands, that when $a = 1$, $\Delta_1 = \Delta_2 = \Delta_3 = 1/3$, when $a = 2$, $\Delta_1 = 4/3, \Delta_2 = 2/3$, when $a = 3$, $\Delta_1 = 3$. $P_\theta^{(int)}$ denotes different power levels of NBI, that the radio band on specific subcarrier, is occupied by one ($P_1^{(int)}$), two ($P_2^{(int)}$) and three ($P_3^{(int)}$) radio users,

respectively. $\bar{H}(f)$ is the average channel attenuation over the bandwidth, where the channel is assumed flat fading in comparison with the frequency selective NBI.

It can be derived that with negligible capacities at the active radio bands, (4.11) reduces to

$$C \approx \frac{1}{N} \sum_{a=0}^{\phi} \sum_{i=1}^{N-a} \pi_a \cdot \log_2 \left(1 + \frac{P_e |H(f_i)|^2}{P_b} \right) \tag{4.14}$$

Let $H_j(f_i)$ denote the jth instantaneous channel frequency response on the ith subcarrier. Assuming the number of subcarriers $N \gg \phi$, the corresponding instantaneous maximum bandwidth efficiency in (4.11) is given by

$$C_j \approx \frac{1}{N} \sum_{i=1}^{N} \log_2 \left(1 + \frac{P_e |H_j(f_i)|^2}{P_b} \right) \tag{4.15}$$

Thus, the average maximum overall bandwidth efficiency under the impact of NBI channel in (4.11) can be simplified as

$$C = \lim_{M \to \infty} \frac{1}{NM} \sum_{j=1}^{M} \sum_{i=1}^{N} \log_2 \left(1 + \frac{P_e |H_j(f_i)|^2}{P_b} \right) \tag{4.16}$$

which implies that the system capacity is dominated by background noise and the channel attenuation.

In Fig. 4.7, the overall maximum bandwidth efficiencies under proposed NBI model given by (4.16) is demonstrated, in comparison with the bandwidth efficiency for the case of AWGN background noise only, and the bandwidth efficiency achieved under the IN channel [58]. The horizontal axis denotes P_e/P_b, the signal-to-background-noise ratio, which varies from 0 dB to 20 dB. It is assumed low occurrence probability of IN, and the presence of NBI is generated using the same parameters as shown in Fig. 4.6, with the number of subcarriers $N = 128$. To compare with the added noise and interference channel, a random PLC channel generator [7] is applied to obtain Fig. 4.7, for broadband PLC transmission. With the effect of channel attenuation, the system performance is significantly degraded.

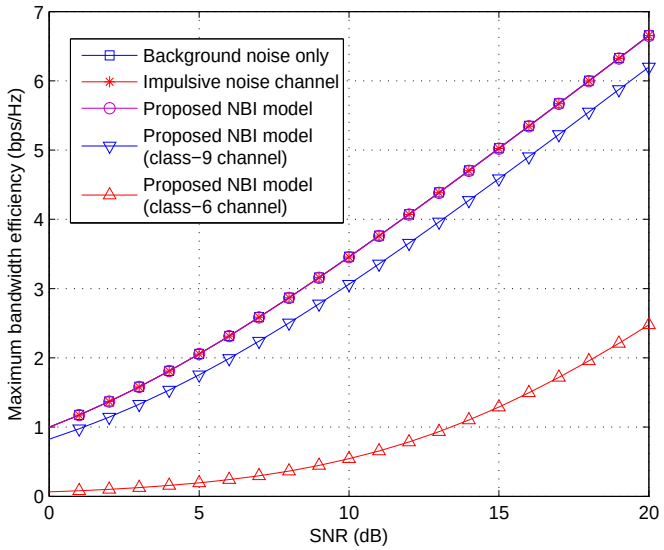

Figure 4.7: Analytical maximum bandwidth efficiency achievable under different channels.

Fig. 4.7 shows that within noise and interference channel, all cases achieve almost the same system capacity, implying that limited number of potential radio interferences, and IN with low occurrence probability have little impact on system performance. In the frequency range of 1.8 MHz-100 MHz, the maximum bandwidth efficiency is lowered by around 0.4 bps/Hz and 3 bps/Hz with class-9 and class-6 channels, respectively, verifying our analysis in (4.16) that the theoretical capacity is dominated by background noise and the channel attenuation.

4.4.3.2 Outage Capacity under both IN and NBI

As shown in (4.2), α, $\beta \in \{0,\ 1\}$ are the parameters indicating the occurrence states (absent or present) of the IN and NBI respectively. Let $\pi(\alpha, \beta) = \Pr(\alpha \cap \beta)$ denote the joint steady-state probabilities of the events IN and NBI. It is assumed that the occurrence of IN and NBI is statistically independent, where $\pi(1, 1) = \Pr(\alpha = 1)\Pr(\beta = 1)$ reflects the probability that both events occur. Thus, the general maximum bandwidth efficiency achievable under IN and NBI scenarios is

given by

$$C = \sum_{\alpha=0}^{1} \sum_{\beta=0}^{1} \pi(\alpha, \beta) C(\alpha, \beta) \tag{4.17}$$

where

$$\begin{bmatrix} \pi(0,0) \\ \pi(0,1) \\ \pi(1,0) \\ \pi(1,1) \end{bmatrix} = \begin{bmatrix} \pi_{I\ 0} \cdot \pi_0 \\ \pi_{I\ 0} \cdot (1-\pi_0) \\ \pi_{I\ 1} \cdot \pi_0 \\ \pi_{I\ 1} \cdot (1-\pi_0) \end{bmatrix}$$

and $C(\alpha, \beta)$ is the maximum bandwidth efficiency under the corresponding scenario. At the time when both IN and NBI occur, the corresponding maximum bandwidth efficiency $C(1,1)$ can be formulated as

$$\begin{aligned} C(1,1) = & \sum_{l=1}^{n} \frac{e^{-A} A^{l-1}}{(l-1)!} \\ & \cdot \left[\frac{\pi_{II\ 0l}}{(1-\pi_0)N} \sum_{a=1}^{\phi} \sum_{i=1}^{N-a} \pi_a \cdot \log_2 \left(1 + \frac{P_e |H(f_i)|^2}{P_b} \right) \right. \\ & \left. + \frac{\pi_{II\ l}}{(1-\pi_0)N} \sum_{a=1}^{\phi} \sum_{i=1}^{N-a} \pi_a \cdot \log_2 \left(1 + \frac{P_e |H(f_i)|^2}{P_l^{(imp)}(f_i) + P_b} \right) \right] \end{aligned} \tag{4.18}$$

Let $H_j(f_i)$ denote the jth instantaneous channel frequency response on the ith subcarrier. Assuming low occurrence probability of IN bursts, *i.e.*, $\pi_{I\ 1}$ is close to 0, and $\pi_{I\ 0} = 1 - \pi_{I\ 1}$ is close to 1, and the number of subcarriers $N \gg \phi$, the corresponding instantaneous maximum bandwidth efficiency in (4.17) is given by

$$C_j \approx \frac{\pi_{I\ 0}}{N} \sum_{i=1}^{N} \log_2 \left(1 + \frac{P_e |H_j(f_i)|^2}{P_b} \right) \tag{4.19}$$

Thus, the average maximum overall bandwidth efficiency under both IN and NBI channel in (4.17) can be simplified as

$$C = \lim_{M \to \infty} \frac{\pi_{I\ 0}}{NM} \sum_{j=1}^{M} \sum_{i=1}^{N} \log_2 \left(1 + \frac{P_e |H_j(f_i)|^2}{P_b} \right) \tag{4.20}$$

which implies that the system capacity is dominated by background noise and the channel attenuation.

Normally, the subcarriers disturbed by NBI are not able to decode the data correctly, which are allowed in outage.

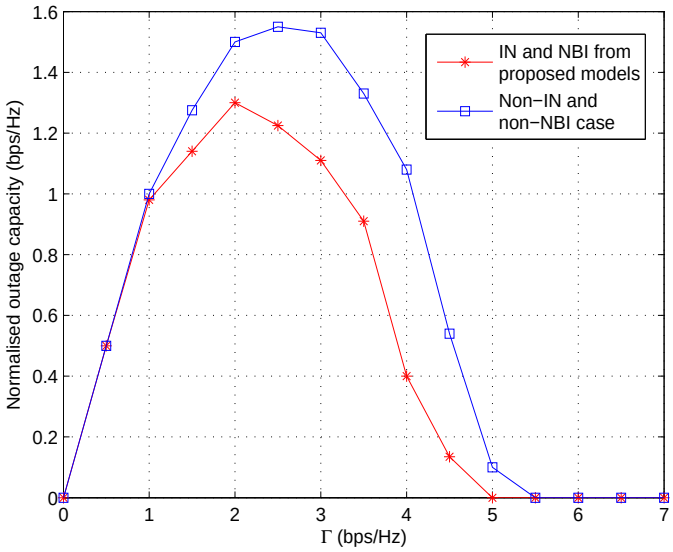

Figure 4.8: Outage capacity of the proposed noise and interference models for an average received SNR = 10 dB at a class-9 channel output.

Let P_{out} be the parameter indicating the probability that the system can be in outage, given by $P_{out} = \Pr(C_i < \Gamma)$. C_i denotes the average capacity for each subcarrier, and Γ is a certain value of the normalised throughput with an associated minimum received signal-to-noise ratio (SNR) γ_{min}, where $\Gamma = \log_2(1 + \gamma_{min})$. For received SNRs below γ_{min}, the data cannot be successfully decoded, and the system declares an outage. Hence, the average outage capacity C_{out} correctly received over a large number of transmissions is given by

$$C_{out} = (1 - P_{out}) \cdot \Gamma \tag{4.21}$$

In Fig. 4.8, the results of maximising outage capacity numerically are shown for an average SNR of 10 dB at a class-9 channel output, with the number of subcarriers $N = 128$. The presence of NBI is generated using the same parameters as shown in Fig. 4.6. It can be seen that with impulsive noise and interference, the maximum outage capacity is lowered by around 0.25 bps/Hz.

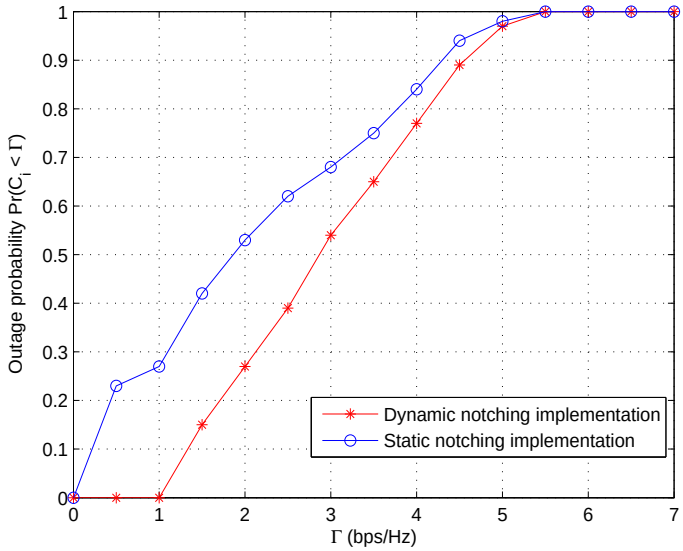

Figure 4.9: Comparison of the theoretical throughput between the dynamic and static notching schemes, in terms of the outage probability that the received SNRs are below a certain value of γ_{min}, for an average SNR = 10 dB at a class-9 channel output.

4.4.3.3 Dynamic Notching Implementation on the Active NBI Bands

Due to the concern about disturbing the surrounding radio users, many of the existing systems do not consider the high frequency (HF) band for PLC [23]. In Future PLC systems, in order to get higher data rate, PLC aims to share spectrum with other radio frequencies. An effective dynamic notching scheme may be essential to protect the valid radio services, and mitigate the effect of narrowband interferences from the active radios at the same time [6, 54]. To resolve the coexistence issue, the spectrum should be monitored and detected in real time, and then adjust the notched frequencies adaptively. An energy-based detector is mentioned in [6], in order to detect out the active radio users. With dynamic notching of the NBI, the maximum bandwidth efficiency under the MC based NBI model can be estimated by (4.14). Normally, a static notching is applied as in the HPAV standard [17], that the subcarrier with NBI and its neighbour ± 4 subcarriers are too notched.

The comparisons of normalised throughput between the dynamic and static notching implementations are reflected in Fig. 4.9, with the number of subcarriers $N = 128$, and average SNR of 10 dB at a class-9 channel output. It is assumed no IN, and the presence of NBI is generated using the same parameters as shown in Fig. 4.6. The results obtained show the significance of using the radio bands for PLC transmission. With the dynamic notching scheme, 25% more subcarriers in average provide the data rate over 2 bps/Hz, than that with the normal static notching approach.

4.5 Summary

In this chapter, measured results have been presented to help investigate the nature of NBI for indoor broadband PLC networks. A 3D MC based statistical model to describe the occurrence dependence of NBI has been proposed, based on the measurement results. The example NBI illustrates that MC is suitable to model the transitions among time states, where it is more realistic to consider multiple NBI states in the 3D MC. The proposed model is validated in reference to the measured results. The analytical throughput considering the impact of both IN and NBI has been investigated. The dynamic spectrum access approach is of the interest in added interference channel, especially for future cognitive PLC solutions, which improves the throughput by sharing the spectrum of radio bands.

The models proposed in Chapter 3 and Chapter 4 are applicable to performance analysis and computer simulations of any broadband PLC systems, and can be easily implemented to test the IN and NBI mitigation for green PLC spectrum and any other performance optimising methods, without carrying out any measurements. The statistical model for the occurrence property of interferences caused by radio users can be a valuable tool of analysing the performance of future cognitive PLC networks.

Chapter 5

Null Subcarriers Assisted Impulsive Noise Mitigation

IN is one of the main sources causing pollution to the PLC spectrum [2], which should be dealt with properly. The models of IN have been presented in Chapter 3. A thorough mitigation of IN at PLC receivers supports an enhancement of system performance in order to achieve effective transmissions.

As learned in Chapter 3, aperiodic IN caused by switching/plugging/unplugging transients of electric appliances is dominant in broadband PLC systems, which degrades the system performance significantly [2, 25]. Aperiodic IN often occurs randomly in a series of impulses, referred to as burst [25], for which the occurrence is statistically modelled in Chapter 3 using the tool of MC. It may hence result in bust errors during data transmissions. This chapter focuses on mitigating aperiodic IN. Most of the existing IN mitigation schemes are executed in OFDM systems through a number of conventional nonlinear techniques, such as blanking [41], clipping/deep clipping [27] and weighted combinations of them [40, 42]. However, the conventional schemes are based on detecting the IN contaminated data tones instead of reconstructing the IN vector and cancelling it out. Hence, the performance of the conventional methods is limited by the high peak-to-average power ratio (PAPR) OFDM signals, where use of the advanced techniques with channel coding schemes [46, 47] is necessary to achieve a satisfactory bit error rate (BER) in OFDM systems [63, 31]. Some sophisticated IN

mitigation schemes were developed in [11, 26] with the aid of compressed sensing [43, 44] and sparse Bayesian learning [45]. However, calculations of the matrix multiplication and inversion are required in these algorithms, and also the acquisition of *a priori* information leads an extra computation. Iterative method applied in [32, 64] is a good trade-off between the IN mitigation performance and complexity. However, it lacks a thorough validation of their proposed algorithms since the adopted IN model cannot simulate the burst environments, and the common disturbance of NBI on the indoor PLC spectrum was not considered. Referring to Chapter 4, NBI at PLC receivers from various nearby radio applications such as broadcast radios and amateur radios [6] is considered in this chapter. Since the unshielded power line can be a good antenna picking up the radios around [6], NBI may become a salient issue that degrades the PLC receiver performance. Also, high power spectral density (PSD) of the intensive NBI may lead a high rate of indistinguishable IN at PLC receivers. Thus, a suitable scheme is required to qualify the IN mitigation at PLC receivers.

In this chapter, the problem of constructing an effective IN mitigation scheme at uncoded OFDM-based PLC receivers is addressed. Our work is different in the following aspects. First, a novel IN mitigation scheme is proposed where the feedback of IN estimation is updated iteratively for a thorough mitigation. The use of null subcarriers leads a reduced number of iterations. Unlike the conventional blanking scheme [40] executed given the test statistics of the received signal, the harmful impact of high PAPR signals on the IN reconstruction is excluded in the proposed scheme. The associated receiver operating characteristic (ROC) is derived to show the performance of IN detection for both schemes. Second, the IN mitigation in the presence of NBI from nearby radio users with different impacts of NBI environments on the proposed receiver is evaluated, which has not been fully investigated previously. The associated analytical expressions for ROC are given to show the ability of IN detection under the disturbance of NBI. In the

case that the system is intensively disturbed by NBI, the IN vector reconstruction becomes ineffective, resulting in an incomplete IN mitigation. Third, null subcarriers aided pre-mitigation blocks are adopted in the proposed receiver to achieve a near-optimal performance without updating the IN estimation iteratively. The pre-mitigation significantly improves the initial IN estimation, while eliminates the impact of intensive NBI when it is present, leading to a joint NBI and IN mitigation. The thresholds for pre-NBI and pre-IN mitigation blocks are set to be sufficiently high, in order to achieve a sufficiently low false alarm rate for outliers detection. The performance of the proposed receiver is much higher than that of the existing blanking nonlinearity especially in the high SNR region. Simulation results are provided to demonstrate an improved BER performance achievable under the proposed IN mitigation scheme compared to the conventional blanking nonlinearity, while the robustness of the proposed receiver is also validated under the intensive disturbance of NBI.

In Section 5.1, a system model is presented to describe the overall IN mitigation scenarios for an indoor broadband PLC. In Section 5.2, the IN vector estimation in the proposed scheme is implemented over a PLC channel for NBI absence and NBI presence, respectively. The performance of the proposed scheme is compared to that of the conventional blanking approach. Simulation results are given in Section 5.3 to validate the proposed IN mitigation approach. The summary is finally remarked in Section 5.4.

5.1 System Model

The block diagram of an indoor broadband PLC system is depicted in Fig. 5.1, where $s(t)$ represents the transmit signal and $r(t)$ is the received signal. A hybrid of the aperiodic IN $n_{\mathrm{i}}(t)$, the NBI $v(t)$ and the background noise $n_{\mathrm{b}}(t)$ are the added disturbance at PLC receiver. While $n_{\mathrm{i}}(t)$ is caused from any potential switching/plug transients of the appliances in the system ($n_{\mathrm{i}}(t) = 0$ means no

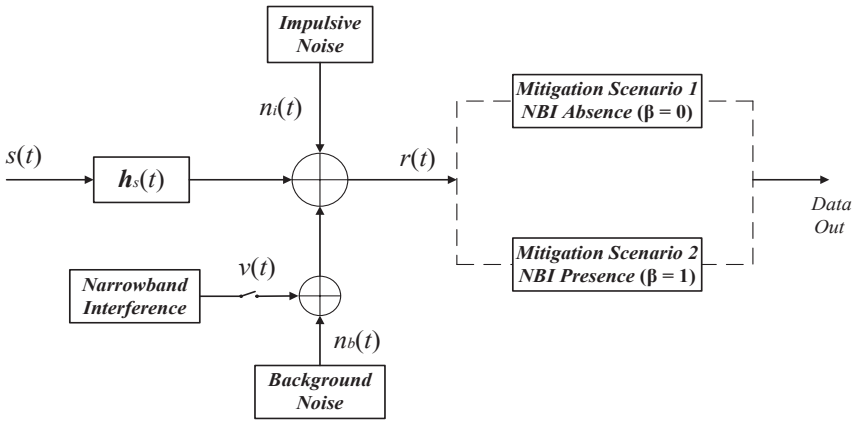

Figure 5.1: Block diagram of a PLC system with IN mitigation.

noise), and $v(t)$ is from various nearby radio applications ($v(t) = 0$ means no interference). We assume IN is present for each transmission. The dashed-line block indicates the proposed IN mitigation scheme at the receiver, considering two different scenarios that NBI is present and NBI is absent, respectively.

In a discrete-time system, the signal at the PLC receiver is a mixture of various noises. Let $r(m)$ denote the mth received signal sample, expressed as:

$$r(m) = \{h_{\mathrm{s}} * s\}(m) + n_{\mathrm{i}}(m) + \beta \cdot v(m) + n_{\mathrm{b}}(m) \tag{5.1}$$

where in (5.1), $\beta \in \{0,\ 1\}$ is the parameter indicating the occurrence states (absent or present) of the NBI, where $\Pr(\beta = 1)$ reflects the NBI occurrence probability.

As shown in Fig. 5.1, the IN mitigation scheme should be implemented in both scenarios of NBI absence ($\beta = 0$) and NBI presence ($\beta = 1$), with the probabilities of $\Pr(\beta = 0)$ and $\Pr(\beta = 1)$, respectively. In this chapter, the statistical models presented in Chapter 3 and Chapter 4 are adopted. PLC systems under the disturbance of IN and NBI can be simulated applying these statistical models, and the effectiveness of the proposed mitigation scheme can be easily evaluated without carrying out any measurements.

Referring to Chapter 3, the impact of aperiodic IN is considered since it is dominant in broadband PLC systems [33]. Aperiodic IN occurs randomly and

often refers to as burst in time domain [25], which has its occurrence probabilities dependent on the previous states, following the MC process [56]. Modelling of the time-domain (TD) occurrence-dependent IN was presented, where a two-level MC-based model was proposed.

It is assumed that each event of the switching/plugging transients produces a noise burst. The occurrence of a burst can be described by the first level MC, and the occurrence of individual impulses within a burst are characterised by the second level MC. The first-order Markov process can be described by its transition probability matrix, which is conditioned by the previous one state. Steady-state probability (SSP) can be applied to define the occurrence probability of an event under discrete-time Markov process, where the next state probabilities have dependence on the current state probabilities and are determined by the transition probability matrix as

$$\boldsymbol{\Pi}_{t+1} = \boldsymbol{P}\boldsymbol{\Pi}_t \tag{5.2}$$

where $\boldsymbol{P}$ is transition probability matrix, which has the elements defined by $\Pr(\{t+1\}|\{t\})$. The probability of the next state '$\{t+1\}$' is conditioned by the current state '$\{t\}$'. $\boldsymbol{\Pi}_t$ is a column vector whose elements represent the state probabilities at time t. In the steady-state, we have $\boldsymbol{\Pi}_{t+1} = \boldsymbol{\Pi}_t$.

For simplicity, it is assumed that the considered PLC system in Fig. 5.1 is hit by one burst from a single IN source during each transmission. We adopt the second level MC to reproduce the impulses in a burst. Let '$\{t\}$' indicate the state in the second level MC at the discrete-time t. The corresponding state has a value of '1' in the presence of an impulse, otherwise '0' represents the absent of IN. Π_{II} indicates the SSP of producing an individual impulse in the second level MC, which can be derived by solving (5.2) as

$$\Pi_{\mathrm{II}} = \frac{\Pr\left(\{t+1\}=1|\{t\}=0\right)}{\Pr(\{t+1\}=1|\{t\}=0) + \Pr(\{t+1\}=0|\{t\}=1)} \tag{5.3}$$

which is weighted by the corresponding transition probabilities.

It is assumed the IN $n_{\mathrm{i}}(m)$ with zero mean and variance σ_{i}^2 has a Gaussian process of $\mathcal{N}(0, \sigma_{\mathrm{i}}^2)$, where $\sigma_{\mathrm{i}}^2 \gg \sigma_{\mathrm{b}}^2$. Thus, the PDF of the combined noise $n = n_{\mathrm{i}} + n_{\mathrm{b}}$ is given by

$$\begin{aligned}\boldsymbol{f}_n(n) &= \begin{bmatrix} f(n|\{t\}=0) & f(n|\{t\}=1) \end{bmatrix} \\ &= \begin{bmatrix} \mathcal{N}(0,\sigma_{\mathrm{b}}^2) & \mathcal{N}(0,\sigma_{\mathrm{b}}^2+\sigma_{\mathrm{i}}^2) \end{bmatrix} \cdot \begin{bmatrix} \Pr(0|0) & \Pr(0|1) \\ \Pr(1|0) & \Pr(1|1) \end{bmatrix} \end{aligned} \tag{5.4}$$

which is conditioned by the current impulse state. In the steady-state of IN, the PDF can be expressed as

$$f_n(n) = (1 - \mathit{\Pi}_{\mathrm{II}}) \cdot \mathcal{N}(n; 0, \sigma_{\mathrm{b}}^2) + \mathit{\Pi}_{\mathrm{II}} \cdot \mathcal{N}(n; 0, \sigma_{\mathrm{b}}^2 + \sigma_{\mathrm{i}}^2) \tag{5.5}$$

where $\mathit{\Pi}_{\mathrm{II}}$ is independent of the initial transition state.

The corresponding arrival rate of the impulses normalised to the sampling interval, follows the reciprocal value of the number of consecutive non-impulse states k between two impulses, which has the probability distribution for remaining in the non-impulse state as

$$P(k) = \Pr(0|0)^{k-1} \cdot (1 - \Pr(0|0)) \tag{5.6}$$

The SSP $\mathit{\Pi}_{\mathrm{II}}$ and the arrival model of the second level MC can describe the particular impulsive scenario in the considered PLC system accurately, which are important to evaluate the performance of the proposed IN mitigation approach.

Referring to Chapter 4, a single level 3D MC model was presented for the reconstruction of NBI in frequency-domain (FD), considering the TD occurrence-dependence. Let $\boldsymbol{P}^{(int)}$ be the transition probability matrix for the number of active radio interferers over the total ϕ potential interferers, which can be formulated as

$$\boldsymbol{P}^{(int)} = \begin{bmatrix} P_{0,0} & P_{1,0} & 0 & \cdots & 0 \\ P_{0,1} & P_{1,1} & \ddots & \ddots & \vdots \\ 0 & P_{1,2} & \ddots & P_{\phi-1,\phi-2} & 0 \\ \vdots & \ddots & \ddots & P_{\phi-1,\phi-1} & P_{\phi,\phi-1} \\ 0 & \cdots & 0 & P_{\phi-1,\phi} & P_{\phi,\phi} \end{bmatrix} \tag{5.7}$$

where $P_{i,j}$ is defined as the transition probability from the number of i tone interferers to j tone interferers, with $i, j = 0, 1, 2, \ldots, \phi$. For simplicity, it is assumed the transition starts from ϕ interferers and $P_{\phi,\phi} = 1$.

IN mitigation for PLC applications is normally considered under the OFDM systems [31]. As specified for the OFDM in HPAV standard [17], about 40% of the total N subcarriers are set to zero to avoid interfering with other applications, referred to as null subcarriers. NBI from radio applications normally presents in those subcarriers from the total N_ξ null subcarriers [11]. Thus, it is assumed the FD sparse NBI vector with N_ξ entries has its ϕ nonzero entries located at ϕ out of all the N_ξ null subcarriers.

The initial ϕ NBI entries are randomly chosen which has the disturbance ratio $\mu = \phi/N_\xi$. The amplitude distribution for each band-limited tone interferer can be modelled by Gaussian noise as described in [11, 65] with the PSD σ_v^2, following a Gaussian distribution of $\mathcal{N}(0, \sigma_v^2)$. The NBI power normalised to the background noise power at the NBI contaminated subcarriers is $p_v = N\sigma_v^2/\phi$.

In the proposed IN mitigation scheme in Section 5.2, null subcarriers are adopted to improve the reconstruction of IN at PLC receiving end. In the presence of NBI, the accuracy of IN estimation is affected by the NBI contaminated subcarriers, which brings challenges for IN mitigation. The environments with NBI can be simulated using the statistical model, which is important to test the proposed mitigation method under the joint impact of IN and NBI.

5.2 Iterative IN Mitigation

In Fig. 5.2, two detailed block diagrams of the proposed IN mitigation scheme at receiver are demonstrated, where the red dashed-line block illustrates a zoom-in on the IN mitigation block using an iterative approach. Basically, IN is estimated using the feedback of soft data detection, and removal of the estimated IN from the received sequence improves the data detection accordingly. Hence,

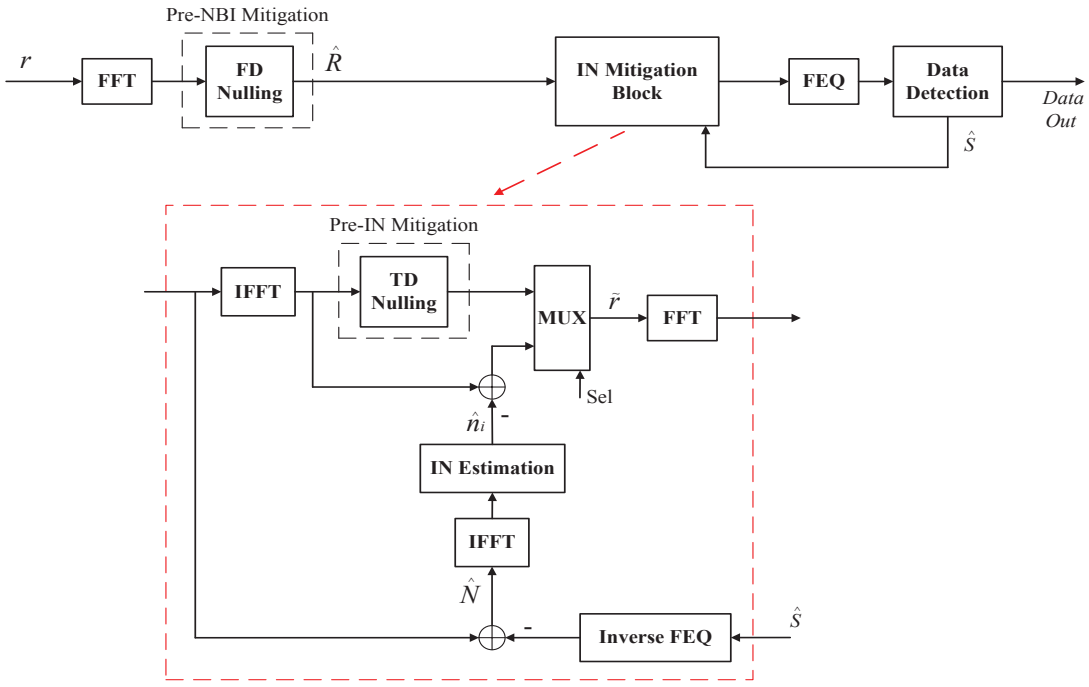

Figure 5.2: Proposed receiver for IN mitigation (FEQ-frequency domain equalization; FD-nulling is applied when NBI is present; TD-nulling is applied when IN is present).

both IN estimation and data detection blocks are updated iteratively until the hard decision is made for data output. The use of null subcarriers improves the iterative method significantly, but also brings challenges on accurate IN reconstruction when some of the subcarriers are contaminated by NBI. The design of pre-NBI mitigation and pre-IN mitigation blocks is to combat the impact of NBI, and further enhances the performance of the proposed mitigation scheme. In this section, the IN mitigation proposed for both scenarios as shown in Fig. 5.1 is described, considering the NBI absence ($\beta = 0$) and the NBI presence ($\beta = 1$), respectively.

5.2.1 IN Mitigation in the Absence of NBI

In this subsection, the environment of IN only is considered, which is widely applied to test the existing mitigation algorithms. First, we look into the conventional blanking scheme reported in the literature. Then, the proposed IN

mitigation scheme is studied, where the performance is also analysed to show the benefit of using null subcarriers.

5.2.1.1 Conventional Blanking Approach

In the case of $\beta = 0$ in (5.1), where NBI from radio applications is absent. The received signal in (5.1) is then simplified to

$$r(m) = \{h_{\mathrm{s}} * s\}(m) + n_{\mathrm{i}}(m) + n_{\mathrm{b}}(m) \tag{5.8}$$

which is usually applied as the received sequence for various indoor PLC communication systems [31, 26]. Thus, most of the existing IN mitigation methods such as [66, 32], are verified through the basic system model in (5.8).

The conventional nonlinear techniques are widely used to mitigate IN at the receiver, including blanking, clipping and weighted combinations of them [27, 42]. Referring to Fig. 5.2, the blanking nonlinearity is normally applied directly on the received signal r before FFT, which can be defined as [40]

$$\bar{r}(m) = \begin{cases} r(m), & |r(m)| \leq \lambda \\ 0, & |r(m)| > \lambda \end{cases} \tag{5.9}$$

where λ denotes the blanking threshold and $\bar{r}(m)$ is the blanked sequence, with $m = 0, 1, \ldots, N-1$.

As described in (5.5), each noise term has a Gaussian PDF. In a large number N of OFDM subcarriers, the transmit signal $s(m)$ filtered by power line channel follows a Gaussian distribution of $\mathcal{N}(0, \sigma_{\mathrm{s}}^2)$. Thus, the PDF of the received signal $r(m)$ in (5.8) can be expressed as

$$f_r(r) = (1 - \Pi_{\mathrm{II}}) \cdot \mathcal{N}(r; 0, \sigma_{\mathrm{s}}^2 + \sigma_{\mathrm{b}}^2) + \Pi_{\mathrm{II}} \cdot \mathcal{N}(r; 0, \sigma_{\mathrm{s}}^2 + \sigma_{\mathrm{b}}^2 + \sigma_{\mathrm{i}}^2) \tag{5.10}$$

The basic principle for the threshold-based techniques is actually to use signal detection theory, where the ROC can be analysed on the test signal statistics [67]. ROC curves explore the trade-offs between the probability of detection $\mathcal{P}_d$ and the probability of false alarm $\mathcal{P}_f$ for a range of varied thresholds. By comparing

the test statistics $|r(m)|$ to a given threshold λ, the associated probabilities $\mathcal{P}_f$ and $\mathcal{P}_d$ are expressed as

$$\mathcal{P}_f = \text{erfc}\left(\frac{\lambda}{\sqrt{2(\sigma_\text{s}^2 + \sigma_\text{b}^2)}}\right) \tag{5.11}$$

$$\mathcal{P}_d = \text{erfc}\left(\frac{\lambda}{\sqrt{2(\sigma_\text{s}^2 + \sigma_\text{b}^2 + \sigma_\text{i}^2)}}\right) \tag{5.12}$$

where erfc is the complementary error function [68].

The corresponding optimal threshold can be determined with respect to a pair of best trade-off probabilities, which can be selected for specific system requirements, and varied according to different criteria [31].

5.2.1.2 IN Estimation Using Data Subcarriers

Under the proposed IN mitigation scheme as shown in Fig. 5.2, IN samples are estimated first and then suppressed from the received signal individually, rather than set the IN contaminated signal samples to zero as described in the conventional blanking approach. The basic principle for the IN estimation is to cancel out the data term at the channel output from the received signal, and then reconstruct the IN vector from the remaining mixed noise terms.

For the considered system in (5.1) with $\beta = 0$, the received signal $r(m)$ is initially passed through the FFT module at the conventional OFDM receiver, yielding

$$R(\mathcal{M}) = \{H_\text{s} \cdot S\}(\mathcal{M}) + \boldsymbol{F} n_\text{i}(\mathcal{M}) + \boldsymbol{F} n_\text{b}(\mathcal{M}) \tag{5.13}$$

where $\boldsymbol{F}$ denotes the N-point DFT matrix and H_s is the channel frequency response, with the subcarrier index $\mathcal{M} = 0, 1, \ldots, N-1$.

Then, the signal can be simply compensated by a frequency-domain equalizer (FEQ) on each subcarrier independently, using the zero-forcing (ZF) method. The channel frequency response can be estimated with overhead, which is considered separately. Assuming perfect channel estimation, *i.e.*, complete knowledge of H_s,

and using a ZF equalizer, the tentative soft decision $\hat{S}(\mathcal{M})$ can be obtained, which is then cancelled out from the received signal in order to find the estimation of noise terms as

$$\hat{N}(\mathcal{M}) = R(\mathcal{M}) - \{H_{\mathrm{s}} \cdot \hat{S}\}(\mathcal{M}) \tag{5.14}$$

To reconstruct the IN vector in TD, inverse fast Fourier transform (IFFT) is performed on $\hat{N}(\mathcal{M})$ in order to obtain the mixed TD noise terms $\hat{n}(m)$. In the proposed scheme, the IN vector can then be estimated by

$$\hat{n}_{\mathrm{i}}(m) = \begin{cases} 0, & |\hat{n}(m)| \leq \lambda \\ \hat{n}(m), & |\hat{n}(m)| > \lambda \end{cases} \tag{5.15}$$

where $\hat{n}_{\mathrm{i}}(m)$ denotes the estimated IN vector and λ is the corresponding threshold.

An accurate detection of the nonzero entries in $\hat{n}_{\mathrm{i}}$ leads a good estimation of the IN vector, and hence improves the performance of the according mitigation techniques. A perfect detection may lead to a thorough IN mitigation. Unlike the conventional blanking approach in (5.9) which takes the detection on IN entries given the received signal vector, the detection in the proposed scheme is performed given the noise terms only. Thus, the impact of high PAPR signals on the threshold-based detection is eliminated. According to (5.15), the test statistics $|\hat{n}(m)|$ is compared to a given threshold λ, resulting in the detection probabilities as

$$\mathcal{P}_f = \mathrm{erfc}\left(\frac{\lambda}{\sigma_{\mathrm{b}}\sqrt{2}}\right) \tag{5.16}$$

$$\mathcal{P}_d = \mathrm{erfc}\left(\frac{\lambda}{\sqrt{2(\sigma_{\mathrm{b}}^2 + \sigma_{\mathrm{i}}^2)}}\right) \tag{5.17}$$

which outperforms the conventional blanking in classifying between the zero and nonzero entries of the IN vector, especially in the high SNR region. For a given false alarm rate $\mathcal{P}_f$ in (5.16), the non-adaptive threshold λ can be simply calculated by the inverse complementary error function.

Then, the estimated IN vector $\hat{n}_{\mathrm{i}}$ can be used as a feedback to obtain a cleaner received signal $\tilde{r}(m)$ as

$$\tilde{r}(m) = r(m) - \hat{n}_{\mathrm{i}}(m) \tag{5.18}$$

where the estimated impulses are suppressed individually from the initially received signal samples and a multiplexer is used to select the updated received signal for further data processing of the proposed receiver.

5.2.1.3 IN Estimation Using Data and Null Subcarriers

In practical, the estimate of the IN vector $\hat{n}_{\mathrm{i}}$ in TD is imperfect, which is affected by the accuracy of $\hat{n}(m)$ estimation and the trade-off thresholding. The tentative soft decision $\hat{S}(\mathcal{M})$ may contain many errors without doing iterations. Thus, after performing the IFFT on (5.14), the estimated noise terms can be expressed by considering decision errors as

$$\hat{n}(m) = \hat{e}(m) + n_{\mathrm{i}}(m) + n_{\mathrm{b}}(m) \tag{5.19}$$

where $\hat{e}(m)$ is caused by the feedback of wrong decisions. In the high SNR region, decision errors are rare and negligible. While in the low SNR region, lots of wrong decisions are made, and $\hat{e}(m)$ can be assumed as Gaussian distributed due to the IFFT operation. Thus, the PDF of $\hat{n}(m)$ in (5.19) can be expressed by

$$f_{\hat{n}}(\hat{n}) = (1 - \mathit{\Pi}_{\mathrm{II}}) \cdot \mathcal{N}(\hat{n}; 0, \sigma_{\hat{\mathrm{e}}}^2 + \sigma_{\mathrm{b}}^2) + \mathit{\Pi}_{\mathrm{II}} \cdot \mathcal{N}(\hat{n}; 0, \sigma_{\hat{\mathrm{e}}}^2 + \sigma_{\mathrm{b}}^2 + \sigma_{\mathrm{i}}^2) \tag{5.20}$$

where $\sigma_{\hat{\mathrm{e}}}^2$ is the variance of $\hat{e}(m)$, which should be lowered to improve the IN estimation. According to the proposed receiver in Fig. 5.2, it normally costs several iterations to minimise $\sigma_{\hat{\mathrm{e}}}^2$.

Most of the power line systems do not use the whole spectrum for data transmission, in order to avoid interfering with other applications. A spectrum mask for HPAV is implemented to stay clear from transmission on some frequencies [69]. This ability can be easily performed at the OFDM transmitter by setting the corresponding subcarriers to zero, referred to as null subcarriers.

At the receiver, the wideband IN spreads its power over all frequencies, which has its components in the null subcarriers. Let ξ be the index set of the null subcarriers, where the total number $N_\xi = |\xi|$ of null subcarriers is considered. In the absence of NBI ($\beta = 0$ in (5.1)), the noise terms from the null subcarriers can be observed at the receiver as

$$R_\xi(\mathcal{M}) = \boldsymbol{F}_\xi n_{\mathrm{i}}(\mathcal{M}) + \boldsymbol{F}_\xi n_{\mathrm{b}}(\mathcal{M}) \tag{5.21}$$

where $(\cdot)_\xi$ indicates the sub-vector which has the entries indexed by the null subcarriers set ξ, *i.e.*, $\mathcal{M} \in \xi$.

The noise terms in null subcarriers are from nature with no decision errors, resulting in a more accurate initial estimate of the IN vector. Hence, the receiver performance can be improved with a certain number of iterations by adopting the null subcarriers. The performance of detecting the nonzero entries in the IN vector given $\hat{n}(m)$ in (5.19) can be evaluated by comparing the test statistics $|\hat{n}(m)|$ to a given threshold λ, yielding the detection probabilities as

$$\mathcal{P}_f = \mathrm{erfc}\left(\frac{\lambda}{\sqrt{2(\sigma_{\hat{\mathrm{e}}}^2 + \sigma_{\mathrm{b}}^2)}}\right) \tag{5.22}$$

$$\mathcal{P}_d = \mathrm{erfc}\left(\frac{\lambda}{\sqrt{2(\sigma_{\hat{\mathrm{e}}}^2 + \sigma_{\mathrm{b}}^2 + \sigma_{\mathrm{i}}^2)}}\right) \tag{5.23}$$

where the mean squared error $\sigma_{\hat{\mathrm{e}}}^2$ is lowered by using null subcarriers since $\boldsymbol{F}_\xi \hat{e} = 0$. After few iterations, $\sigma_{\hat{\mathrm{e}}}^2$ is negligible and equals zero in the high SNR region.

For a maximum allowed false alarm rate $\mathcal{P}_f$ in (5.22), the threshold can be derived as

$$\lambda = \sqrt{2}\sigma_{\hat{\mathrm{n}}} \cdot \mathrm{erfc}^{-1}(\mathcal{P}_f) \tag{5.24}$$

where $\sigma_{\hat{\mathrm{n}}}$ is the standard derivation of the noise vector $\hat{n}(m)$ in (5.19) and erfc^{-1} denotes the inverse complementary error function. The chosen threshold is adaptive since $\sigma_{\hat{\mathrm{e}}}^2$ is varied from the different values of SNR.

With the assistance of null subcarriers and adaptive thresholding, feedback of the improved IN vector $\hat{n}_{\mathrm{i}}$ estimation can be obtained to mitigate the IN thoroughly by costing a reduced number of iterations.

5.2.1.4 Pre-Time Domain Processing using Null Subcarriers

To further improve the IN mitigation algorithm, the feedback of an accurate initial estimated IN vector $\hat{n}_{\mathrm{i}}$ is the key to achieve a satisfactory performance of the proposed receiver, without updating the IN vector $\hat{n}_{\mathrm{i}}$ iteratively.

A pre-processing block is applied to improve the tentative soft decision $\hat{S}(\mathcal{M})$ before the initial IN estimation. Hence, a lower mean squared error $\sigma^2_{\hat{\mathrm{e}}}$ caused by wrong decisions can be obtained to achieve a better initial IN estimation. The pre-processing vector can be reconstructed by using the null subcarriers as

$$R_{\mathrm{pre}}(\mathcal{M}) = \begin{cases} R_{\xi}(\mathcal{M}), & \mathcal{M} \in \xi \\ 0, & \mathcal{M} \in \bar{\xi} \end{cases} \tag{5.25}$$

where $\bar{(\cdot)}$ indicates the set complement. Let $r_{\mathrm{pre}}(m)$ denote the IFFT counterpart of (5.25), with $m = 0, 1, \ldots, N-1$.

In the absence of NBI, the pre-TD processing is meant to remove the strong portion in $r_{\mathrm{pre}}(m)$ from the received signal $r(m)$, which can be formulated by

$$r^{(\mathrm{TD})}_{\mathrm{pre}}(m) = \begin{cases} r(m), & |r_{\mathrm{pre}}(m)| \leq \lambda_{\mathrm{pre}} \\ r(m) - r_{\mathrm{pre}}(m), & |r_{\mathrm{pre}}(m)| > \lambda_{\mathrm{pre}} \end{cases} \tag{5.26}$$

where λ_{pre} denotes the threshold for pre-TD processing, which can be determined using the standard derivation of $r_{\mathrm{pre}}(m)$ through (5.24). The threshold λ_{pre} is non-adaptive to SNR since the test statistics $|r_{\mathrm{pre}}(m)|$ only includes the noise terms from nature.

Instead of the received signal $r(m)$, the vector $r^{(\mathrm{TD})}_{\mathrm{pre}}$ in (5.26) is passed through the conventional OFDM receiver in order to obtain an improved initial feedback of the tentative decision $\hat{S}(\mathcal{M})$. Thus, the initial IN estimation using (5.14) and (5.15) can be refined accordingly.

5.2.2 IN Mitigation in the Presence of NBI

The previous subsection demonstrates the proposed IN mitigation scheme in the absence of NBI. With the aid of null subcarriers, the initial estimate of the IN vector can be significantly improved. According to the system model in Fig. 5.1, NBI is a common event for indoor PLC where the NBI contaminated subcarriers bring challenges for the IN vector reconstruction. In this subsection, first, the proposed receiver performance in the presence of NBI is analysed, and then a joint mitigation of the NBI and IN before the estimate of the IN vector is applied, in order to combat the effect of NBI as shown in Fig. 5.2.

5.2.2.1 IN Estimation Using Data and Null Subcarriers

The NBI from radio applications such as emergencies, amateur and mobile-radios often happens to indoor scenarios. The use of null subcarriers for the OFDM PLC avoids interfering with other applications, and on the other hand, improves the proposed IN estimation when NBI is absent as learned in Subsection 5.2.1. In the case of $\beta = 1$ in (5.1), the IN estimation should be performed in the presence of NBI, where the IN samples observed in null subcarriers are polluted by the NBI. Thus, the noise terms added at receiver from the null subcarriers can be formulated as

$$R_{\xi}(\mathcal{M}) = \boldsymbol{F}_{\xi} n_{\mathrm{i}}(\mathcal{M}) + \boldsymbol{F}_{\xi} v(\mathcal{M}) + \boldsymbol{F}_{\xi} n_{\mathrm{b}}(\mathcal{M}) \tag{5.27}$$

where the subcarrier index $\mathcal{M} \in \xi$. Let the complement set $\bar{\xi}$ denote the index set of the data subcarriers where $\boldsymbol{F}_{\bar{\xi}} v(\mathcal{M}) = 0$. Thus, the received signal from the data subcarriers can be represented by (5.13) with $\mathcal{M} \in \bar{\xi}$.

According to the proposed receiver in Fig. 5.2, the received signal before the FFT operation equals

$$r(m) = \{h_{\mathrm{s}} * s\}(m) + n_{\mathrm{i}}(m) + v(m) + n_{\mathrm{b}}(m) \tag{5.28}$$

which can be adopted after FFT to obtain the estimated noise terms as in (5.14).

Hence, the IFFT counterpart of (5.14) can be expressed as

$$\hat{n}(m) = \hat{e}(m) + n_{\mathrm{i}}(m) + v(m) + n_{\mathrm{b}}(m) \tag{5.29}$$

where the amplitude distribution for the NBI $v(m)$ follows the random Gaussian of $\mathcal{N}(0, \sigma_v^2)$. Thus, the PDF of $\hat{n}(m)$ in (5.29) can be expressed by

$$\begin{aligned} f_{\hat{n}}(\hat{n}) =& (1 - \mathit{\Pi}_{\mathrm{II}}) \cdot \mathcal{N}(\hat{n}; 0, \sigma_{\hat{\mathrm{e}}}^2 + \sigma_{\mathrm{b}}^2 + \sigma_v^2) \\ &+ \mathit{\Pi}_{\mathrm{II}} \cdot \mathcal{N}(\hat{n}; 0, \sigma_{\hat{\mathrm{e}}}^2 + \sigma_{\mathrm{b}}^2 + \sigma_v^2 + \sigma_{\mathrm{i}}^2) \end{aligned} \tag{5.30}$$

where the estimated IN vector $\hat{n}_{\mathrm{i}}(m)$ can be obtained in (5.15) by comparing the test statistics $|\hat{n}(m)|$ modelled in (5.30) to a given threshold. In the presence of NBI, the performance of detecting the nonzero entries in the IN vector can be evaluated by

$$\mathcal{P}_f = \mathrm{erfc}\left(\frac{\lambda}{\sqrt{2(\sigma_{\hat{\mathrm{e}}}^2 + \sigma_{\mathrm{b}}^2 + \sigma_v^2)}}\right) \tag{5.31}$$

$$\mathcal{P}_d = \mathrm{erfc}\left(\frac{\lambda}{\sqrt{2(\sigma_{\hat{\mathrm{e}}}^2 + \sigma_{\mathrm{b}}^2 + \sigma_v^2 + \sigma_{\mathrm{i}}^2)}}\right) \tag{5.32}$$

where the ingress of the intensive NBI ($\sigma_v^2 \gg \sigma_{\mathrm{b}}^2$) can cause a harmful impact on the detection performance. For a maximum allowed false alarm rate $\mathcal{P}_f$ in (5.31), the associated threshold λ can be calculated using (5.24) given the standard derivation of $\hat{n}(m)$ in (5.29).

In the presence of intensive NBI, although the mean squared error $\sigma_{\hat{\mathrm{e}}}^2$ can be reduced iteratively, the high PSD σ_v^2 can still disturb the reconstruction of the IN vector, leading an incomplete IN mitigation in (5.18). The intensive NBI in null subcarriers should be removed in advance to enhance the performance of the proposed IN mitigation scheme.

5.2.2.2 Pre-Joint Frequency Domain/Time Domain Nulling

The presence of NBI with high PSD σ_v^2 brings challenges for the IN detection given the vector $\hat{n}(m)$ in (5.29), where the entries with weak IN would be indis-

tinguishable from the entries with the combined terms of background noise, NBI and decision errors only.

A pre-joint mitigation on the intensive NBI and IN is required to improve the reconstruction of IN in the presence of NBI, which is indicated by the dashed-line blocks in Fig. 5.2. The pre-FD nulling is meant to detect and null the NBI contaminated subcarriers, which can be formulated by

$$R_{\text{pre}}^{(\text{FD})}(\mathcal{M}) = \begin{cases} R_{\xi}(\mathcal{M}), & |R_{\xi}(\mathcal{M})| \leq \Lambda_{\text{pre}} \\ 0, & |R_{\xi}(\mathcal{M})| > \Lambda_{\text{pre}} \end{cases} \tag{5.33}$$

where $R_{\text{pre}}^{(\text{FD})}$ is the output vector from the pre-FD nulling block with $\mathcal{M} \in \xi$, and Λ_{pre} denotes the threshold for the pre-FD nulling. Detection of the NBI contaminated subcarriers would be accurate since it has much higher intensity of the FD component compared to that of the IN and background noise. Hence, the chosen threshold can be sufficiently high to keep a low rate of false alarm. For a sufficiently low false alarm rate $\mathcal{P}_f$, the threshold Λ_{pre} is given by

$$\Lambda_{\text{pre}} = \sqrt{2(\sigma_{\text{b}}^2 + \mathit{\Pi}_{\text{II}}\sigma_{\text{i}}^2)} \cdot \text{erfc}^{-1}(\mathcal{P}_f) \tag{5.34}$$

where Λ_{pre} is non-adaptive to the SNR. The refined received signal $\hat{R}(\mathcal{M})$ can be reconstructed by

$$\hat{R}(\mathcal{M}) = \begin{cases} R_{\text{pre}}^{(\text{FD})}(\mathcal{M}), & \mathcal{M} \in \xi \\ R_{\bar{\xi}}(\mathcal{M}), & \mathcal{M} \in \bar{\xi} \end{cases} \tag{5.35}$$

which excludes the influence of NBI and has its IFFT counterpart $\hat{r}(m)$, with $m = 0, 1, \ldots, N-1$.

Following the pre-FD nulling, it is possible to detect the IN from TD more accurately. The pre-TD nulling is meant to detect and null the strong portion in $\hat{r}(m)$, which is defined as

$$r_{\text{pre}}^{(\text{TD})}(m) = \begin{cases} \hat{r}(m), & |\hat{r}(m)| \leq \lambda_{\text{pre}} \\ 0, & |\hat{r}(m)| > \lambda_{\text{pre}} \end{cases} \tag{5.36}$$

where $r_{\text{pre}}^{(\text{TD})}$ indicates the output vector from the pre-TD nulling block. λ_{pre} denotes the threshold for the pre-TD nulling, which can be set for a maximum

allowed false alarm rate $\mathcal{P}_f$ as

$$\lambda_{\text{pre}} = \sqrt{2}\sigma_{\hat{\text{r}}} \cdot \text{erfc}^{-1}(\mathcal{P}_f) \tag{5.37}$$

where $\sigma_{\hat{\text{r}}}$ is the standard derivation of the refined received signal $\hat{r}(m)$ by the pre-FD nulling. At this stage, a sufficiently low $\mathcal{P}_f$ is expected that λ_{pre} should be high enough, and the impact of strong IN would be mitigated. The chosen threshold varies with $\sigma_{\hat{\text{r}}}$, which is adaptive of various SNR values.

With the benefit of pre-joint FD/TD nulling, an improved initial feedback of the tentative soft decision $\hat{S}(\mathcal{M})$ can be obtained before the IN reconstruction. Meanwhile, the estimation on noise terms is given by

$$\hat{N}(\mathcal{M}) = \hat{R}(\mathcal{M}) - \{H_{\text{s}} \cdot \hat{S}\}(\mathcal{M}) \tag{5.38}$$

which eliminates the influence of NBI by using $\hat{R}(\mathcal{M})$ instead of the received signal $R(\mathcal{M})$ as in (5.14). Therefore, after the IFFT process, even the initial IN estimation through (5.15) can be fairly good.

5.3 Numerical Results

The performance of the proposed IN mitigation scheme is evaluated through extensive simulations over the PLC system in Fig. 5.1, where both scenarios of NBI absence and NBI presence are considered. The results of BER are obtained from an uncoded OFDM system with a total of $N = 256$ subcarriers. As specified in the HPAV standard [17], about 40% of the total N subcarriers are set to zero to avoid interference with other applications, *i.e.*, the number of null subcarriers is set to $N_\xi = 112$, 40% of the total 256 subcarriers during the transmission. A random PLC channel generator in [7] is applied to obtain the class-9 PLC channel which is assumed perfectly estimated at the receiver. The IN environment is generated statistically using the arrival model in (5.6) with $\Pr(0|0) = 0.98$, where $\mathit{\Pi}_{\text{II}} = 0.1$ and $\sigma_{\text{i}}^2 = 1000\sigma_{\text{b}}^2$. Three different NBI environments are considered

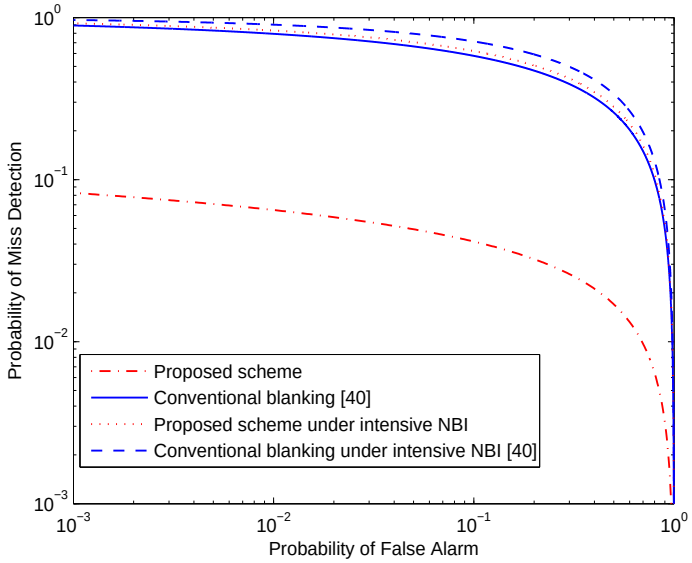

Figure 5.3: Complementary ROC curves for different IN detection schemes over the PLC system.

as: weakly disturbed ($\mu = 0.01$; $p_v/\sigma_{\rm b}^2 = 20$ dB), strongly disturbed ($\mu = 0.9$; $p_v/\sigma_{\rm b}^2 = 20$ dB) and intensively disturbed ($\mu = 0.1$; $p_v/\sigma_{\rm b}^2 = 40$ dB). Figs. 5.4, 5.5 and 5.6 are carried out in the absence of NBI ($\beta = 0$), while the BER performance in Figs. 5.7 and 5.8 is evaluated in the presence of NBI ($\beta = 1$). Moreover, the results obtained from the proposed scheme are compared to those from the previous IN mitigation with the optimal blanking threshold in [40].

In Fig. 5.3, the performance of detecting the nonzero entries in the IN vector of the proposed scheme is evaluated, in comparison with the conventional detection-based blanking scheme, using the complementary ROC ($1 - \mathcal{P}_d$ versus $\mathcal{P}_f$) over the non-NBI and intensive NBI scenarios. The curves are illustrated for SNR = 25 dB, which is high enough to achieve a negligible $\sigma_{\hat{\rm e}}^2$ for the proposed scheme. It can be seen in Fig. 5.3 that the proposed scheme which can achieve a sufficiently high detection rate by causing a negligible false alarm rate, outperforms the conventional blanking in terms of the ability of IN entries detection. According to the test statistics for the blanking nonlinearity, the associated threshold-based IN detection is disturbed by the high PAPR, resulting in a poor ROC performance.

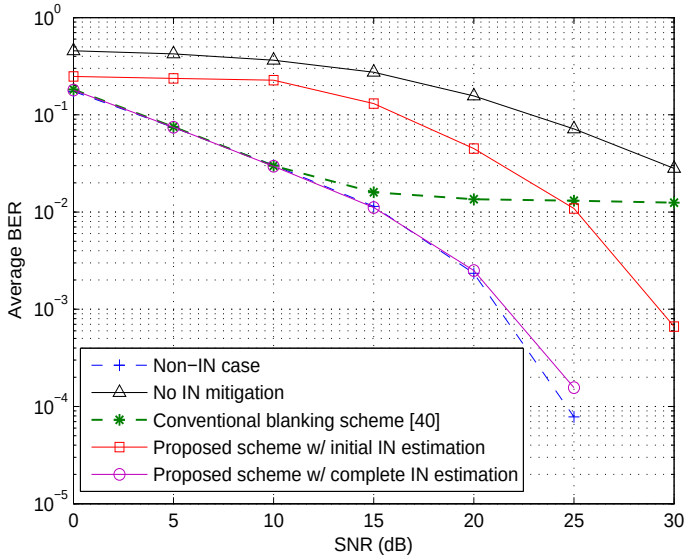

Figure 5.4: BER performance comparison of different mitigation schemes over the PLC system using data subcarriers only ($\beta = 0$).

Meanwhile, the curves reveal that when the system is intensively disturbed by added NBI, the rate of indistinguishable IN becomes quite high for both schemes under the impact of high NBI power.

Fig. 5.4 shows the BER performance comparison between the proposed IN mitigation scheme and the conventional blanking scheme using data subcarriers only. Let P_e indicate the transmitted PSD. The horizontal axis denotes the signal-to-background noise power ratio $P_e/\sigma_{\mathrm{b}}^2$, which varies from 0 dB to 30 dB. For a maximum allowed false alarm rate $\mathcal{P}_f = 10^{-3}$ in (5.22), the according threshold value normalised to $\sigma_{\hat{\mathrm{n}}}$ in (5.24) is set as 3.29. It can be observed that the proposed scheme with complete IN estimation clearly exhibits a much better performance than the conventional blanking scheme especially in high SNR region, where the curve for blanking illustrates an error floor over various SNR values. According to (5.9) and (5.15), the high SNR would disturb the IN detection for blanking nonlinearity, which however provides benefits on the proposed scheme by causing a fairly low mean squared decision error $\sigma_{\hat{\mathrm{e}}}^2$. Thus, even with initial IN estimation, the curves reveal that the proposed IN mitigation outperforms

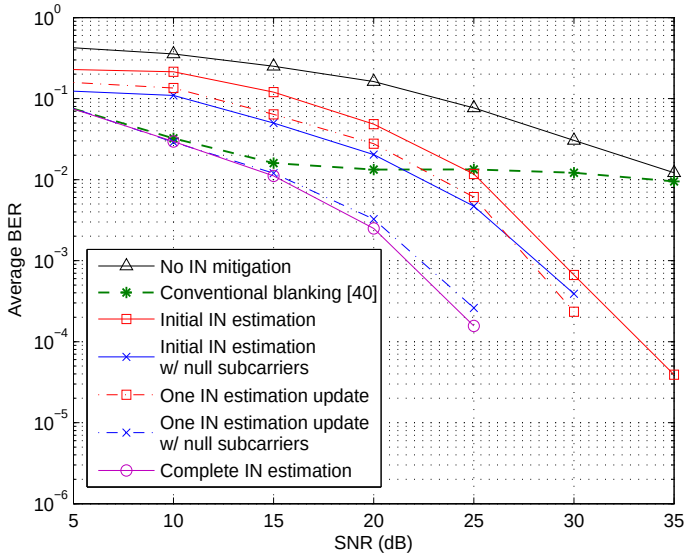

Figure 5.5: BER performance comparison of different mitigation schemes to show the benefit of using null subcarriers in the proposed scheme ($\beta = 0$).

the blanking nonlinearity when the SNR value achieves 25 dB or above. The complete IN estimation using data subcarriers only normally costs four or five iterations, where the soft decision $\hat{S}$ cannot be improved any more and should serve as the hard decision for data output.

The benefit of adopting null subcarriers in the proposed mitigation scheme is learned in Fig. 5.5 in terms of BER performance. According to (5.21), use of the null subcarriers containing no decision errors results in a lower $\sigma_{\hat{\epsilon}}^2$, yielding an improved IN estimation. Hence, the IN can be thoroughly mitigated using the feedback of the estimated IN as in (5.18) with a reduced number of iterations. The results show that with the aid of null subcarriers, only one update of the estimated IN vector is required to lead a BER performance approaching that from the complete IN estimation.

In Fig. 5.6, a pre-processing block is adopted to extend the use of null subcarriers, where the performance of the proposed receiver is further enhanced by the feedback of an improved initial IN estimation. It can be seen that the proposed scheme with pre-TD processing achieves 5 dB SNR gain over that without

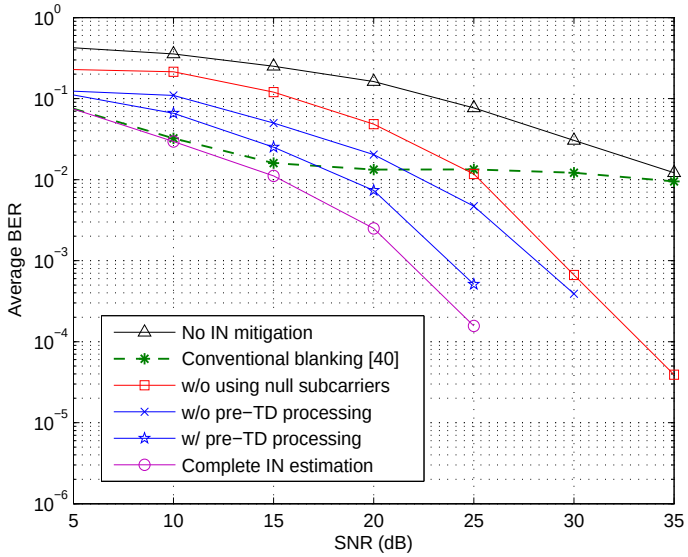

Figure 5.6: BER performance comparison under the proposed scheme with initial IN estimation to show the benefit of adopting the pre-TD processing ($\beta = 0$).

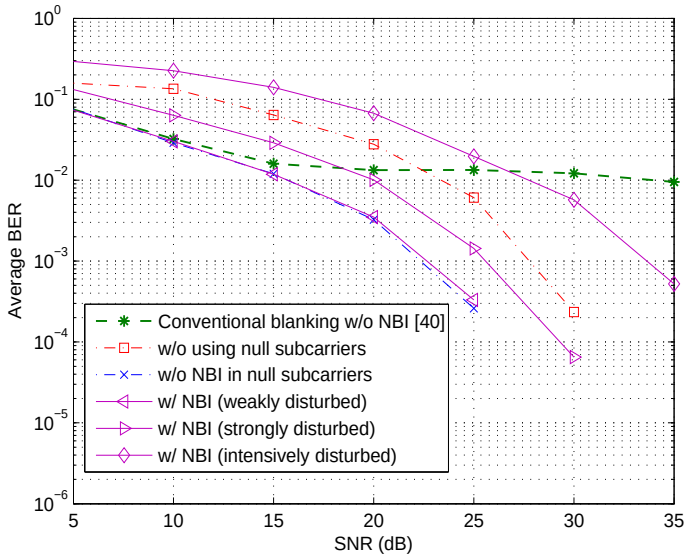

Figure 5.7: BER performance comparison under the proposed scheme with one update of the IN estimation to see different impacts of NBI on the IN estimation ($\beta = 1$).

pre-TD processing. Under the pre-TD processing aided initial IN estimation, a fairly good BER performance can be obtained without iteratively updating the estimated IN vector.

In the presence of NBI ($\beta = 1$), the performance of detecting the nonzero

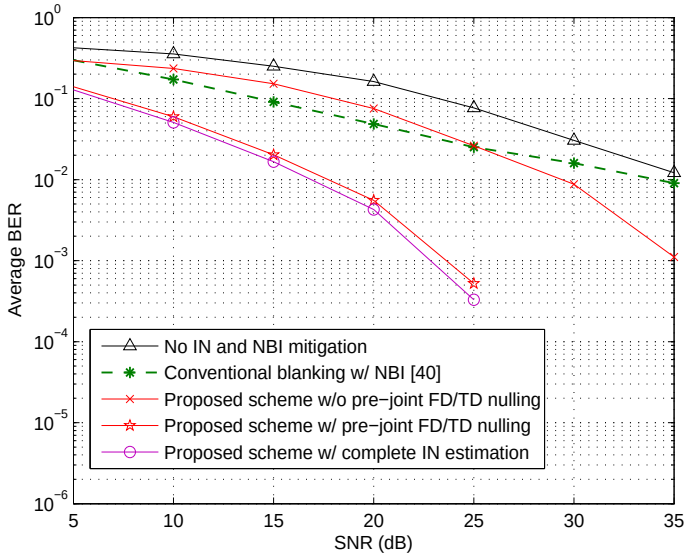

Figure 5.8: BER performance comparison under the proposed scheme with the initial IN estimation intensively disturbed by NBI to show the benefit of adopting the pre-joint FD/TD nulling ($\beta = 1$).

entries in the IN vector is affected by the added σ_v^2 in (5.31) and (5.32), which may result in an incomplete IN mitigation. The impacts of different NBI environments are depicted in Fig. 5.7 in terms of BER performance. It can be observed that the proposed receiver works well under the weak disturbance of NBI, which achieves BER values close to that with no NBI. In the case of strong disturbance which has a high value of NBI disturbance ratio $\mu = 0.9$, the null subcarriers assisted method requires 2.5 dB SNR gain to achieve the same BER of no NBI, which however still outperforms that without using null subcarriers by approximately 2.5 dB. When the system is intensively disturbed where the NBI to background noise power ratio at the NBI contaminated subcarriers is considered as 40 dB, the according BER curve reveals a harmful impact from the ingress of the intensive NBI, which requires to be eliminated properly before the IN vector reconstruction.

In Fig. 5.8, the benefit of adopting the pre-joint FD/TD nulling is evaluated under the impact of intensive NBI disturbance. To achieve a sufficiently low false alarm rate $\mathcal{P}_f = 10^{-4}$, the threshold for pre-FD nulling in (5.34) normalised to

σ_{b} is set as 39.10, while the pre-TD nulling threshold in (5.37) normalised to $\sigma_{\hat{\mathrm{r}}}$ has its value of 3.89. It can be seen that the deployment of the pre-joint FD/TD nulling at the proposed receiver, results in a near-optimal BER performance with the initial IN estimation only. The IN vector is accurately reconstructed by the initial estimation in the proposed scheme with the aid of pre-joint FD/TD nulling, which outperforms that without pre-mitigation and the conventional blanking scheme at the BER of 10^{-2} by approximately 12 dB and 17 dB, respectively. The effectiveness of the proposed IN mitigation scheme is validated by simulation results, even under the environment of intensive NBI.

5.4 Summary

In this chapter, the IN mitigation for OFDM-based PLC systems have been studied. A null subcarriers assisted iterative receiver has been proposed to reconstruct the IN vector, considering the potential NBI contaminated null subcarriers. The proposed IN mitigation scheme has been evaluated in the scenarios of NBI absence and NBI presence, respectively. The ROC expressions of detecting nonzero entries in the IN vector have been given, which are conditioned by the presence of NBI. In the absence of NBI, the improvement in IN detection capability of the proposed scheme over the conventional blanking scheme, has been quantified by the complementary ROC curves. While both schemes can be harmfully affected under the disturbance of intensive NBI. Moreover, a pre-FD/TD nulling block has been adopted as an extended use of null subcarriers in the proposed receiver, in order to improve the initial IN estimation by joint mitigating the high-amplitude NBI and IN. The associated thresholds for the detection of NBI and IN can be simply computed, given a desired false alarm rate. Furthermore, simulation results have demonstrated a much better BER performance of the proposed receiver than that of the blanking scheme especially in the high SNR region, meanwhile, a reduced number of iterations is required with the aid of

null subcarriers in the proposed scheme. In the presence of intensive NBI that the power of the NBI contaminated subcarriers is extremely high, the IN vector cannot be reconstructed accurately. Hence, the pre-mitigation is implemented, which makes it possible to achieve a BER performance with initial IN estimation only close to that with complete IN estimation. The proposed IN mitigation scheme is particularly useful at PLC receivers since it combats the disturbance of NBI whenever the NBI is present, and can probably be applied to any other communication systems disturbed by both IN and NBI.

Chapter 6

Higher-Order Statistics Assisted Narrowband Interference Detection

Cognitive PLC is of the interest [52] to increase the transmission frequencies by using the available radio frequencies. NBI is one of the main sources causing pollution to the PLC spectrum [2], which should be dealt with properly. Accurate detection of NBI supports system performance enhancement in order to achieve effective transmission, and also provides a reliable protection of radio applications for cognitive PLC.

As learned in Chapter 4, NBI from radio systems may become a salient issue that degrades the PLC system performance, since the unshielded power line can be a good antenna picking up the radios around [6]. Here, we focus on detecting the NBI from various nearby radio applications, since it has great impact on system performance and is significant for cognitive PLC. Most existing NBI detection schemes are for cognitive radio applications, such as matched filtering, amplitude detection and energy detection methods [4, 51]. The well-known energy detector is simple and fast, however, it is sensitive to threshold setting and can not operate for low-power scenarios. A cooperative energy detection scheme was proposed for cognitive PLC in [54], however, NBI was detected from different networks rather than at the receiver of a single network. Higher-order statistics

(HOS) based detection techniques [70] are an alternative solution to the cooperative method, which has significantly better performance especially in low-power NBI scenarios. However, there lacks a generic theoretical analysis of detection performance and the previous work did not consider the common disturbance of IN for PLC systems. Referring to Chapter 3, PLC aperiodic IN incurred by switching/plugging/unplugging transients of electric appliances such as heater, oven and incandescent lamp [18, 30] is considered in this chapter. The IN often occurs randomly in bursts and degrades the PLC system performance significantly [2, 25]. Also, the time-domain IN has its energy spread over a wideband channel and increases the overall power line noise level, which brings a huge challenge to the conventional NBI detectors. A suitable detection scheme is required to qualify the NBI detection over PLC systems.

In this chapter, we propose a novel HOS based detection scheme for NBI from radio applications in cognitive PLC systems. Our work is different in the following aspects. First, our detection scheme is based on HOS of radio signals only, and is less complex than the method in [70], where both third-order and fourth-order statistics are used for NBI detection. It also outperforms the existing NBI detection schemes based on amplitude level [31] and energy level [71], and in particular, demonstrates more robustness against low-power NBI. Second, we consider the presence of IN, which is a challenging and practical problem, but was not addressed in the previous work on NBI detection. The two-level hierarchical MC based model proposed in Chapter 3 is applied to generate the occurrence-dependent IN. Third, we present a closed-form analysis, including analysis of the NBI detection probability for various detection schemes (amplitude-, energy- and HOS-based detection schemes), as well as analysis of the system capacity. While the work in [70] was verified by simulations only. The proposed scheme is shown to lead to a higher system capacity than the previous schemes, and is therefore more suitable for cognitive PLC networks.

In Section 6.1, a system model is presented to describe the NBI detection scenarios for PLC. In Section 6.2, the proposed NBI scheme is presented. NBI detection probability is analysed for the proposed HOS based scheme and also for the conventional schemes in Section 6.3. In Section 6.4, the system capacity analysis is presented. The conclusion is remarked in Section 6.5.

6.1 System Model

The block diagram of an indoor broadband PLC system is depicted in Fig. 6.1, where $s(t)$ represents the transmit signal and $r(t)$ is the received signal. A hybrid of the aperiodic IN $n_{\mathrm{i}}(t)$, the NBI $v(t)$ and the background noise $n_{\mathrm{b}}(t)$ are the added disturbance at PLC receiver. While $n_{\mathrm{i}}(t)$ is caused from any potential switching/plug transients of the appliances in the system ($n_{\mathrm{i}}(t) = 0$ means no noise), and $v(t)$ is from various nearby radio applications ($v(t) = 0$ means no interference). The dashed-line block indicates the proposed NBI detection scheme at the receiver, considering two different scenarios. Without loss of generality, we assume only one aperiodic IN source and one narrowband interferer. The background noise $n_{\mathrm{b}}(m)$ is assumed to be AWGN with zero mean and variance σ_{b}^2. $n_{\mathrm{i}}(m)$ is the considered IN at PLC receiver, which has a zero mean and variance σ_{i}^2 . It is assumed that the variance of the background noise is much lower than that of the IN, *i.e.*, $\sigma_{\mathrm{b}}^2 \ll \sigma_{\mathrm{i}}^2$. The NBI $v(m)$ is from various nearby radio applications.

Overall Disturbance Model: In a discrete-time system, since both IN and NBI occur with probabilities, the general added disturbance $n(m)$ can be expressed as

$$n(m) = \alpha \cdot n_{\mathrm{i}}(m) + \beta \cdot v(m) + n_{\mathrm{b}}(m) \tag{6.1}$$

In (6.1), α, $\beta \in \{0,\ 1\}$ are the parameters indicating the occurrence states (absence or presence) of the IN and NBI respectively. $\Pr(\alpha = 1)$ denotes the IN occurrence probability, while $\Pr(\beta = 1)$ reflects the NBI occurrence probability.

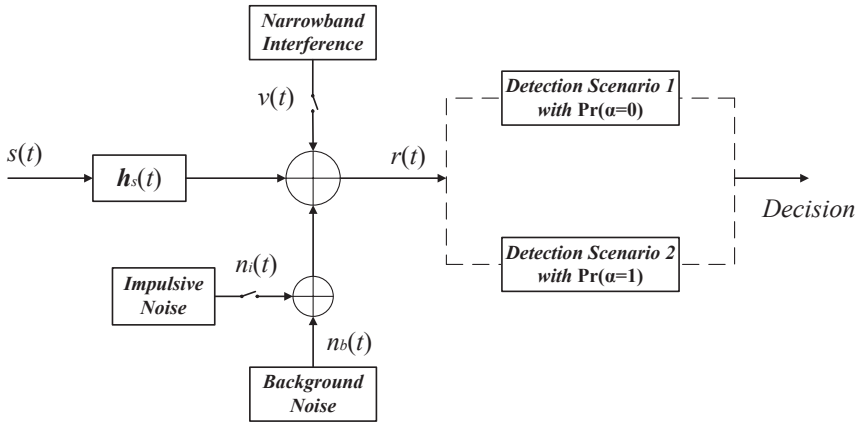

Figure 6.1: Block diagram of a PLC system with NBI detection.

Impulsive Noise Model: Referring to Chapter 3, it is assumed that each event of the switching/plugging transients produces a noise burst. The burst IN often occurs with much higher power over the background noise, which increases the overall power line noise level and brings challenges for NBI detection. The occurrence of a burst can be described by the first level MC, and the occurrence of individual impulses within a burst are characterised by the second level MC. The first-order Markov process can be described by its transition probability matrix, which is conditioned by the previous one state. Steady-state probability (SSP) can be applied to define the occurrence probability of an event under discrete-time Markov process, where the next state probabilities have dependence on the current state probabilities and are determined by the transition probability matrix as

$$\boldsymbol{\Pi}_{t+1} = \boldsymbol{P}\boldsymbol{\Pi}_t \tag{6.2}$$

where $\boldsymbol{P}$ is transition probability matrix, which has the elements defined by $\Pr(\{t+1\}|\{t\})$. The probability of the next state '$\{t+1\}$' is conditioned by the current state '$\{t\}$'. $\boldsymbol{\Pi}_t$ is a column vector whose elements represent the state probabilities at time t. In the steady state, we have $\boldsymbol{\Pi}_{t+1} = \boldsymbol{\Pi}_t$.

Let Π_{I} denote the SSP of incurring a burst in the first level MC, and '$\{t\}_{\mathrm{I}}$' indicate the state of first level MC at the discrete-time t. The corresponding state

has a value of '1' in the presence of a burst, otherwise '0' represents the absent of noise burst, solving (6.2) yields

$$\Pi_{\mathrm{I}} = \frac{\Pr(\{t+1\}_{\mathrm{I}}=1|\{t\}_{\mathrm{I}}=0)}{\Pr(\{t+1\}_{\mathrm{I}}=1|\{t\}_{\mathrm{I}}=0)+\Pr(\{t+1\}_{\mathrm{I}}=0|\{t\}_{\mathrm{I}}=1)} \tag{6.3}$$

which is weighted by the corresponding transition probabilities. Π_{II} indicates the SSP of producing an individual impulse in the second level MC, which can be derived in a similar way as

$$\Pi_{\mathrm{II}} = \frac{\Pr(\{t+1\}_{\mathrm{II}}=1|\{t\}_{\mathrm{II}}=0)}{\Pr(\{t+1\}_{\mathrm{II}}=1|\{t\}_{\mathrm{II}}=0)+\Pr(\{t+1\}_{\mathrm{II}}=0|\{t\}_{\mathrm{II}}=1)} \tag{6.4}$$

where the steady-state probabilities Π_{I} and Π_{II} are independent of the initial transition probabilities.

In the presence of a noise burst, the corresponding arrival rate of the sample impulses normalised to the sampling interval, follows the reciprocal value of the number of consecutive non-impulse states k between two impulses, which has the probability distribution for remaining in the non-impulse state as

$$P(k) = \Pr(0|0)^{k-1} \cdot (1 - \Pr(0|0)) \tag{6.5}$$

The steady-state probabilities Π_{I}, Π_{II} and the arrival model can describe the particular impulsive environment in the considered PLC system accurately, which are important to verify the effectiveness of the proposed NBI detection scheme in the presence of IN.

6.2 HOS-based NBI Detection

As shown in Fig. 6.1, the NBI detection scheme should be implemented in both scenarios of IN absence ($\alpha = 0$) and IN presence ($\alpha = 1$), with the probabilities of $\Pr(\alpha = 0)$ and $\Pr(\alpha = 1)$, respectively.

The proposed NBI detection scheme is actually to classify between the following two hypotheses

$$n(m) = \begin{cases} \alpha \cdot n_{\mathrm{i}}(m) + n_{\mathrm{b}}(m) & \mathcal{H}_0, \\ \alpha \cdot n_{\mathrm{i}}(m) + v(m) + n_{\mathrm{b}}(m) & \mathcal{H}_1. \end{cases} \tag{6.6}$$

where $\alpha = 0$ denotes that NBI detection is performed in the absence of PLC IN, while $\alpha = 1$ indicates the scenario often applied to indoor PLC systems that wideband IN is present during the NBI detection. The two hypotheses of $\mathcal{H}_0$ and $\mathcal{H}_1$ refer to NBI absence and NBI presence, respectively.

Generally, to test the two hypotheses $\mathcal{H}_0$ and $\mathcal{H}_1$, the test statistics $\mathcal{K}$ for the k^{th}-order statistics can be expressed as

$$\mathcal{K} = \sum_{m=1}^{N} |n(m)|^k \tag{6.7}$$

The decision can be obtained by comparing the test statistics of $\mathcal{K}$ against a certain threshold λ. The performance of a detector can be evaluated by the probability of detection $\mathcal{P}_d$ and the probability of a false alarm $\mathcal{P}_f$, which are defined as

$$\mathcal{P}_d = \Pr(\mathcal{K} > \lambda | \mathcal{H}_1) \tag{6.8}$$

$$\mathcal{P}_f = \Pr(\mathcal{K} > \lambda | \mathcal{H}_0) \tag{6.9}$$

where $\mathcal{P}_d$ denotes the probability that a signal is correctly detected when an NBI event occurs, and $\mathcal{P}_f$ represents the probability that an NBI occurrence event is wrongly detected when there is no NBI present. $\mathcal{P}_d$ and $\mathcal{P}_f$ of a detector are two key interrelated parameters to assess the detection performance. The given threshold λ results in a trade-off, since a high value of $\mathcal{P}_d$ and a low value of $\mathcal{P}_f$ are expected. A best trade-off can be selected for specific system requirements, and varies according to different criteria [31]. The decision threshold λ varies according to different values of test statistics $\mathcal{K}$ for a given $\mathcal{P}_f$, and is conditioned by the parameter value of α.

HOS is an effective tool for NBI detection. In [70], an HOS based method was empirically evaluated by a testbed for cognitive radio. The bounds of the probability distributions of the HOS were given in [72] according to the Chebyshev inequality. There lacks analysis of the probability distributions of HOS

and analytical connection between statistics of different orders. In the following, closed-form expressions are presented for the HOS-based probabilities.

With a large number of OFDM subcarriers, a large number N of OFDM subcarriers, the unknown signal $v(m)$ follows a Gaussian distribution of $\mathcal{N}(0, \sigma_v^2)$. For the fourth-order statistics of $\mathcal{K}$, it follows an example of K-distribution [73], which can be defined as a product distribution of two random variables having a gamma distribution. For $\mathcal{K} > 0$, the PDF of a generalized K-distribution with the normalised average power can be shown as [74]

$$f(\mathcal{K}; \nu, L) = \frac{2(L\nu)^{(L+\nu)/2}}{\Gamma(L)\Gamma(\nu)} \mathcal{K}^{\frac{L+\nu}{2}-1} K_{\nu-L}\left(2\sqrt{L\nu\mathcal{K}}\right) \tag{6.10}$$

where $\Gamma(\cdot)$ denotes the gamma function [68], ν and L are shaping parameters. $K_m(\cdot)$ in (6.10) is the mth-order modified Bessel function of the second kind. To simplify the K-distribution algorithm, an accurate approximation to the PDF of K-distribution has been given in [75], in order to avoid detailed calculation involving modified Bessel functions of the second kind. Hence, with $2N$ degrees of freedom that $L = \nu = N$, (6.10) can be simplified as

$$f(\mathcal{K}; \sigma_{n,\alpha}^2) = \frac{N^2\sqrt{\pi}\left(N\mathcal{K}^{1/2}\right)^{2N-\frac{5}{2}}}{\left(\sqrt{2}\sigma_{n,\alpha=0}\right)^{4N-1}\Gamma^2(N)} \cdot e^{-\frac{N\mathcal{K}^{1/2}}{\sigma_{n,\alpha}^2}} \tag{6.11}$$

where $n = 1, 2$, with $\sigma_{1,\alpha=0}^2 = \sigma_{\mathrm{b}}^2$ and $\sigma_{2,\alpha=0}^2 = \sigma_{\mathrm{b}}^2 + \sigma_v^2$ for non-impulsive scenarios. While, $\sigma_{1,\alpha=1}^2 = \sigma_{\mathrm{b}}^2 + \mathit{\Pi}_{\mathrm{II}}\sigma_{\mathrm{i}}^2$ and $\sigma_{2,\alpha=1}^2 = \sigma_{\mathrm{b}}^2 + \mathit{\Pi}_{\mathrm{II}}\sigma_{\mathrm{i}}^2 + \sigma_v^2$ when the scheme is disturbed by IN.

The cumulative distribution function (CDF) of the K-distribution can be defined as $F(\mathcal{K}; \lambda) = \Pr(\mathcal{K} \leq \lambda)$, which is the integral of its PDF in (6.11) and expressed as

$$F(u; \lambda) = \int_0^{\lambda} \begin{cases} f(u; \sigma_{1,\alpha}^2) & \mathcal{H}_0 \\ f(u; \sigma_{2,\alpha}^2) & \mathcal{H}_1 \end{cases} du. \tag{6.12}$$

In threshold-aided signal detection, $\bar{F}(\mathcal{K}; \lambda) = \Pr(\mathcal{K} > \lambda) = 1 - F(\mathcal{K}; \lambda)$ denotes the complementary cumulative distribution function (CCDF), which has

applications in statistical hypothesis testing. For the proposed HOS-based detector, CCDF of $\mathcal{K}$ can be obtained by solving (6.12), and used to evaluate the detection probabilities.

In OFDM systems, the decision metric of $\mathcal{K}$ in (6.7) is equivalent to the test statistics of the frequency-domain fourth order cumulants [76] after performing the fast Fourier transform (FFT), which can be expressed as

$$\begin{aligned}\mathcal{C}_4(\omega) =& \frac{1}{N}\sum\nolimits_z n^2(z)n^2(z+\omega) - \left[\frac{1}{N}\sum\nolimits_z n^2(z)\right]^2 \\ & - 2\left[\frac{1}{N}\sum\nolimits_z n(z)n(z+\omega)\right]^2 \end{aligned} \tag{6.13}$$

The frequency-domain kurtosis is estimated by setting $\omega = 0$,

$$\mathcal{C}_4(0) = \frac{1}{N}\sum\nolimits_z n^4(z) - 3\left[\frac{1}{N}\sum\nolimits_z n^2(z)\right]^2 \tag{6.14}$$

(6.13) has its inverse FFT counterpart to be shown as [77]

$$F^{-1}\{\mathcal{C}_4(\tau)\} = \left|\{n * n\}(\tau)\right|^2 - \left[\mathcal{C}_2(0)\right]^2\delta(\tau) - 2\{R * R\}(\tau) \tag{6.15}$$

where $*$ denotes the discrete-time convolution, *e.g.*, $\{n * n\}(\tau) = \sum_m n(m)n(\tau - m)$, the variance $\mathcal{C}_2(0) = E[n^2(m)]$ and $R(\tau)$ is the autocorrelation of $n(m)$. Thus, we have

$$F^{-1}\{\mathcal{C}_4(0)\} = \left[\mathcal{C}_2(0)\right]^2 - \left[\mathcal{C}_2(0)\right]^2 - 2\{R * R\}(\tau)|_{\tau=0} \tag{6.16}$$

i.e.,

$$\left|F^{-1}\{\mathcal{C}_4(0)\}\right| = 2\sum\nolimits_m |n(m)|^4 \tag{6.17}$$

which is the test statistics of the proposed HOS-based method in (6.7) with $k = 4$.

6.3 Analysis of NBI Detection Probabilities

In this section, we present an analysis of the NBI detection probabilities, including the correct detection probability and false alarm probability of an NBI occurrence in Subsection 6.3.1, and the overall NBI detection probability in Subsection 6.3.2.

6.3.1 Receiver Operating Characteristic Performance

In order to evaluate the proposed detector performances, the receiver operating characteristic (ROC) curve and its variants are commonly used [67]. ROC curves explore the relationship between the probability of detection and the probability of false alarm for a range of varied thresholds. Different NBI detection approaches result in different ROC curves for the considered PLC system and hence, it provides a valuable tool to select a more reliable detector according to the ROC performance comparisons among a number of different detectors. For a given probability of false alarm, the higher the probability of detection, the better the detection technique is. On the other hand, with a robust detector, it is possible to meet the requirement of the probability of detection for a reduced probability of false alarm.

The complementary ROC performance [67], defined as $(1-\mathcal{P}_d)$ vs. $\mathcal{P}_f$, is to explore the relationship between the probability of miss detection and the probability of false alarm. In the following, we present analysis of $\mathcal{P}_d$ and $\mathcal{P}_f$ for the proposed HOS based detection scheme, and also for the first-order based scheme [31] and the second-order statistics (SOS) based scheme [71], which were not analysed in the literature.

In the steady state of IN, the PDF of the combined power line impulsive and background noise is given by

$$f(\mathcal{H}_0) = (1-\mathit{\Pi}_{\rm II})\cdot\mathcal{N}(0,\sigma_{\rm b}^2) + \mathit{\Pi}_{\rm II}\cdot\mathcal{N}(0,\sigma_{\rm b}^2+\sigma_{\rm i}^2) \tag{6.18}$$

HOS based Detection: For the proposed HOS-based NBI detector, CCDF of $\mathcal{K}$ can be obtained by solving the complementary of (6.12) *i.e.*, $\bar{F}(\mathcal{K};\lambda) = 1-F(\mathcal{K};\lambda)$. Under $\mathcal{H}_0$ in (6.6), $\mathcal{P}_{f,\alpha}$ can be evaluated using the CCDF $\bar{F}(\mathcal{K};\lambda|\mathcal{H}_0)$ yields

$$\mathcal{P}_{f,\alpha} = \frac{\sqrt{\pi}}{2^{2N-\frac{3}{2}}\Gamma^2(N)}\cdot\Gamma\left(2N-\frac{1}{2},\frac{\lambda}{4\sigma_{1,\alpha}^4}\right) \tag{6.19}$$

where $\Gamma(\cdot,\cdot)$ denotes the upper incomplete gamma function [68]. $\mathcal{P}_{f,\alpha}$ is the

probability of false alarm. Likewise, under $\mathcal{H}_1$ in (6.6), the probability of detection $\mathcal{P}_{d,\alpha}$ can be obtained similarly as

$$\mathcal{P}_{d,\alpha} = \frac{\sqrt{\pi}}{2^{2N-\frac{3}{2}}\Gamma^2(N)} \cdot \Gamma\left(2N - \frac{1}{2}, \frac{\lambda}{4\sigma_{2,\alpha}^4}\right) \tag{6.20}$$

where the values of both $\mathcal{P}_{f,\alpha}$ and $\mathcal{P}_{d,\alpha}$ are conditioned by the occurrence status of IN. In the absence of IN ($\alpha = 0$), the detection and false alarm probabilities can be derived using $\sigma_{1,\alpha=0}^2 = \sigma_{\mathrm{b}}^2$ and $\sigma_{2,\alpha=0}^2 = \sigma_{\mathrm{b}}^2 + \sigma_v^2$. While, in the presence of IN ($\alpha = 1$), the associated probabilities can be calculated with $\sigma_{1,\alpha=1}^2 = \sigma_{\mathrm{b}}^2 + \mathit{\Pi}_{\mathrm{II}}\sigma_{\mathrm{i}}^2$ and $\sigma_{2,\alpha=1}^2 = \sigma_{\mathrm{b}}^2 + \mathit{\Pi}_{\mathrm{II}}\sigma_{\mathrm{i}}^2 + \sigma_v^2$.

First-Order based Detection: The first-order statistics of $\mathcal{K}$ follow a Gaussian distribution according to these assumptions. Thus, for an amplitude-level based detector [31], the detection and false alarm probabilities can be expressed as

$$\mathcal{P}_{f,\alpha} = \mathrm{erfc}\left(\frac{\lambda}{\sigma_{1,\alpha}\sqrt{2}}\right) \tag{6.21}$$

$$\mathcal{P}_{d,\alpha} = \mathrm{erfc}\left(\frac{\lambda}{\sigma_{2,\alpha}\sqrt{2}}\right) \tag{6.22}$$

where erfc is the complementary error function [68]. For the non-IN case, $\sigma_{1,\alpha=0}^2 = \sigma_{\mathrm{b}}^2$ and $\sigma_{2,\alpha=0}^2 = \sigma_{\mathrm{b}}^2 + N\sigma_v^2$. Under the disturbance of IN, $\sigma_{1,\alpha=1}^2 = \sigma_{\mathrm{b}}^2 + \mathit{\Pi}_{\mathrm{II}}\sigma_{\mathrm{i}}^2$ and $\sigma_{2,\alpha=1}^2 = \sigma_{\mathrm{b}}^2 + \mathit{\Pi}_{\mathrm{II}}\sigma_{\mathrm{i}}^2 + N\sigma_v^2$.

SOS based Detection: For the second-order statistics of $\mathcal{K}$, which is widely applied in spectrum sensing techniques, $\mathcal{K}$ follows a chi-square distribution with $2N$ degrees of freedom (special case of gamma distribution). Hence, the probabilities $\mathcal{P}_{f,\alpha}$ and $\mathcal{P}_{d,\alpha}$ of an energy detector [71] can be calculated as

$$\mathcal{P}_{f,\alpha} = \frac{\Gamma\left(N, \frac{\lambda}{2\sigma_{1,\alpha}^2}\right)}{\Gamma(N)} \tag{6.23}$$

$$\mathcal{P}_{d,\alpha} = \frac{\Gamma\left(N, \frac{\lambda}{2\sigma_{2,\alpha}^2}\right)}{\Gamma(N)} \tag{6.24}$$

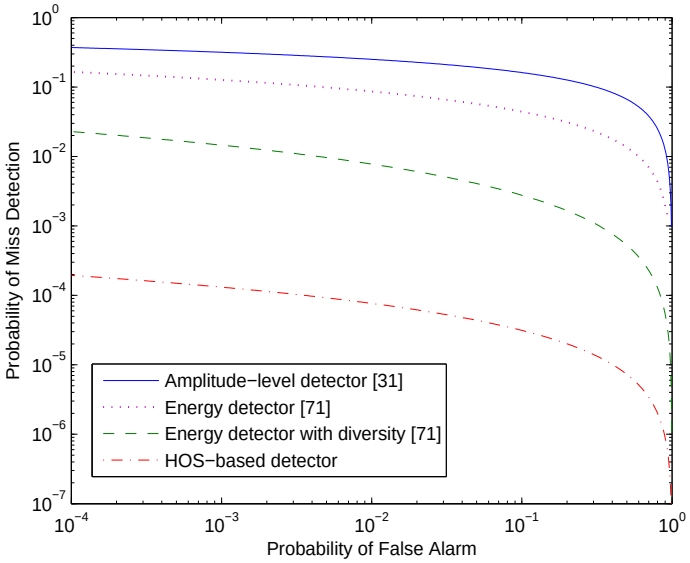

Figure 6.2: Complementary ROC curves for different NBI detection schemes in the case of background noise only.

where $\sigma^2_{1,\alpha=0} = \sigma^2_{\rm b}$ and $\sigma^2_{2,\alpha=0} = \sigma^2_{\rm b} + \sigma^2_v$ for non-impulsive scenarios. While, $\sigma^2_{1,\alpha=1} = \sigma^2_{\rm b} + \Pi_{\rm II}\sigma^2_{\rm i}$ and $\sigma^2_{2,\alpha=1} = \sigma^2_{\rm b} + \Pi_{\rm II}\sigma^2_{\rm i} + \sigma^2_v$ when the scheme is disturbed by IN.

In Fig. 6.2, the complementary ROC performances of different NBI detection schemes are shown for the case with background noise only ($\alpha = 0$), with $N = 128$, $\sigma^2_{\rm b} = 1$ and the 20 dB NBI power normalised to the background noise power. The proposed method performs much better than the approaches in [31, 71] and maintains almost a perfect detection at a negligible false alarm rate.

It can be seen that the widely used SOS based energy detector has a moderate performance with a simple and fast operation. However, it is sensitive to threshold and can not operate for a relatively low NBI power (weakly disturbed) scenario. [71] proposes to apply diversity schemes such as square-law combining (SLC) and square-law selection (SLS) to improve the energy detection capability. The proposed HOS-based detection method can be treated as implementing a second-order diversity of the SLC, which has the property that

$$\Pr\left(\sum_{i=1}^{\mathcal{L}} \mathcal{K}_i > \lambda\right) \sim \Gamma\left(\mathcal{L}N, \lambda\right) \tag{6.25}$$

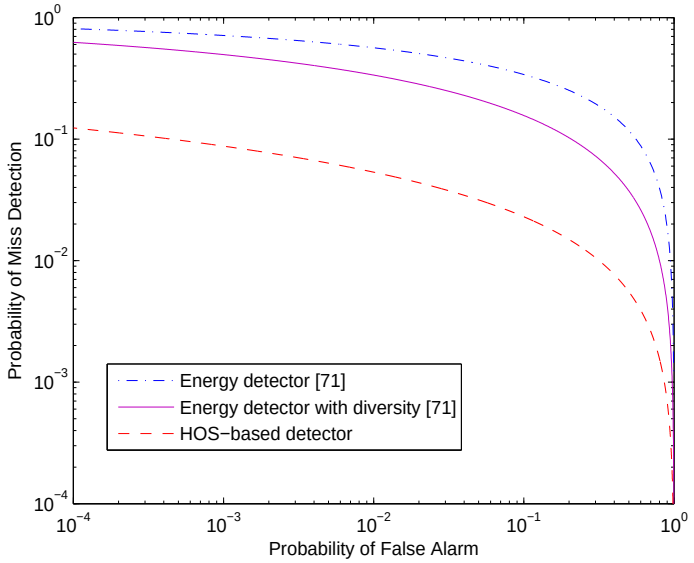

Figure 6.3: Complementary ROC curves for different NBI detection schemes in the presence of IN ($\sigma_{\mathrm{i}}^2/\sigma_{\mathrm{b}}^2 = 100$, $\Pi_{\mathrm{II}} = 0.1$ and $\Pr(0|0) = 0.98$).

where $\mathcal{L}$ diversity branches are assumed. In the case that $\mathcal{L} = 2$ and N is large enough, the improved energy detector performance is analogous to that of our proposed detector in analytical form as (6.19) and (6.20). However, due to the higher performance sensitivity to HOS of NBI than that to the NBI energy, approximately half of the gain over the amplitude-level detector is lost when applying the energy detector with diversity scheme.

In Fig. 6.3, the complementary ROC performance considering the impact of power line IN ($\alpha = 1$) for $\sigma_{\mathrm{i}}^2 = 100\sigma_{\mathrm{b}}^2$, $\Pi_{\mathrm{II}} = 0.1$ and $\Pr(0|0) = 0.98$ is evaluated, rather than for the background noise only case as shown in Fig. 6.2. In PLC channel, the wideband IN power normalised to the background noise power is 10 dB since the time-domain IN spreads its power over the whole PLC frequency spectrum, which causes an increase of the average noise level. Thus, the radio interference has relatively low power above the noise level and the weak NBI would be submerged in the strong power line noise, increasing the risk of high miss detection rate. It can be seen in Fig. 6.3 that the rate of indistinguishable NBI is quite high by deploying the energy detector under IN, while the proposed HOS-

based method presents a similar performance as the energy detector achieved for background noise only.

6.3.2 Overall Detection Performance

For the considered PLC system in Fig. 6.1, the potential IN source separates the NBI detection into two scenarios, with the probability $\Pr(\alpha = 0)$ for the scenario 1 of IN absence and the probability $\Pr(\alpha = 1)$ for the scenario 2 of IN presence. Here, we evaluate the overall detection performance of the proposed HOS-based method considering both scenarios.

Let $\pi(0)$ and $\pi(1)$ be the SSP for the scenario of IN absence and the scenario of IN presence, respectively. The overall probability of false alarm $\bar{\mathcal{P}}_f$ and the overall probability of detection $\bar{\mathcal{P}}_d$ can be written as

$$\bar{\mathcal{P}}_f = \sum\nolimits_{\alpha=0}^{1} \pi(\alpha) \cdot \mathcal{P}_{f,\alpha} \tag{6.26}$$

$$\bar{\mathcal{P}}_d = \sum\nolimits_{\alpha=0}^{1} \pi(\alpha) \cdot \mathcal{P}_{d,\alpha} \tag{6.27}$$

where $\sum_{\alpha=0}^{1} \pi(\alpha) = \Pr(\alpha = 0) + \Pr(\alpha = 1) = 1$, and assuming that $\Pr(\alpha = 1) = \mathit{\Pi}_{\mathrm{I}}$, applying $\mathcal{P}_{f,\alpha}$ in (6.19) and $\mathcal{P}_{d,\alpha}$ in (6.20), the overall NBI detection probabilities achievable for the considered PLC system can be formulated as

$$\begin{aligned}\bar{\mathcal{P}}_f =&(1 - \mathit{\Pi}_{\mathrm{I}}) \frac{\sqrt{\pi}}{2^{2N-\frac{3}{2}}\Gamma^2(N)} \cdot \Gamma\left(2N - \frac{1}{2}, \frac{\lambda}{4\sigma_{\mathrm{b}}^4}\right) \\ &+ \frac{\mathit{\Pi}_{\mathrm{I}}\sqrt{\pi}}{2^{2N-\frac{3}{2}}\Gamma^2(N)} \cdot \Gamma\left(2N - \frac{1}{2}, \frac{\lambda}{4\sigma_{1,\alpha=1}^4}\right)\end{aligned} \tag{6.28}$$

$$\begin{aligned}\bar{\mathcal{P}}_d =&(1 - \mathit{\Pi}_{\mathrm{I}}) \frac{\sqrt{\pi}}{2^{2N-\frac{3}{2}}\Gamma^2(N)} \cdot \Gamma\left(2N - \frac{1}{2}, \frac{\lambda}{4\sigma_{2,\alpha=0}^4}\right) \\ &+ \frac{\mathit{\Pi}_{\mathrm{I}}\sqrt{\pi}}{2^{2N-\frac{3}{2}}\Gamma^2(N)} \cdot \Gamma\left(2N - \frac{1}{2}, \frac{\lambda}{4\sigma_{2,\alpha=1}^4}\right)\end{aligned} \tag{6.29}$$

where $\sigma_{1,\alpha=1}^2 = \sigma_{\mathrm{b}}^2 + \mathit{\Pi}_{\mathrm{II}}\sigma_{\mathrm{i}}^2$, $\sigma_{2,\alpha=0}^2 = \sigma_{\mathrm{b}}^2 + \sigma_v^2$ and $\sigma_{2,\alpha=1}^2 = \sigma_{\mathrm{b}}^2 + \mathit{\Pi}_{\mathrm{II}}\sigma_{\mathrm{i}}^2 + \sigma_v^2$.

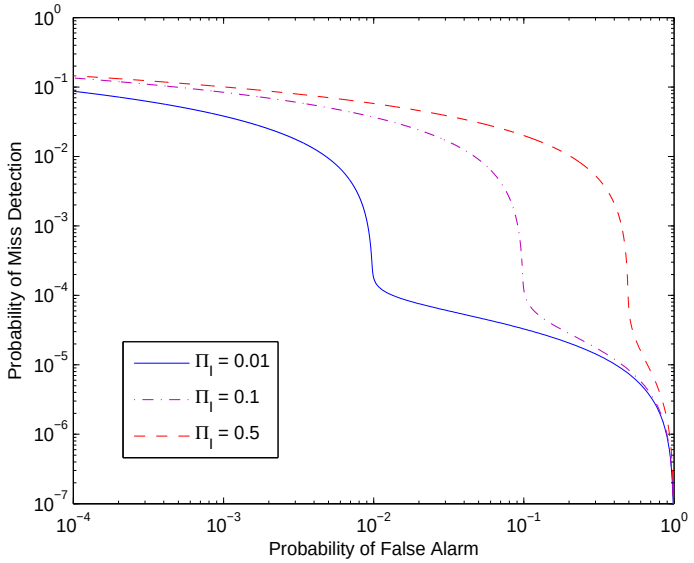

Figure 6.4: Complementary ROC curves of the proposed NBI detection scheme for different IN occurrence probabilities over the PLC system.

In Fig. 6.4, the overall capability of the proposed HOS-based detector is evaluated across the considered PLC system for different occurrence probabilities of the IN event, including $\Pi_{\mathrm{I}} = 0.01$ for the weak impact, $\Pi_{\mathrm{I}} = 0.1$ for the medium impact and $\Pi_{\mathrm{I}} = 0.5$ for the strong impact. $\sigma_{\mathrm{i}}^2 = 100\sigma_{\mathrm{b}}^2$, $\Pi_{\mathrm{II}} = 0.1$ and $\Pr(0|0) = 0.98$ are assumed. It can be seen that with high impulsive to background noise power ratio, the increase in the threshold results in the decrease in the detection rate, but barely results in reduction of the overall false alarm rate due to the occurrence of IN, yielding a sharp increase in the probability of miss detection perspective. The false alarm rate achieved on the sharp increase in the miss detection rate is determined by the occurrence probability of IN, *i.e.*, Π_{I}, and 1/10 times of the value of Π_{I} yields a gain of one order of magnitude in the probability of false alarm perspective.

6.4 System Performance Analysis

The proposed NBI detection and false alarm probabilities considering the IN disturbance have been learned. In this section, an intensive performance analysis

of the proposed detection scheme is provided for the considered PLC system.

6.4.1 Markov's Inequality

For the proposed HOS-based NBI detection capability as (6.19) and (6.20), PLC IN $n_{\mathrm{i}}(m)$ may not have the Gaussian PDF for the wideband distribution. The Markov's inequality [78] yields an upper bound of the probability that the non-negative random variable $\mathcal{K}$ lies above the threshold for any $\lambda > 0$, which refers to the CCDF of $\mathcal{K}$, *i.e.*,

$$\Pr(\mathcal{K} > \lambda) < \frac{4\sigma_{n,\alpha=1}^{4}}{\lambda} \tag{6.30}$$

where $n = 1, 2$, with $\sigma_{1,\alpha=1}^{2} = \sigma_{\mathrm{b}}^{2} + \Pi_{\mathrm{II}}\sigma_{\mathrm{i}}^{2}$ and $\sigma_{2,\alpha=1}^{2} = \sigma_{\mathrm{b}}^{2} + \Pi_{\mathrm{II}}\sigma_{\mathrm{i}}^{2} + \sigma_{v}^{2}$. Hence, the probabilities $\mathcal{P}_{f,\alpha=1}$ and $\mathcal{P}_{d,\alpha=1}$ satisfy

$$\mathcal{P}_{f,\alpha=1} < \frac{4\left(\sigma_{\mathrm{b}}^{2} + \Pi_{\mathrm{II}}\sigma_{\mathrm{i}}^{2}\right)^{2}}{\lambda} \tag{6.31}$$

$$\mathcal{P}_{d,\alpha=1} < \frac{4\left(\sigma_{\mathrm{b}}^{2} + \Pi_{\mathrm{II}}\sigma_{\mathrm{i}}^{2} + \sigma_{v}^{2}\right)^{2}}{\lambda} \tag{6.32}$$

The occurrence of time-domain IN varies significantly according to different events [58], hence in OFDM system, it is natural to assume an unknown distribution of IN across the subcarriers. The Markov's inequality applies to arbitrary probability distribution, and the probabilities are upper bounded as expressed in (6.31) and (6.32). In the case that the number of OFDM subcarriers is sufficiently large, the noise distribution follows Gaussian and the detection probabilities can be evaluated using (6.19) and (6.20).

6.4.2 Maximum Bandwidth Efficiency Achievable under IN and NBI

In this subsection, we analyse the system capacity (maximum bandwidth efficiency achievable) with the proposed NBI detection scheme. As shown in

(6.1), α, $\beta \in \{0,\ 1\}$ are the parameters indicating the occurrence states (absent or present) of the IN and NBI respectively. Let $\pi(\alpha, \beta) = \Pr(\alpha \cap \beta)$ denote the joint steady-state probabilities of the events of IN and NBI. It is assumed that the occurrence of IN and NBI is statistically independent, where $\pi(1,1) = \Pr(\alpha = 1)\Pr(\beta = 1)$ reflects the probability that both events occur. Let probabilities $\pi(\eta)$, $\eta \in \{0,\ 1\}$ indicate the NBI detection performance, where $\pi(\eta)|_{\eta=1}$ reflects the probability of detection and the probability of false alarm for the scenarios of NBI presence and NBI absence, respectively. The value of $\pi(\eta)|_{\eta=1}$ is conditioned by the event of IN as learned previously in Subsection 6.3.1, and $\pi(\eta)|_{\eta=0} = 1 - \pi(\eta)|_{\eta=1}$. Let $C(\alpha, \beta, \eta)$ be the corresponding maximum bandwidth efficiency under the specific scenario. Thus, the general maximum bandwidth efficiency achievable for the considered PLC system in Fig. 6.1 is given by

$$C = \sum_{\alpha=0}^{1} \sum_{\beta=0}^{1} \sum_{\eta=0}^{1} \pi(\alpha, \beta, \eta) C(\alpha, \beta, \eta) \tag{6.33}$$

where

$$\begin{bmatrix} \pi(\alpha,0,0) \\ \pi(\alpha,0,1) \\ \pi(\alpha,1,0) \\ \pi(\alpha,1,1) \end{bmatrix} = \begin{bmatrix} \mathcal{P}(\mathcal{H}_0) \cdot (1 - \mathcal{P}_{f,\alpha}) \\ \mathcal{P}(\mathcal{H}_0) \cdot \mathcal{P}_{f,\alpha} \\ \mathcal{P}(\mathcal{H}_1) \cdot (1 - \mathcal{P}_{d,\alpha}) \\ \mathcal{P}(\mathcal{H}_1) \cdot \mathcal{P}_{d,\alpha} \end{bmatrix}$$

and

$$\begin{bmatrix} \pi(0,\beta,\eta) \\ \pi(1,\beta,\eta) \end{bmatrix} = \begin{bmatrix} 1 - \Pi_{\mathrm{I}} \\ \Pi_{\mathrm{I}} \end{bmatrix}$$

$\mathcal{P}(\mathcal{H}_0)$ and $\mathcal{P}(\mathcal{H}_1)$ denote the probabilities of NBI absence and presence, respectively. We have

$$\begin{bmatrix} \mathcal{P}_{f,\alpha=0} \\ \mathcal{P}_{d,\alpha=0} \\ \mathcal{P}_{f,\alpha=1} \\ \mathcal{P}_{d,\alpha=1} \end{bmatrix} = \begin{bmatrix} \Pr(\eta = 1|_{\alpha=0,\beta=0}) \\ \Pr(\eta = 1|_{\alpha=0,\beta=1}) \\ \Pr(\eta = 1|_{\alpha=1,\beta=0}) \\ \Pr(\eta = 1|_{\alpha=1,\beta=1}) \end{bmatrix}$$

which has been defined in (6.19) and (6.20). For the scenario that NBI is present and has been successfully detected using our proposed method when IN also occurs at the same time, the associated probability $\pi(1,1,1)$ can be formulated

as

$$\pi(1,1,1) = \frac{\Pi_{\mathrm{I}}\mathcal{P}(\mathcal{H}_1)\sqrt{\pi}}{2^{2N-\frac{3}{2}}\Gamma^2(N)} \cdot \Gamma\left(2N - \frac{1}{2}, \frac{\lambda}{4\sigma^4_{2,\alpha=1}}\right) \tag{6.34}$$

We analyse the system capacity for the application of spectrum sharing cognitive PLC, where the so called NBI at PLC receiver is assumed from the radio primary, such as some narrowband amateur radio users around and operated inside the broadband PLC spectrum [5]. Cognitive PLC should be able to adapt the transmit power based on the decision of the NBI detection. Let P_0 be the normal transmit power to be used when NBI is not detected, and it should be reduced to a lower power P_1 when NBI is detected to protect the radio primary. Due to imperfect NBI detection, in the scenario of positive detection ($\eta = 1$), the associated capacity can be classified into four different cases based on the status of radio users and IN as

$$\begin{bmatrix} C(0,0,1) \\ C(0,1,1) \\ C(1,0,1) \\ C(1,1,1) \end{bmatrix} = \begin{bmatrix} \log_2\left(1 + P_1|H(f)|^2/\sigma^2_{\mathrm{b}}\right) \\ \log_2\left(1 + P_1|H(f)|^2/(\sigma^2_{\mathrm{b}} + \sigma^2_v)\right) \\ \log_2\left(1 + P_1|H(f)|^2/(\sigma^2_{\mathrm{b}} + \Pi_{\mathrm{II}}\sigma^2_{\mathrm{i}})\right) \\ \log_2\left(1 + P_1|H(f)|^2/(\sigma^2_{\mathrm{b}} + \Pi_{\mathrm{II}}\sigma^2_{\mathrm{i}} + \sigma^2_v)\right) \end{bmatrix}$$

where $H(f)$ denotes the average PLC channel attenuation.

In the scenario that NBI is present and has been successfully detected given IN occurs, cognitive PLC will transmit with a lower power P_1 on a higher power line noise level, and hence has harmful impact on the system performance with significantly reduced capacity in $C(1,1,1)$. Since NBI occurs frequency selectively in comparison with wideband IN and background noise, orthogonal frequency-division multiplexing (OFDM) can be applied to mitigate the impact of NBI, which is also specified in current PLC standard [17]. In OFDM PLC, the subcarriers with NBI have negligible capacities, thus $C(1,1,1)$ can be derived as

$$\begin{aligned} C(1,1,1) \approx & \frac{(1-\Pi_{\mathrm{II}})}{N} \cdot \sum_{i=1}^{N} \log_2\left(1 + \frac{P_1|H(f_i)|^2}{P_b}\right) \\ & + \frac{\Pi_{\mathrm{II}}}{N} \cdot \sum_{i=1}^{N} \log_2\left(1 + \frac{P_1|H(f_i)|^2}{P_b + P^{(imp)}}\right) \end{aligned} \tag{6.35}$$

where P_b is the background noise power spectral density (PSD), which is denoted by σ_{b}^2, N is the number of subcarriers. $P^{(imp)}$ denotes the PSD of IN.

Given the scenario of NBI presence ($\beta = 1$), a power constraint is imposed to limit the average interference within a tolerable power level by the radio users, and it can be formulated as

$$\sum_{\alpha=0}^{1} \sum_{\eta=0}^{1} \pi(\alpha, 1, \eta) P_\eta \leq P_{max} \tag{6.36}$$

where P_{max} indicates the maximum tolerable average interference normalised by the average channel gain between the cognitive PLC transmitter and the radio receiver. When $\alpha = 0$, a simplified formulation of (6.36) in [61] was considered for cognitive radio with AWGN only. Moreover, we consider the presence of IN ($\alpha = 1$) for cognitive PLC, and hence (6.36) is equivalent to

$$\begin{aligned} &(1 - \Pi_{\mathrm{I}})\mathcal{P}(\mathcal{H}_1)(1 - \mathcal{P}_{d,\alpha=0})P_0 + (1 - \Pi_{\mathrm{I}})\mathcal{P}(\mathcal{H}_1)\mathcal{P}_{d,\alpha=0}P_1 \\ &+ \Pi_{\mathrm{I}}\mathcal{P}(\mathcal{H}_1)(1 - \mathcal{P}_{d,\alpha=1})P_0 + \Pi_{\mathrm{I}}\mathcal{P}(\mathcal{H}_1)\mathcal{P}_{d,\alpha=1}P_1 \leq P_{max} \end{aligned} \tag{6.37}$$

Inserting the overall probability of detection for the considered PLC system in (6.27), yields

$$(1 - \bar{\mathcal{P}}_d)\mathcal{P}(\mathcal{H}_1)P_0 + \bar{\mathcal{P}}_d\mathcal{P}(\mathcal{H}_1)P_1 \leq P_{max} \tag{6.38}$$

thus, it can be derived that

$$\bar{\mathcal{P}}_d \geq \frac{\mathcal{P}(\mathcal{H}_1)P_0 - P_{max}}{\mathcal{P}(\mathcal{H}_1)(P_0 - P_1)} \tag{6.39}$$

where the average probability of detection should meet a minimum required value to protect the radio primary, and for a given probability of false alarm, the higher the probability of detection, the more protection to the radio users. Hence, the NBI detection scheme with higher ROC performance can protect the radio users more effectively.

Given the scenario of NBI absence ($\beta = 0$), and assuming low occurrence probability of IN bursts, *i.e.*, Π_{I} is close to 0, and using the overall probability

of false alarm in (6.26), the maximum bandwidth efficiency in (6.33) can be expressed as

$$C = \frac{(1-\Pi_{\mathrm{I}})\mathcal{P}(\mathcal{H}_0)}{N}\left[(1-\bar{\mathcal{P}}_f)\sum_{i=1}^{N}\log_2\left(1+\frac{P_0|H(f_i)|^2}{P_b}\right)\right.$$
$$\left.+\,\bar{\mathcal{P}}_f\sum_{i=1}^{N}\log_2\left(1+\frac{P_1|H(f_i)|^2}{P_b}\right)\right] \tag{6.40}$$

which implies that the overall system capacity is dominated by the adaptive transmit power, background noise and the channel attenuation. For a given probability of detection following the constraint in (6.39), it can be seen in (6.40) that the lower the probability of false alarm, the higher the capacity achievable for spectrum sharing cognitive PLC. Hence, the NBI detection scheme with higher ROC performance results in a better system performance.

In Fig. 6.5, the maximum bandwidth efficiencies achievable in (6.40) are demonstrated for different detection schemes. For a target $\bar{\mathcal{P}}_d$ following the constraint in (6.39), the corresponding $\bar{\mathcal{P}}_f$ varies from different detectors. The horizontal axis denotes the signal-to-background noise power ratio P_0/P_b, which varies from 0 dB to 20 dB. A random PLC channel generator in [7] is applied to obtain the class-9 channel from 1.8 MHz-100 MHz. We consider $\Pi_{\mathrm{I}} = 0.01$, $\mathcal{P}(\mathcal{H}_0) = 0.9$, $P_1 = 0.1P_0$, $N = 128$ and the target probability of miss detection $(1-\bar{\mathcal{P}}_d)$ is 10^{-3}. It can be seen in Fig. 6.5 that under the target probability of miss detection, the proposed HOS-based detector has its average probability of false alarm low enough yielding a negligible loss in the system capacity. Using the amplitude-level detector, the maximum bandwidth efficiency is lowered by around 2 bps/Hz for SNR = 10 dB, comparing to the perfect case with no false alarm.

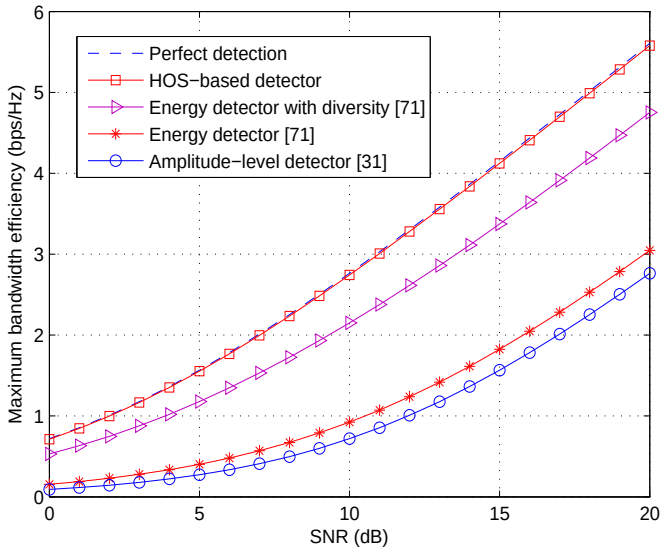

Figure 6.5: Maximum bandwidth efficiency achievable under different NBI detection schemes for a target probability of miss detection ($1 - \bar{\mathcal{P}}_d = 10^{-3}$).

6.4.3 Dynamic Notching Implementation on the NBI Frequencies

Due to the concern about disturbing the surrounding radio users, many of the existing systems do not consider some HF bands for PLC transmission [79]. Normally, a static notching is applied as in the HPAV standard [17], that the subcarrier with NBI and its neighbour ± 4 subcarriers are too notched. In Future PLC systems, in order to get higher data rate, PLC aims to share spectrum with other radio frequencies. An effective dynamic notching scheme may be essential to protect the valid radio services, and mitigate the effect of NBI from the active radios at the same time [6, 54]. To resolve the coexistence issue, the spectrum should be monitored and detected in real time, and then adjust the notched frequencies adaptively.

The comparisons of normalised throughput between the dynamic and static notching implementations are reflected in Fig. 6.6, with $N = 128$, $\mathcal{P}(\mathcal{H}_1) = 0.1$, and average SNR of 10 dB at a class-9 channel output. Assuming no IN occurs, and the NBI frequencies are pre-known with a perfect detection of the

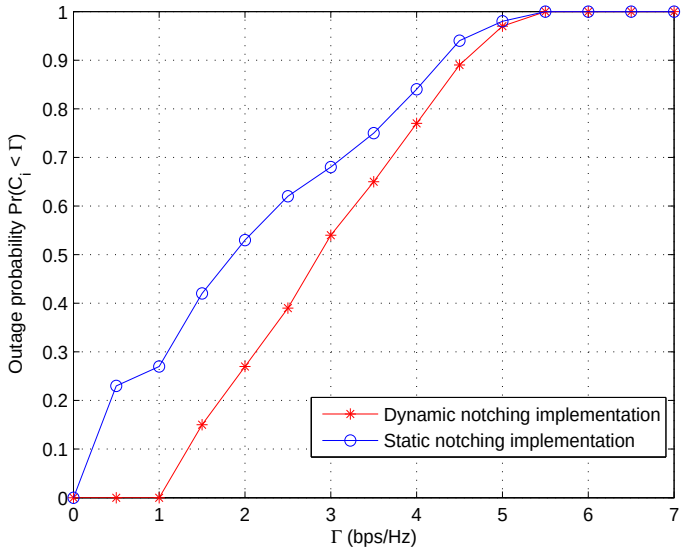

Figure 6.6: Comparison of the theoretical throughput between the dynamic and static notching schemes, in terms of the outage probability that the received SNRs are below a certain value of γ_{min}, for an average SNR = 10 dB at a class-9 channel output.

NBI presence. It can be seen that with the dynamic notching scheme, 25% more subcarriers in average provide the data rate over 2 bps/Hz, than the normal static notching approach. The results obtained show the significance of implementing an effective detection of the NBI from radio bands for cognitive PLC.

6.5 Summary

In this chapter, an HOS-based NBI detection scheme has been proposed, considering the occurrence model of power line IN. Analytical expressions for the probability of detection, which is conditioned by the presence of wideband IN have been given. The proposed detection scheme has been implemented in both scenarios of IN absence and IN presence, respectively. The improvement in detection capability of the proposed scheme over the conventional methods, has been quantified using the complementary ROC curves. The HOS-based NBI detection scheme is shown to be more suitable for PLC systems as it is robust against IN. Simulation results have demonstrated a near perfect system capacity achievable

with the proposed NBI detection scheme, indicating its suitability for cognitive PLC networks by allowing sharing of the spectrum of radio frequencies. The dynamic spectrum access approach is of the interest in added interference channels, especially for future cognitive PLC solutions, which improves the throughput by sharing the spectrum of radio frequencies.

Chapter 7

Conclusions and Future Work

7.1 Conclusions

In this thesis, a thorough study has been made on IN and NBI for indoor broadband PLC, ranging from measurement, modelling, detection and mitigation techniques, and performance analysis. The main achievements of the study are highlighted in the following:

- In Chapter 3, a hybrid statistical model to describe the correlation of IN, and a two-level MC based model to describe the occurrence dependence of IN has been proposed, based on the measurement results. The models are generic and adaptive to different scenarios (the BG model [2] can be treated as a special case where impulses are independent). By simply adjusting the value of the weight coefficient in the hybrid model, the level of correlation between consecutive impulses can be changed. The example IN illustrates that MC is suitable to model the transitions among time states, where it is more realistic to consider multiple impulse states in the two-level MC. The proposed models are validated in reference to the measured results.

- In Chapter 4, a 3D MC based statistical model to describe the occurrence dependence of NBI has been proposed, based on the measurement results. The example NBI illustrates that MC is suitable to model the transitions among time states, where it is more realistic to consider multiple NBI states

in the 3D MC. The proposed model is validated in reference to the measured results. The analytical throughput considering the impact of both IN and NBI has been investigated. The dynamic spectrum access approach is of the interest in added interference channel, especially for future cognitive PLC solutions, which improves the throughput by sharing the spectrum of radio bands.

- In Chapter 5, the IN mitigation for OFDM-based PLC systems have been studied. A null subcarriers assisted iterative receiver has been proposed to reconstruct the IN vector, considering the potential NBI contaminated null subcarriers. The proposed IN mitigation scheme has been evaluated in the scenarios of NBI absence and NBI presence, respectively. The ROC expressions of detecting nonzero entries in the IN vector have been given, which are conditioned by the presence of NBI. In the absence of NBI, the improvement in IN detection capability of the proposed scheme over the conventional blanking scheme, has been quantified by the complementary ROC curves. While both schemes can be harmfully affected under the disturbance of intensive NBI. Moreover, a pre-FD/TD nulling block has been adopted as an extended use of null subcarriers in the proposed receiver, in order to improve the initial IN estimation by joint mitigating the high-amplitude NBI and IN. The associated thresholds for the detection of NBI and IN can be simply computed, given a desired false alarm rate. Furthermore, simulation results have demonstrated a much better BER performance of the proposed receiver than that of the blanking scheme especially in the high SNR region, meanwhile, a reduced number of iterations is required with the aid of null subcarriers in the proposed scheme. In the presence of intensive NBI that the power of the NBI contaminated subcarriers is extremely high, the IN vector cannot be reconstructed accurately. Hence, the pre-mitigation is implemented, which makes it possible to achieve a BER

performance with initial IN estimation only close to that with complete IN estimation.

- In Chapter 6, we have proposed an HOS-based NBI detection scheme for broadband cognitive PLC networks, considering the occurence model of IN. Closed-form expressions for the probabilities of detection have been given. The improvement in detection capability of the proposed NBI detection over the conventional methods, has been quantified using the complementary ROC curves. The HOS based NBI detection scheme is shown to be more suitable for PLC systems as it is robust against IN. Simulation results have demonstrated a near perfect system capacity achievable with the proposed NBI detection scheme, indicating its suitability for cognitive PLC networks by allowing sharing of the spectrum of radio frequencies.

As a conclusion, the proposed work in this thesis is applicable to the PLC systems under the disturbance of both IN and NBI, and also optimises the system performance.

7.2 Future Work

Following this thesis, it is desirable to extend the work in the future as:

- The performance of PLC suffering from IN and NBI is analysed in an OFDM system in this thesis. Future work includes performance optimisation techniques in a single-carrier frequency-domain equalisation (SC-FDE) system [80, 81] in order to reduce the high PAPR of signals in OFDM systems.

- IN and NBI mitigation can be extended in a SC-FDE based PLC system. The NBI from radio applications normally appears at null subcarriers, where the frequencies are notched from the PLC transmit power spectrum. Some of the unexpected NBI may have the ingress at data subcarriers.

Mitigation of NBI on data subcarriers in a SC-FDE system can be studied. Moreover, hybrid SC-FDE/OFDM PLC systems can be considered.

- Dynamic channel frequency response due to the connection/disconnection of electric appliances inside the grid can be investigated with extensive measurement. Different PLC channel attenuation models will be considered. As learned in Chapter 3, different plugging/unplugging operations reproduce different statistics of IN, which can be applied as a signature for channel estimation. Hence, the patterns of burst IN can be further analysed for the dynamic channel variations.

- Extensive work can be conducted on spectrum sharing cognitive PLC for the demand of high throughput indoor PLC networking. Specifically, as learned in Chapter 6, PLC limits the transmit power from the higher power P_0 to the lower power P_1, in order to avoid causing intolerable interference to the radio users. The ratio of P_1/P_0 is not given, since it is bounded by the values of maximum tolerable interference and the total aggregated interference at the radio receivers. The connection between P_0 and P_1 can be further studied. Also, the aggregated interference from the power line network to radio receivers can be learned.

- The IN mitigation scheme proposed in this thesis is at the OFDM receiving end. IN mitigation can be further considered at OFDM transmitters. For example, clipping of the large magnitude signals to reduce the high PAPR problem and make the IN reconstruction more accurate. Also, it is an interesting technique to add a random phase rotation in the transmit OFDM symbol, and rotated back at receiver to avoid the tail of noise PDF.

Appendix A

Derivation of the Autocorrelation Function of Impulsive Noise

The autocorrelation function of $n_{\mathrm{i}}(m)$ can be expressed as $R(k) = E[n_{\mathrm{i}}(m+k) \cdot n_{\mathrm{i}}(m)]$. By using (3.2), it becomes

$$R(k) = R_{xx}(k) + w \cdot R_{xn_{\mathrm{i}}}(k+1) + w \cdot R_{n_{\mathrm{i}}x}(k-1) \tag{A.1}$$

where $R_{n_{\mathrm{i}}x}(k)$ is the cross-correlation between $n_{\mathrm{i}}(m)$ and $x(m)$, expressed as

$$\begin{aligned} R_{n_{\mathrm{i}}x}(k) &= E[n_{\mathrm{i}}(m+k) \cdot x(m)] \\ &= \frac{w}{\sqrt{1+w^2}} R_{n_{\mathrm{i}}x}(k-1) + \frac{1}{\sqrt{1+w^2}} R_{xx}(k) \end{aligned} \tag{A.2}$$

$R_{xx}(k)$ in (A.1) and (A.2) is the autocorrelation function of $x(m)$, and $R_{xx}(k) = \sigma_x^2 \cdot \delta(k)$. Thus, we derive $R_{n_{\mathrm{i}}x}(k)$ as

$$R_{n_{\mathrm{i}}x}(k) = \frac{1}{\sqrt{1+w^2}} \cdot \sigma_x^2 \left(\frac{w}{\sqrt{1+w^2}} \right)^k u(k) \tag{A.3}$$

where $u(k)$ is the step function, and the cross-correlation $R_{xn_{\mathrm{i}}}(k) = R_{n_{\mathrm{i}}x}(-k)$ can be solved as

$$R_{xn_{\mathrm{i}}}(k) = \frac{1}{\sqrt{1+w^2}} \cdot \sigma_x^2 \left(\frac{w}{\sqrt{1+w^2}} \right)^{-k} u(-k) \tag{A.4}$$

Thus, by substituting (A.3) and (A.4) into (A.1), the autocorrelation function in (3.3) can be derived.

Appendix B

Derivation of the PSD of Impulsive Noise

The PSD of $n_{\mathrm{i}}(m)$ can be defined as the discrete-time Fourier transform of its autocorrelation function as $S(f) = \sum_k R(k) e^{-j2\pi kf/f_s}$. By applying (3.3), it can be expressed as

$$S(f) = \sigma_x^2 \sum_{k=-\infty}^{\infty} \left(\frac{w}{\sqrt{1+w^2}} \right)^{|k|} e^{-j2\pi kf/f_s} \tag{B.1}$$

which is equivalent to

$$\begin{aligned} S(f) = \sigma_x^2 \cdot \Bigg[& \sum_{k=-\infty}^{-1} \left(\frac{w}{\sqrt{1+w^2}} \right)^{-k} e^{-j2\pi kf/f_s} \\ & + \sum_{k=0}^{\infty} \left(\frac{w}{\sqrt{1+w^2}} \right)^{k} e^{-j2\pi kf/f_s} \Bigg] \end{aligned} \tag{B.2}$$

where (B.2) can simply be expressed as

$$\begin{aligned} S(f) = \sigma_x^2 \cdot \Bigg[& \frac{1}{1-(w/\sqrt{1+w^2})e^{-j2\pi f/f_s}} \\ & - \frac{w/\sqrt{1+w^2}}{w/\sqrt{1+w^2} - e^{-j2\pi f/f_s}} \Bigg] \end{aligned} \tag{B.3}$$

It can be derived that

$$\begin{aligned} |S(f)|^2 &= S(f)S^*(f) \\ &= \sigma_x^4 \Bigg[\frac{1+(w/\sqrt{1+w^2})^2}{1+(w/\sqrt{1+w^2})^2 - 2(w/\sqrt{1+w^2})\cos(2\pi f/f_s)} \\ &\quad - \frac{4(w/\sqrt{1+w^2})^2}{\Big(1+(w/\sqrt{1+w^2})^2 - 2(w/\sqrt{1+w^2})\cos(2\pi f/f_s)\Big)^2} \end{aligned}$$

$$+\frac{2(w/\sqrt{1+w^2})(1+(w/\sqrt{1+w^2})^2)\cos(2\pi f/f_s)}{\left(1+(w/\sqrt{1+w^2})^2-2(w/\sqrt{1+w^2})\cos(2\pi f/f_s)\right)^2}\Bigg]$$

$$=\sigma_x^4\cdot\frac{1}{\left(1-2w\sqrt{1+w^2}\cos(2\pi f/f_s)+2w^2\right)^2} \tag{B.4}$$

Thus, the expression of the PSD in (3.7) can be derived.

Bibliography

[1] P. Amirshahi, F. Canete, K. Dostert, S. Galli, M. Katayama, and M. Kavehrad, *Power Line Communications: Theory and Applications for Narrowband and Broadband Communications over Power Lines*. New York: Wiley, 2010.

[2] L. D. Bert, P. Caldera, D. Schwingshackl, and A. M. Tonello, "On noise modeling for power line communications," *in Proc. ISPLC 2011*, pp. 283–288, Apr. 2011, Udine, Italy.

[3] C. Paul, *Analysis of Multiconductor Transmission Lines*. New Jersey: John Wiley and Sons, 2008.

[4] T. Yucek and H. Arslan, "A survey of spectrum sensing algorithms for cognitive radio applications," *IEEE Commun. Surveys & Tutorials*, vol. 11, pp. 116–130, 2009.

[5] *Amateur Radio Band Plans*. Radio Society of Great Britain, 2015, [Online]. Available: http://www.hflink.com/bandplans/UK_bandplan.pdf.

[6] B. Praho, M. Tlich, P. Pagani, A. Zeddam, and F. Nouvel, "Cognitive detection method of radio frequencies on power line networks," *in Proc. ISPLC 2010*, pp. 225–230, Mar. 2010.

[7] M. Tlich, A. Zeddam, F. Moulin, and F. Gauthier, "Indoor powerline communications channel characterization up to 100 MHz-Part II: Time-frequency

analysis," *IEEE Trans. Power Delivery*, vol. 23, no. 3, pp. 1402–1409, Jul. 2008.

[8] A. M. Tonello and F. Versolatto, "Bottom-up statistical PLC channel modeling-Part II: Inferring the statistics," *IEEE Trans. Power Del.*, vol. 25, no. 4, pp. 2356–2363, Oct. 2010.

[9] L. Lampe, A. M. Tonello, and D. Shaver, "Power line communications for automation networks and smart grid [Guest Editorial]," *IEEE Commun. Mag.*, vol. 49, no. 12, pp. 26–27, Dec. 2011.

[10] G. Acciani, V. Amoruso, G. Fornarelli, and A. Giaquinto, "A supervised method for the automatic detection of impulsive noise in naval powerline communications," *in Proc. ISPLC 2011*, pp. 90–95, Apr. 2011, Udine, Italy.

[11] S. Liu, F. Yang, W. Ding, and J. Song, "Double kill: Compressive sensing based narrowband interference and impulsive noise mitigation for vehicular communications," *IEEE Trans. Veh. Technol.*, vol. 65, no. 7, pp. 5099–5109, Jul. 2016.

[12] E. A. Teixeira, F. S. Marques, S. G. de Araujo, E. M. de Souza, T. M. Johnson, and M. V. Ribeiro, "Modeling and performance analysis of PLC channels with external interference in outdoor and indoor environments," *in Proc. ISPLC*, pp. 222–227, 2008.

[13] W. Liu, H. Widmer, and P. Raffin, "Broadband PLC access systems and field deployment in European power line networks," *IEEE Communications Magazine*, vol. 41, no. 5, pp. 114–118, May 2003.

[14] S. Galli, A. Scaglione, and Z. Wang, "For the grid and through the grid: The role of Power Line Communications in the Smart Grid," *Proceedings of the IEEE*, vol. 99, no. 6, pp. 998–1027, Jun. 2011.

[15] S. Galli and O. Logvinov, "Recent developments in the standardization of power line communications within the IEEE," *IEEE Commun. Mag.*, vol. 46, no. 7, pp. 64–71, Jul. 2008.

[16] V. Oksman and S. Galli, "G.hn: The new ITU-T home networking standard," *IEEE Commun. Mag.*, vol. 47, no. 10, pp. 138–45, Oct. 2009.

[17] *HomePlug AV white paper*. HomePlug Powerline Alliance, 2015, [Online]. Available: http://www.homeplug.org/tech-resources/resources/.

[18] J. A. Cortes, L. Dez, F. J. Canete, and J. J. Sanchez-Martnez, "Analysis of the indoor broadband power-line noise scenario," *IEEE Trans. Electromagnetic Compatibility*, vol. 52, no. 4, pp. 849–858, Nov. 2010.

[19] T. Esmailian, F. R. Kschischang, and P. G. Gulak, "In-building power lines as high-speed communication channels: Channel characterization and a test channel ensemble," *Int. J. Commun.*, vol. 16, pp. 381–400, Jun. 2003.

[20] V. Degardin, M. Lienard, A. Zeddam, F. Gauthier, and P. Degauque, "Classification and characterization of impulsive noise on indoor power line used for data communications," *Consum. Electron.*, vol. 48, no. 4, pp. 913–918, Nov. 2002.

[21] H. Meng, Y. L. Guan, and S. Chen, "Modeling and analysis of noise effects on broadband power-line communications," *IEEE Trans. Power Del.*, vol. 20, no. 2, pp. 630– 637, Apr. 2005.

[22] D. Middleton, "Statistical-physical models of electro-magnetic interference," *IEEE Trans. Electromagnetic Compatibility*, vol. 19, no. 3, Aug. 1977.

[23] M. Katayama, T. Yamazato, and H. Okada, "A mathematical model of noise in narrowband power line communication systems," *IEEE J. Sel. Areas Commun.*, vol. 24, no. 7, pp. 1267–1276, Jul. 2006.

[24] G. Ren, S. Qiao, H. Zhao, C. Li, and Y. Hei, "Mitigation of periodic impulsive noise in OFDM-based power-line communications," *IEEE Trans. Power Del.*, vol. 28, no. 2, pp. 825–834, Apr. 2013.

[25] M. Zimmermann and K. Dostert, "Analysis and modeling of impulsive noise in broad-band powerline communications," *IEEE Trans. Electromagnetic Compatibility*, vol. 44, no. 1, pp. 249–258, Feb. 2002.

[26] J. Lin, M. Nassar, and B. Evans, "Impulsive noise mitigation in powerline communications using sparse Bayesian learning," *IEEE J. Sel. Areas. Commun.*, vol. 31, no. 7, pp. 1172–1183, Jul. 2013.

[27] F. Juwono, Q. Guo, D. Huang, and K. P. Wong, "Deep clipping for impulsive noise mitigation in OFDM-based power-line communications," *IEEE Trans. Power Del.*, vol. 29, no. 3, pp. 1335–1343, Jun. 2014.

[28] S. P. Herath, N. H. Tran, and T. Le-Ngoc, "On optimal input distribution and capacity limit of Bernoulli-Gaussian impulsive noise channels," *in Proc. IEEE ICC 2012*, Jun. 2012, Ottawa, Canada.

[29] C. Lopes, J. M. M. Pinto, and J. B. Gerald, "Dealing with unknown impedance and impulsive noise in the power-line communications channel," *IEEE Trans. Power Delivery*, vol. 28, no. 1, pp. 58–66, Jan. 2013.

[30] M. Babic, M. Hagenau, K. Dostert, and J. Bausch, "D4: Theoretical postulation of PLC channel model," *EC/IST FP6 Project*, vol. 2, no. 507667, Mar. 2005.

[31] G. Ndo, P. Siohan, and M. Hamon, "Adaptive noise mitigation in impulsive environment: application to power-line communications," *IEEE Trans. Power Delivery*, vol. 25, no. 2, pp. 647–656, Apr. 2010.

[32] Y.-R. Chien, "Iterative channel estimation and impulsive noise mitigation algorithm for OFDM-based receivers with application to power-line communications," *IEEE Trans. Power Del.*, vol. 30, no. 6, pp. 2435–2442, Dec. 2015.

[33] M. Antoniali, F. Versolato, and A. M. Tonello, "An experimental characterization of the PLC noise at the source," *IEEE Trans. Power Delivery*, vol. 31, no. 3, pp. 1068–1075, Jun. 2016.

[34] G. Liu, X. Zhu, and G. Zhu, "Impact of variance of heterogeneous spectrum on performance of cognitive radio ad hoc networks," *in Proc. IEEE ICC 2012*, Jun. 2012, Ottawa, Canada.

[35] P. Cardieri, "Modeling interference in wireless ad hoc networks," *IEEE Communications Surveys & Tutorials*, vol. 12, no. 4, pp. 551–572, Fourth quarter 2010.

[36] A. M. Tonello and F. Versolatto, "Bottom-up statistical PLC channel modeling-Part I: Random topology model and efficient transfer function computation," *IEEE Trans. Power Del.*, vol. 26, no. 2, pp. 891–898, Apr. 2011.

[37] M. Zimmermann and K. Dostert, "A multipath model for the powerline channel," *IEEE Trans. Commun.*, vol. 50, no. 4, pp. 553–559, Apr. 2002.

[38] E. Biglieri, "Coding and modulation for a horrible channel," *IEEE Communications Magazine*, vol. 41, no. 5, pp. 92–98, May 2003.

[39] D. F. Tseng, R. B. Yang, T. R. Tsai, Y. S. Han, and W. H. Mow, "Efficient clipping for broadband power line systems in impulsive noise environment," *in Proc. ISPLC 2012*, pp. 362–367, 2012, Beijing.

[40] S. V. Zhidkov, "Analysis and comparison of several simple impulsive noise mitigation schemes for OFDM receivers," *IEEE Trans. Commun.*, vol. 56, no. 1, pp. 5–9, Jan. 2008.

[41] ——, "Performance analysis and optimization of OFDM receiver with blanking nonlinearity in impulsive noise environment," *IEEE Trans. Veh. Technol.*, vol. 55, no. 1, pp. 234–242, Jan. 2006.

[42] V. N. Papilaya and A. J. H. Vinck, "Investigation on a new combined impulsive noise mitigation scheme for OFDM transmission," *in Proc. ISPLC*, pp. 86–91, 2013.

[43] D. Donoho, "Compressed sensing," *IEEE Trans. Inf. Theory*, vol. 52, no. 4, pp. 1289–1306, Apr. 2006.

[44] L. Lampe, "Bursty impulse noise detection by compressed sensing," *in Proc. ISPLC*, pp. 29–34, 2011.

[45] D. Wipf and B. Rao, "Sparse Bayesian learning for basis selection," *IEEE Trans. Signal Process.*, vol. 52, no. 8, pp. 2153–2164, 2004.

[46] D. Umehara, H. Yamaguchi, and Y. Morihiro, "Turbo decoding in impulsive noise environment," *in Proc. IEEE Globecom*, Dec. 2004.

[47] H. Nakagawa, D. Umehara, S. Denno, and Y. Morihiro, "A decoding for low density parity check codes over impulsive noise channels," *in Proc. ISPLC*, pp. 85–89, 2005.

[48] Q. H. Mahmoud, *Cognitive Networks: Towards Self-Aware Networks.* John Wiley, 2007.

[49] H. Arslan, *Cognitive Radio, Software Defined Radio, and Adaptive Wireless Systems.* Springer, 2007.

[50] *Notice of proposed rule making and order: Facilitating opportunities for flexible, efficient, and reliable spectrum use employing cognitive radio technologies*. Federal Communications Commission, Feb. 2005.

[51] M. Matinmikko, J. D. Ser, T. Rauma, and M. Mustonen, "Fuzzy-logic based framework for spectrum availability assessment in cognitive radio systems," *IEEE J. Sel. Areas Commun.*, vol. 31, no. 11, pp. 2173–2184, Nov. 2013.

[52] H. Gao, G. Bumiller, W. Liu, and J. Li, "A new digital front end structure for cognitive PLC systems," *in Proc. ISPLC*, pp. 250–255, 2015.

[53] A. M. Tonello, "PLC physical layer advances," *WSPLC 2009 OMEGA PLC tutorial*, Oct. 2009, Udine, Italy.

[54] Y. Lu and W. Liu, "Spectrum analyzer based measurement and detection of MW/SW broadcast radios on power lines for cognitive PLC," *in Proc. ISPLC*, pp. 103–108, Mar. 2013.

[55] D. Malone, K. Duffy, and D. Leith, "Modeling the 802.11 distributed coordination function in nonsaturated heterogeneous conditions," *IEEE/ACM Trans. Networking*, vol. 15, no. 1, pp. 159–172, Feb. 2007.

[56] E. N. Gilbert, "Capacity of burst-noise channels," *Bell Syst. Tech. J.*, vol. 39, pp. 1253–1266, 1960.

[57] N. H. Nedev, S. McLaughlin, and D. I. Laurenson, "Estimating errors in transmission systems due to impulse noise," *in IEE Proc. Commun.*, vol. 153, no. 5, pp. 651–656, Oct. 2006.

[58] J. Yin, X. Zhu, and Y. Huang, "Modeling of amplitude-correlated and occurrence-dependent impulsive noise for power line communication," *in Proc. IEEE ICC*, Jun. 2014, Sydney, Australia.

[59] M. Tlich, H. Chaouche, A. Zeddam, and P. Pagani, "Novel approach for PLC impulsive noise modelling," *in Proc. ISPLC*, pp. 20–25, Apr. 2009.

[60] K. C. Wiklundh, P. F. Stenumgaard, and H. M. Tullberg, "Channel capacity of Middleton's class A interference channel," *Electron. Lett.*, vol. 45, no. 24, pp. 1227–1229, Nov. 2009.

[61] S. Akin and M. Gursoy, "On the throughput and energy efficiency of cognitive MIMO transmissions," *IEEE Trans. Veh. Technol.*, vol. 62, no. 7, pp. 3245–3260, Sept. 2013.

[62] F. Tuchiya, H. Misawa, T. Nakajo, I. Tomizawa, J. Nakajima, M. Ohishi, M. Tokumaru, T. Ono, and A. Morioka, "Interference measurements in HF and UHF bands caused by extension of power line communication bandwidth for astronomical purpose," *in Proc. ISPLC*, pp. 265–269, Apr. 2003.

[63] F. Abdelkefi, P. Duhamel, and F. Alberge, "Impulsive noise cancellation in multicarrier transmission," *IEEE Trans. Commun.*, vol. 53, no. 1, pp. 94–106, Jan. 2005.

[64] S. V. Zhidkov, "Impulsive noise suppression in OFDM based communication systems," *IEEE Trans. Consum. Electron.*, vol. 4, no. 9, pp. 944–948, Nov. 2003.

[65] A. Tonello and F. Pecile, "Efficient architectures for multiuser FMT systems and application to power line communications," *IEEE Trans. Commun.*, vol. 57, no. 5, pp. 1275–1279, May 2009.

[66] K. Rabie and E. Alsusa, "Preprocessing-based impulsive noise reduction for power-line communications," *IEEE Trans. Power Del.*, vol. 29, no. 4, pp. 1648–1658, Aug. 2014.

[67] P. Khurd, B. Liu, and G. Gindi, "Ideal AFROC and FROC observers," *IEEE Trans. Med. Imag.*, vol. 29, no. 2, pp. 375–385, Feb. 2010.

[68] I. S. Gradshteyn, I. M. Ryzhik, A. Jeffrey, and D. Zwillinger, *Table of Integrals, Series, and Products.* Seventh (7th) edition. Academic Press, 2007.

[69] G. Avril, F. Moulin, A. Zeddam, M. Tlich, and F. Nouvel, "Impulsive noise detection on masked carriers," *in Proc. ISPLC*, pp. 369–373, 2008.

[70] D. Denkovski, V. Atanasovski, and L. Gavrilovska, "HOS based goodness-of-fit testing signal detection," *IEEE Commun. Lett.*, vol. 16, no. 3, pp. 310–313, Mar. 2012.

[71] F. F. Digham, M.-S. Alouini, and M. K. Simon, "On the energy detection of unknown signals over fading channels," *IEEE Trans. Commun.*, vol. 55, no. 1, pp. 21–24, 2007.

[72] C. Saragiotis, L. Hadjileontiadis, I. Rekanos, and S. Panas, "Automatic P phase picking using maximum kurtosis and -statistics criteria," *IEEE Geosci. Remote Sens. Lett*, vol. 1, no. 3, pp. 147–151, Jul. 2004.

[73] N. J. Redding, *Estimating the Parameters of the K Distribution in the Intensity Domain.* DSTO Electronics and Surveillance Laboratory, 1999, South Australia.

[74] I. S. Ansari, S. Al-Ahmadi, F. Yilmaz, M. S. Alouini, and H. Yanikomeroglu, "A new formula for the BER of binary modulations with dual-branch selection over generalized-K composite fading channels," *IEEE Trans. Commun.*, vol. 59, no. 10, pp. 2654–2658, Oct. 2011.

[75] J. Tunaley, *K-distribution Algorithm.* London Research and Development Corporation, Aug. 2010.

[76] M. V. Ribeiro, C. A. G. Marques, C. A. Duque, A. S. Cerqueira, and J. L. R. Pereira, "Detection of disturbances in voltage signals for power quality analysis using HOS," *EURASIP Journal on Advances in Signal Processing*, Feb. 2007.

[77] E. Nemer, R. Goubran, and S. Mahmoud, "Robust voice activity detection using higher-order statistics in the LPC residual domain," *IEEE Trans. Speech Audio Process.*, vol. 9, no. 3, pp. 217–231, Mar. 2001.

[78] G. Grimmett and D. Stirzaker, *Probability and Random Processes*. Third (3rd) edition, Oxford University Press, 2001.

[79] N. Weling, "SNR-based detection of broadcast radio stations on powerlines as mitigation method toward a cognitive PLC solution," *in Proc. ISPLC*, pp. 52–59, Mar. 2012.

[80] K. M. Rabie and E. Alsusa, "Single-carrier FDMA with blanking/clipping for mitigating impulsive noise over PLC channels," *in Proc. ISPLC*, pp. 340–345, 2014, Glasgow.

[81] Y. h. Qi, b. Wang, P. w. Huang, and W. h. Cai, "Coded SC-FDE system over impulsive noise channels," *IET Conference on Wireless, Mobile and Sensor Networks*, pp. 1070–1072, 2007, Shanghai.